THE IMPLICATIONS AND FLOW BEHAVIOR OF THE HYDRAULICALLY FRACTURED WELLS IN SHALE GAS FORMATION

A Thesis

by

ANAS MOHAMMADALI S. ALMARZOOQ

Submitted to the Office of Graduate Studies of
Texas A&M University
in partial fulfillment of the requirements for the degree of

MASTER OF SCIENCE

December 2010

Major Subject: Petroleum Engineering

THE IMPLICATIONS AND FLOW BEHAVIOR OF THE HYDRAULICALLY FRACTURED WELLS IN SHALE GAS FORMATION

A Thesis

by

ANAS MOHAMMADALI S. ALMARZOOQ

Submitted to the Office of Graduate Studies of
Texas A&M University
in partial fulfillment of the requirements for the degree of

MASTER OF SCIENCE

Approved by:

Chair of Committee,	Robert A. Wattenbarger
Committee Members,	Yuefeng Sun
	Bryan Maggard
Head of Department,	Steve Holditch

December 2010

Major Subject: Petroleum Engineering

ABSTRACT

The Implications and Flow Behavior of the Hydraulically Fractured Wells in Shale Gas Formation.

(December 2010)

Anas Mohammadali S. Almarzooq, B.Sc., King Fahad University of Petroleum and Minerals, Saudi Arabia

Chair of Advisory Committee: Dr. Robert Wattenbarger

Shale gas formations are known to have low permeability. This low permeability can be as low as 100 nano darcies. Without stimulating wells drilled in the shale gas formations, it is hard to produce them at an economic rate. One of the stimulating approaches is by drilling horizontal wells and hydraulically fracturing the formation. Once the formation is fractured, different flow patterns will occur. The dominant flow regime observed in the shale gas formation is the linear flow or the transient drainage from the formation matrix toward the hydraulic fracture. This flow could extend up to years of production and it can be identified by half slop on the log-log plot of the gas rate against time. It could be utilized to evaluate the hydraulic fracture surface area and eventually evaluate the effectiveness of the completion job. Different models from the literature can be used to evaluate the completion job. One of the models used in this work assumes a rectangular reservoir with a slab shaped matrix between each two hydraulic fractures. From this model, there are at least five flow regions and the two regions discussed are

the Region 2 in which bilinear flow occurs as a result of simultaneous drainage form the matrix and hydraulic fracture. The other is Region 4 which results from transient matrix drainage which could extend up to many years. The Barnett shale production data will be utilized throughout this work to show sample of the calculations.

This first part of this work will evaluate the field data used in this study following a systematic procedure explained in Chapter III. This part reviews the historical production, reservoir and fluid data and well completion records available for the wells being analyzed. It will also check for data correlations from the data available and explain abnormal flow behaviors that might occur utilizing the field production data. It will explain why some wells might not fit into each model. This will be followed by a preliminary diagnosis, in which flow regimes will be identified, unclear data will be filtered, and interference and liquid loading data will be pointed. After completing the data evaluation, this work will evaluate and compare the different methods available in the literature in order to decide which method will best fit to analyze the production data from the Barnett shale. Formation properties and the original gas in place will be evaluated and compared for different methods.

DEDICATION

I dedicate my work to my family and all those who have lovingly supported me throughout life.

ACKNOWLEDGEMENTS

First, I would like to give praises and honor to Allah almighty for his infinite mercies and blessings.

I would like to express my gratitude to the management of Saudi Aramco for the scholarship award to pursue my graduate studies.

I would like to thank my academic advisor, Dr. Robert. A. Wattenbarger for his unparalleled academic guidance and support through my years of study.

I would like to thank my graduate advisory committee member, Dr. Bryan Maggard for his advice, ideas and suggestions.

I would like to thank both Dr. William Bryant and Dr. Yuefeng Sun for their support to complete this work.

Special thanks to my colleagues in the research group, for the constructive discussions and their friendship.

TABLE OF CONTENTS

Page

LIST OF TABLES

LIST OF FIGURES

FIGURE Page

FIGURE Page

FIGURE Page

FIGURE Page

CHAPTER I

INTRODUCTION

1.1 Barnett Shale Geology and Production

More wells are being drilled each day in the tight gas, shale gas, heavy oil, and coalbed methane in order to meet the world's increasing demand for hydrocarbon. One of the unconventional sources being developed and produced is the Barnett shale gas formation. It is one of the largest shale Gas plays in the United States and is located in Texas. Its area is estimated to be around 5,000 square miles and cover at least 18 counties[1]. Fig. 1.1. shows the Barnett shale location in Fort Worth Basin North Texas and other shale basins currently being developed.

Unconventional hydrocarbon resources gained a lot of attention with the increasing demand for energy. They differ from conventional reservoirs with respect of production. The unconventional reservoirs cannot be produced at an economic rates or volumes of hydrocarbons without being stimulated or have a special recovery process and technology. [2] Some causes for being unconventional are the low permeabilities and formation properties. These unconventional formations have benefitted from the advances in drilling and completions technology to enhance their production performances.

This thesis follows the style of *Society of Petroleum Engineers Journal*.

One way to overcome the uneconomic production problem is to drill horizontal wells and stimulate the formation by creating number of hydraulic fractures or stimulating the existing natural fractures. This will generate a bigger contact surface area between the formation and the producing well to facilitate production from the unconventional shale gas formation. The first slick water hydraulic fracturing in the Barnett shale started in 1997. It was performed on a vertical well using 28,000 barrels of water.[2]

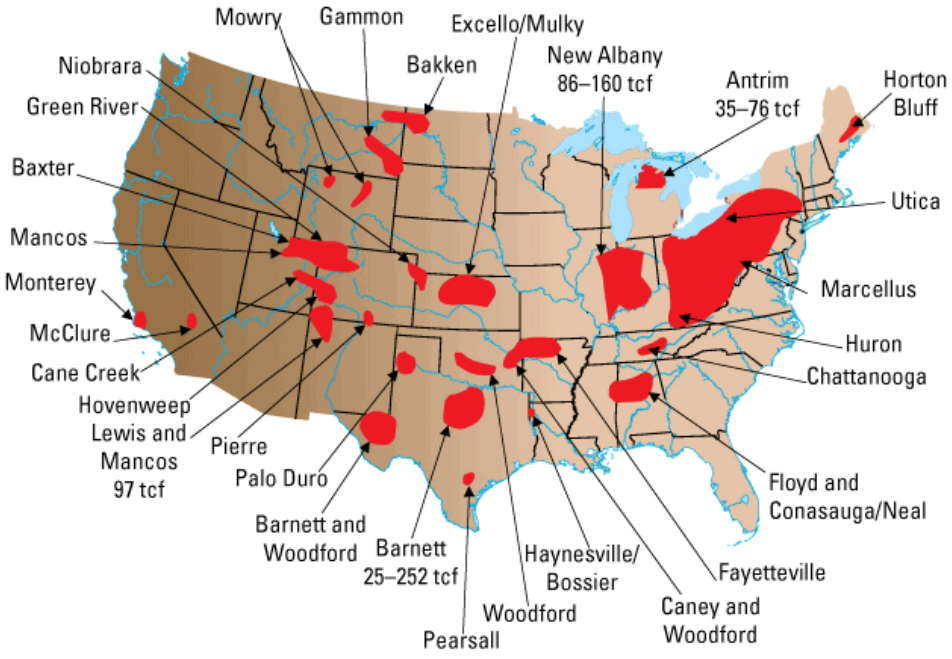

Fig. 1.1 Unconventional gas plays-major U.S. shale gas basins.[3]

The Barnett is naturally fractured with the natural fractures orientation towards the Northwest-Southeast while the induced hydraulic fractures are created perpendicular toward the Northeast-Southwest. This results mainly because of the change of the in-situ

stress direction. This also affected the way wells being drilled and completed in the Barnett shale formation.[2]

The usual practice when drilling a naturally fractured formation is trying to make the well intercept as many natural fractures as possible by drilling perpendicular to the natural fractures. However, this is not the practice in the Barnett shale. Wells usually drilled parallel to the natural fractures towards the Northwest-Southeast and then hydraulically fractured. This will results in the hydraulic fractures or the induced fractures being perpendicular to the natural fractures. [2]

Drilling and completion costs vary depending on the completion type and the area. For example it costs around $1 million to drill and complete a vertical well in the core area, the East and North of the Barnett shale, while it costs around $2 million to drill and complete a horizontal well in the same area. But the same well costs $1.5 million if drilled in Tier 2, which is in the west side of the Barnett.[2-4]

The operations have increased and more attention is given to these unconventional resources. HPDI[5] shows the updated number of wells operating in the Barnett Shale. According to the Rail Road Commission of Texas, there are more than 220 operators in Barnett shale field.[6] The first well drilled in the Barnett shale was in 1981 and by the year 2000, only 726 wells were drilled. This number kept increasing as shown in Fig. 1.2 and in 2005, the total number of wells reached 4,532 wells. The HPDI production data[5] application shows that in May 2010, the total number of wells reached 15,452 and this is an indication of how much attention is the Barnett shale having now.

Fig. 1.2. shows the number of wells being completed in the Barnett shale from 1993 up to 2009. Within the last 10 years, the number of wells increased more than 20 times.

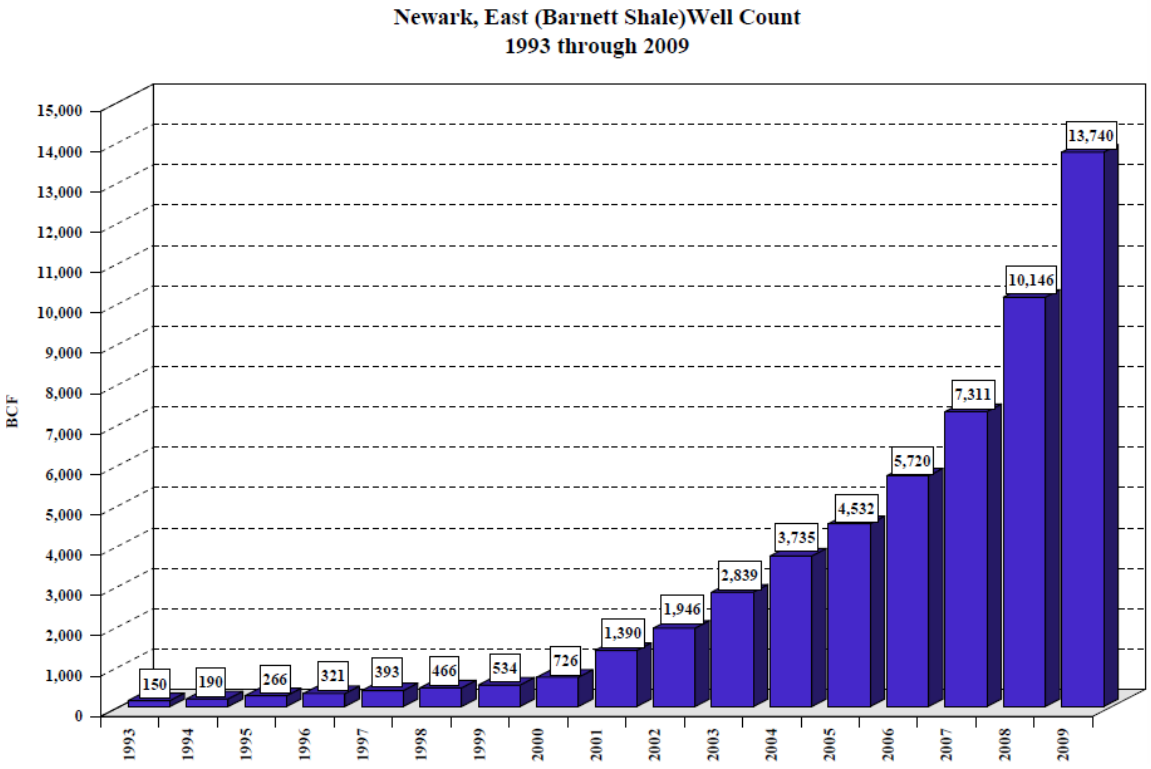

Fig. 1.2 Increase in number of wells being drilled in the Barnett shale.[1]

This increasing number of wells in Barnett shale is followed by an increase in gas production. Fig. 1.3. shows the cumulative gas production in the Barnett shale from 1993 to 2009. The significant increase after 2004 is due to the horizontal drilling becoming the norm when drilling and completing the wells. The Development of the Barnett shale started in 1981 and the main problems facing the producing wells are the Ellenburger water and the closing fractures. [2]

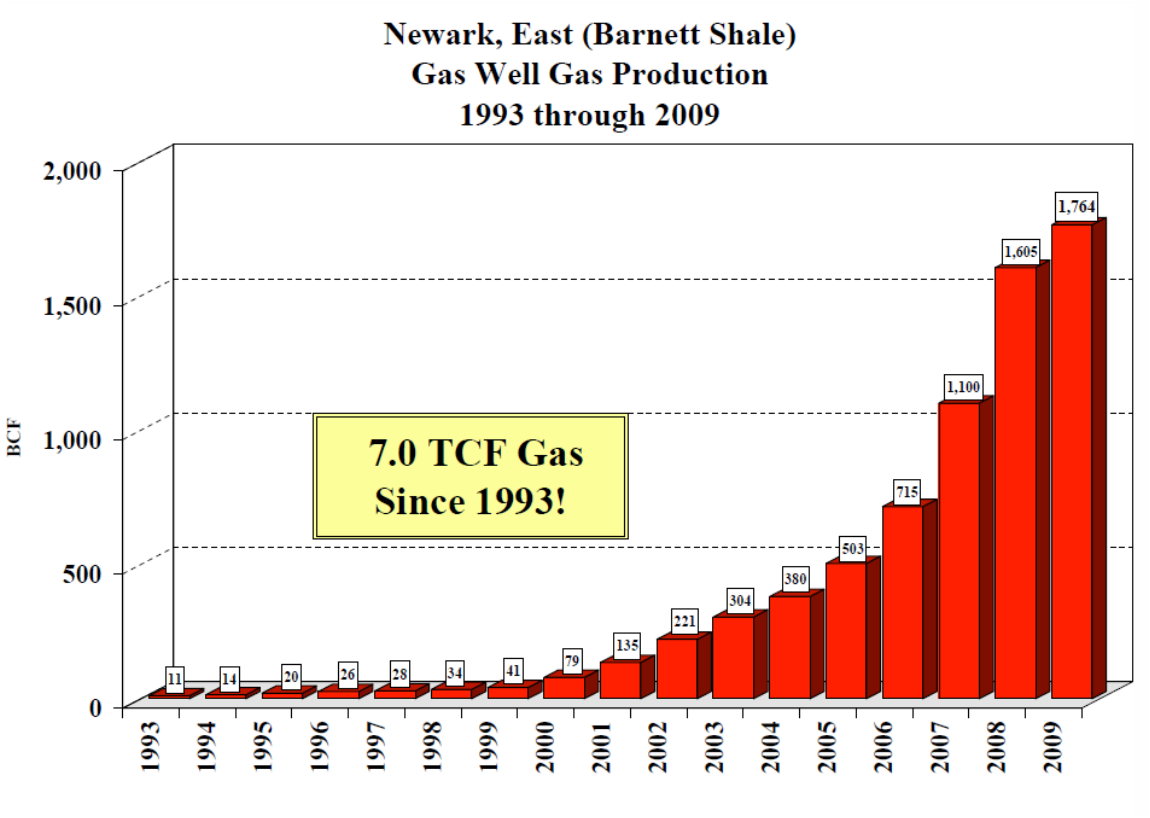

Fig. 1.3 Cumulative production from the Barnett shale in years 1993 to 2009 and the affect of horizontal wells being drilled.[1]

Fig. 1.4 shows the Barnett Shale gas production compared to the most dominant unconventional plays in the United States.

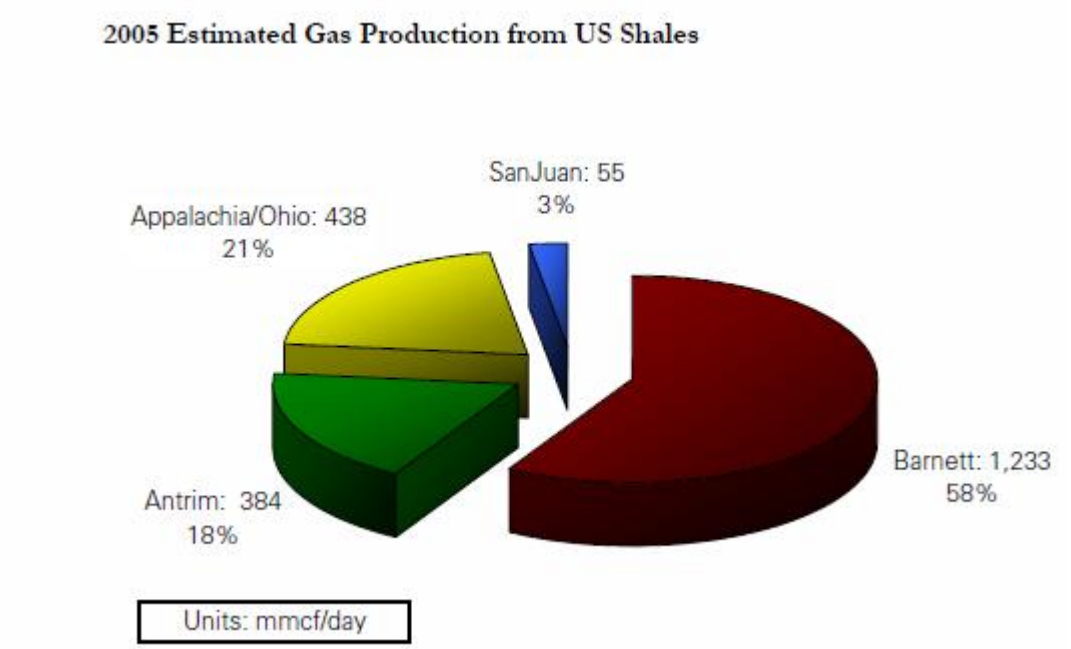

Fig. 1.4 – Comparison of shale gas plays in US showing that Barnett is the most active among them.[4]

The Barnett shale age goes back to the Mississipian and found at depth ranging from 6500 to 8500 feet deep. The net thickness rages from 100 to 600 feet while the average porosity varies from 4 to 5%. The average pressure is between 3,000 to 4,000 psi. The Barnett Shale is bounded in the west by Bend Arch and from the east by Ouachita Thrust-fold belt and the Muenster Arch. Fig 1.5 shows the Barnett shale is divided into lower and upper Barnett as we move toward the northeast. It is separated by the Forestburg limestone formation. Drilling operations usually target the lower Barnett when they are separated.[4]

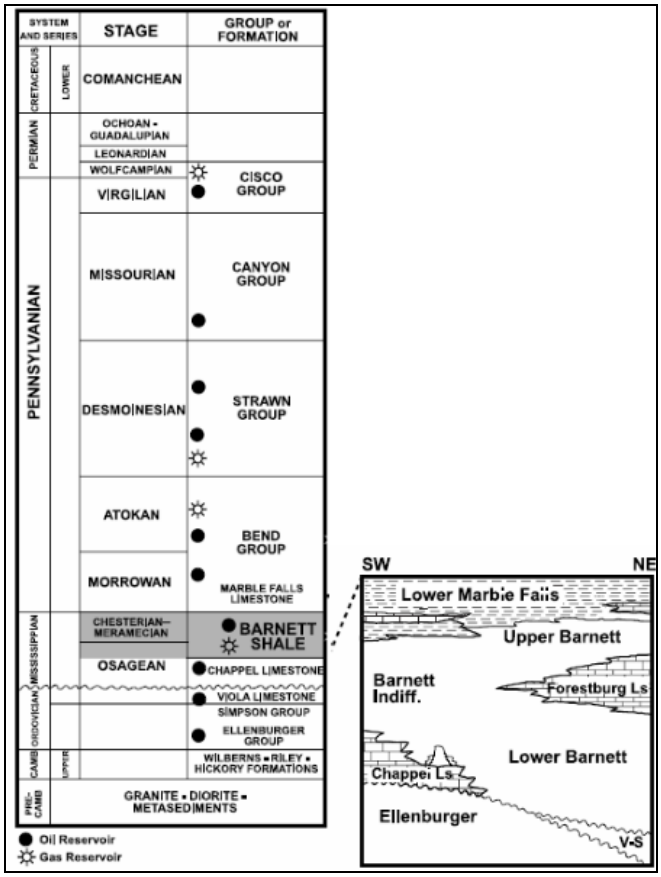

Fig. 1.5 – Stratigraphic column showing the upper and lower Barnett separated by Forestburg limestone underneath is the Viola limestone and the water bearing Ellenburger.[4]

Two cross-sections for the Barnett shale are shown in Fig. 1.6. From the cross-section, it shows the Forestburg Lime formation separating the Barnett into upper and lower layers mainly in the East and North areas. Moreover, the cross section shows the missing Viola Simpson formation in the South and West of the Barnett shale. The Viola Simpson formation is important because it separates the Barnett from the Ellenberger formation water bearing fomation[2].

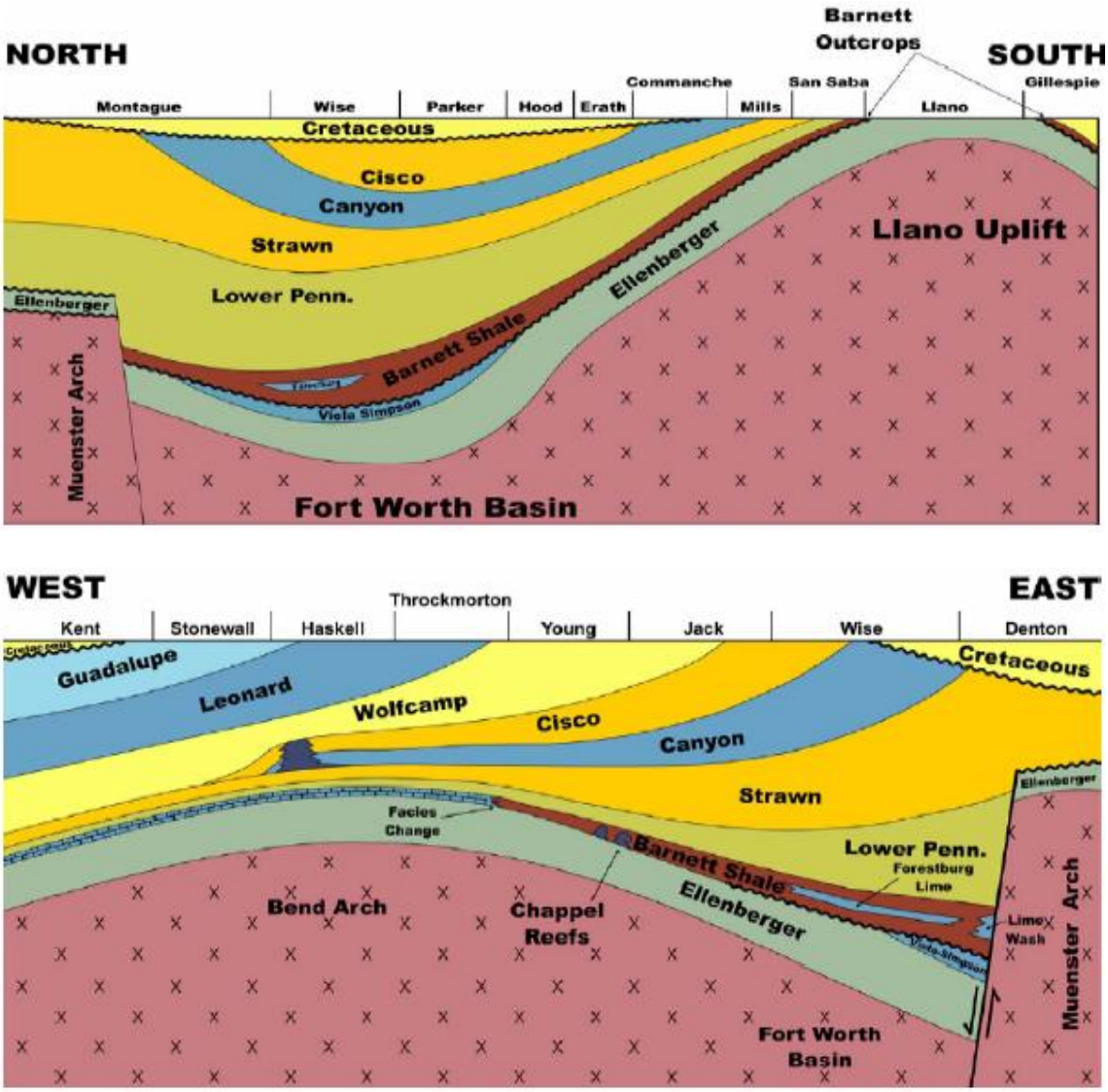

Fig.1.6 – Two cross sections showing the stratigraphic formations of the Barnett shale. The Viola Simpson separating the Ellenberger from the Barnett shale is missing when moving towards the West and South (Humble Geochemical).[4]

1.2 Problem Description

The advantages of the horizontal drilling and hydraulic fracturing have led the operations to increase in the Barnett shale. Back in year 2000, there were only 726 wells[1]

in the Barnett shale and this number has increase to more than 15,452 wells by 2010[5]. The hydraulic fracturing is an essential process help to produce this unconventional shale gas formation at an economic rate. Now that it is almost every horizontal well drilled is being hydraulically fractured, it is important to evaluate the effectiveness these completions and try to improve them. The hydraulic fracturing is a multiple-stages process. Once the well is placed at the target formation, fracture fluid and sand will be utilized to fracture the formation. The wells then flow back to clean the fracture from fluid and create flow paths for gas. Different flow regimes will occur based on the formation, fracture properties and well completion. The dominant flow observed in shale gas formation is the linear flow or the transient drainage from the formation matrix toward the hydraulic fracture. This flow could extend up to years of production and it can be identified by a half slop on the log-log plot of the gas rate against time. It could be utilized to evaluate the reservoir properties, hydraulic fracture surface area and eventually evaluate the effectiveness of the completion job. Fig. 1.7 shows an example of production data on a log-log plot of rate vs. time. There are three flowing periods appearing on this plot. The first interval was identified by Bello[7-8] as an early skin affecting the flow and lasting for less than 10 days. Then an early bilinear flow is identified by a dashed green line having a quarter slope extending up to 40 days and followed by a long linear flow identified by a solid black line with a half slope. The linear flow extends up to 1995 days and this flow can be utilized to evaluate the drainage volume, the interface between hydraulic fracture and matrix, A_{cm} and different reservoir parameters. Production data are provided for 378 wells from the Barnett shale gas

formation. The completion job of these well have been evaluated. In the process of identifying the best production data analysis approach for the Barnet shale, this work will evaluate and prepare the data provided for analysis, show the procedure and apply different purposed models to estimate the original gas in place, OGIP.

The main objective of this work is to apply the production data analysis approaches available in the literature to field data and try to identify the best fit for the Barnett shale gas formation. Identifying the best approach will help in better estimation of reserves and more accurate results to forecast the production. This is an important step that can even lead to better planning a field when trying to determine the best spacing between wells. Different factors affecting the interpretation are shown in this work with examples such as wells having interference, liquid loading, and gas lift installments. Observed production trends are also identified in addition to evaluating the completion job for 378 wells.

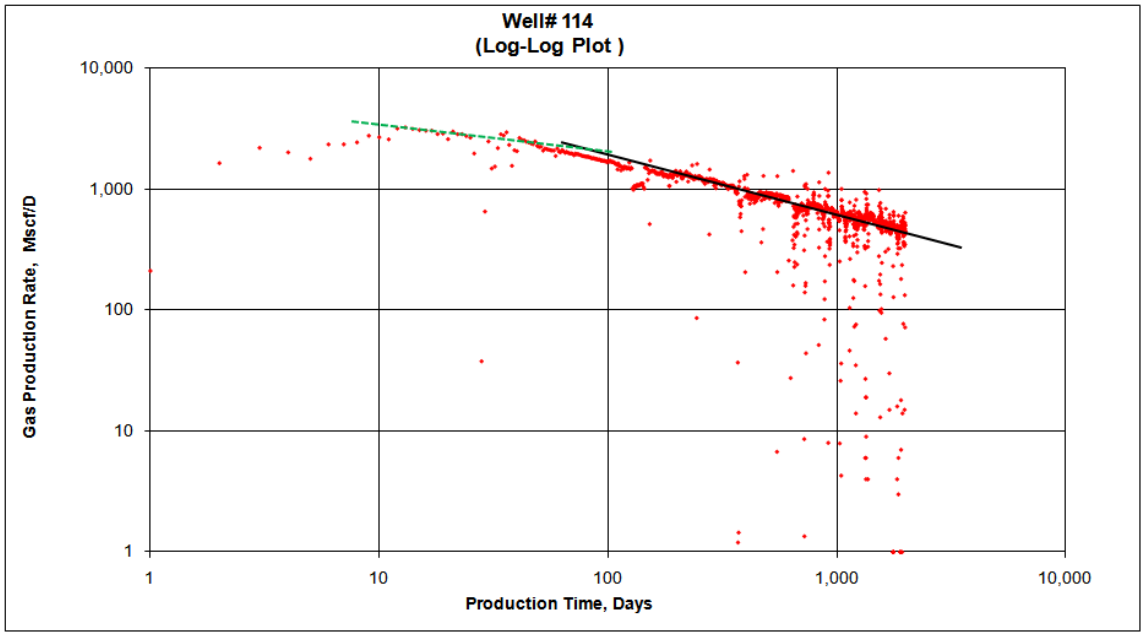

Fig. 1.7 - Example of linear and bilinear flow behavior on log-log plot showing a half (solid black) and quarter (dashed green) slopes.

1.3 Objectives

- Validate the production data then Identify and characterize the flow behaviors of hydraulically fractured wells in shale gas formation.
- Evaluate the completions effectiveness of 378 wells from Barnett shale and showing, recovery of injected water with forecasting production. This part is shown as a supplementary report because of the size of the data.
- Identify different flow behaviors utilizing the production data, completion reports, schematics, formation properties and location of wells. This part will include different plots to identify the flow regimes such as log-log plots, specialized square root and fourth root of time plot, derivative plots with respect to square root and fourth root of time.

- Illustrate different methods available to evaluate the early linear and bilinear flow and apply them to field cases.
- Evaluate different production data analysis methods, from the literature, using field data to show which method will best characterize the Barnett shale production. These methods include; Normalized Pseudotime with Superposition, Material Balance Time, Dynamic Material Balance, Flowing Material Balance, and Model Based Calculations based on the square root of time plot, and Blasingame Type Curve.

1.4 Organization of This Thesis

The study is divided into six chapters. The outline and organization of this thesis are as follows:

Chapter I present an overview of Barnett shale gas production and geology. An overview of the research problem is described and the goals and objectives are presented.

Chapter II presents a literature review. This part will include the dual porosity model and its flow implications, early work done to analyze transient linear and bilinear flow.

Chapter III describes the data preparation showing the field data validation, checking for data correlation and imposing the model for analysis. This part includes the liquid loading effect, gas lift trends and a combination of plots for identifying the different flow regimes.

Chapter IV shows different implications of the linear and bilinear production along with different recommended models for analyzing production data. Field data are used to illustrate the procedures with different samples of calculations to evaluate the formation properties and OGIP.

Chapter IV show the modern advanced production data analysis methods and compare their results in order to identify the best approach that can be applied to analyze Barnett shale production.

Chapter VI presents conclusions and recommendations of this study.

CHAPTER II

LITERATURE REVIEW

2.1 Introduction

In hydraulically fractured shale gas wells, bilinear and linear flow regimes can last for years. Identifying and analyzing these production data can be utilized to evaluate formation properties and completion job effectiveness. This section reviews of technical literature for dual porosity formation and associated flow regimes.

There are different models, semi-analytical, analytical and numerical solutions for liquid and gas developed for different inner and outer boundary conditions. These models are developed for different well and fracture cases. They include vertical wells with hydraulic fractures, vertical wells with horizontal and inclined fractures, and horizontal wells with longitudinal fractures.

2.2 Work Done For Linear Flow

Shale gas formations are known to have low permeability and natural fractures. The formation provides the storage for the fluid while the fractures facilitate the flow.[2] This kind of formation is described as a dual porosity and it can be used in well test analysis following Warren and Root model.[9] The dual porosity formation produced different flow regimes. The linear flow is the dominant flow which can extend up to year of production and in some wells it is the only flow observed. There can be many causes for the linear flow. Recent years have provided more researches to better understand the linear flow.

The first transient dual porosity model for linear reservoir was presented by El-Banbi[10]. He presented new semi-analytical and numerical Laplace solutions for the analysis of production data. He used both old solution to new interpretation models and new solution to solve different cases including the dual porosity models for linear reservoirs with constant pressure and constant rates productions.

Arevalo[11] presented new model for matrix and fracture flow and discusses different physical scenarios that may result in linear flow in tight gas formation. One of these scenarios is the linear flow perpendicular to hydraulic fractures in tight gas formation.

Yilidz and Ozkan [12] investigated the influence of a well orientation on the transient pressure and concluded that in order to have an intermediate time linear flow, the well axis must be normal to the maximum permeability direction.

Arevalo-Vaillagran et al. [13] studied different history cases for long linear flow in tight gas wells and suggested that different geometrical effects result in linear flow behavior such as the existence of parallel natural fractures and vertical flow in steaks of high permeability. The authors also presented a procedure to analyze the linear flow observed in tight gas wells. Furthermore, they concluded that the original gas in place can be evaluated once the outer boundary effect has been reached. Table 2.1 shows linear flow interpretation formulas for constant rate and constant p_{wf}. Fig. 2.1 shows an example of specialized square root of time plot for constant p_{wf} production of a tight gas well. This specialized plot is $\Delta m(p)/q \; vs. \; t^{0.5}$ on Cartesian axis shows a straight

line with a slope $\tilde{m}_{CPL}$ = 25,000 (psia2-D1/2)/(Mscf-cp). The end of the straight line or linear flow is around 18.2 years. This plot can be utilized to evaluate different reservoir parameters and OGIP.

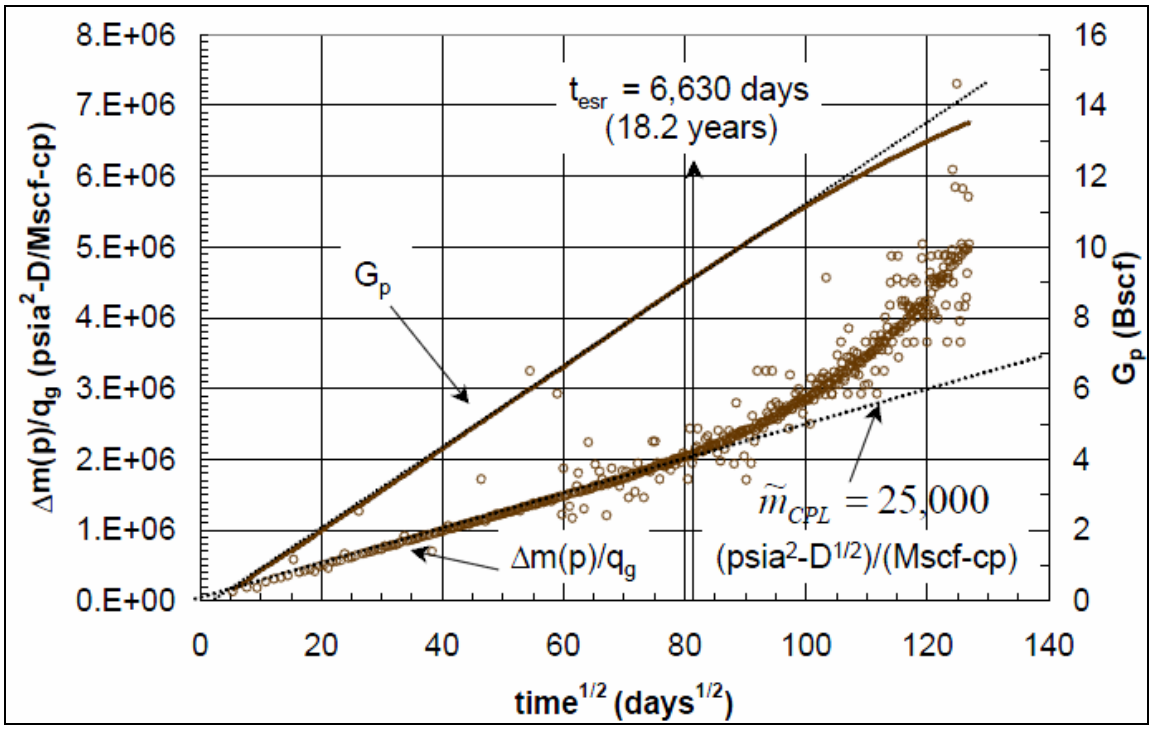

Fig. 2.1 –Specialized square root of time plot for constant p_{wf} production tight gas well with a clear slope that can be used to evaluate different reservoir parameters and OGIP. [13]

Table 2.1 - Constant rate production and constant p_{wf} production formulas for linear flow.[13]

Constant q_g production	Constant p_{wf} production
$\sqrt{k}A_c = \frac{803.24T}{\sqrt{(\phi\mu_g c_t)_i}}\left(\frac{1}{\tilde{m}_{CRL}}\right)$	$\sqrt{k}A_c = \frac{1261.73T}{\sqrt{(\phi\mu_g c_t)_i}}\left(\frac{1}{\tilde{m}_{CPL}}\right)$
$A = \frac{127.80T}{(\phi\mu_g c_t)_i}\left(\frac{\sqrt{t_{esr}}}{\tilde{m}_{CRL}\, h}\right)$	$A = \frac{224.46T}{(\phi\mu_g c_t)_i}\left(\frac{\sqrt{t_{esr}}}{\tilde{m}_{CPL}\, h}\right)$
$V_P = \frac{127.80T}{(\mu_g c_t)_i}\left(\frac{\sqrt{t_{esr}}}{\tilde{m}_{CRL}}\right)$	$V_P = \frac{224.46T}{(\mu_g c_t)_i}\left(\frac{\sqrt{t_{esr}}}{\tilde{m}_{CPL}}\right)$
$OGIP = \frac{127.80T\, S_{gi}}{(\mu_g c_t B_g)_i}\left(\frac{\sqrt{t_{esr}}}{\tilde{m}_{CRL}}\right)$	$OGIP = \frac{224.46T\, S_{gi}}{(\mu_g c_t B_g)_i}\left(\frac{\sqrt{t_{esr}}}{\tilde{m}_{CPL}}\right)$
$y_e = 0.1591\sqrt{\frac{k\, t_{esr}}{(\phi\mu_g c_t)_i}}$	$y_e = 0.1779\sqrt{\frac{k\, t_{esr}}{(\phi\mu_g c_t)_i}}$

Fraim and Wattenbarger[14] developed a normalized time for gas reservoirs producing at a constant wellbore pressure at boundary dominated flow. Their method matches the exponential decline to type-curve to evaluate different reservoir parameters. The normalized time does not have a significant effect on the transient flow and can be used for any reservoir shape.

Palacio and Blasingame[15] presented new modified time function and algorithm that can lead to harmonic declines and used to analyze gas production data of either gas

or oil using type curves analysis. These type curves can by utilized to evaluate gas in place from variable rate or variable pressure production data.

Agarwal et al. [16] presented new production decline curves published specifically for hydraulically fracture wells of infinite and finite conductivity to analyze oil and gas production data from radial and vertically fractured wells. These type curves can be utilized to evaluation gas in place and different formation and completion properties. He combined the type curve and decline curve analysis concepts to present new declines curves that can be used for gas production to estimate the OGIP in addition to formation properties. Their set of type curves include rate time, rate-cumulative and cumulative-time production. The two models for which the type curves can be used are radial model and well with vertically fractures.

Spivey and Semmelbeck[17] presented a procedure to forecast fractured coal and shale gas reservoirs with adsorption using slab geometry, dual porosity, and constant pressure production model.

Ibrahim et al.[18] introduced a new normalized pseudo time plotting function that can be used in the superposition method to provide more accurate estimation of the OGIP. The method has an advantage of the ability to analyze the fluctuating field data of being variable-pressure and variable rate. The presented method is more accurate specially in highly depleted reservoirs.

Gringarten et al. [19] investigated the affect of the shape of fractures in with both vertical and horizontal fractures affecting the wells behavior on log-log type-curve. They tried to illustrate whether from this behavior, the orientation can be fracture determined.

They concluded that the presented type curve solutions are applicable and represent many field data.

Aguilera[20] presented equations for linear flow evaluation in dual porosity natural fractured reservoirs. He illustrated his method using a log-log plot of $\Delta p \, vs. time$ indicating two parallel lines with a half slope in which the duration depends on the interporosity flow and the matrix block shape. Another plot of $\Delta p \, vs. time$ gave two lines with different slopes. The ration of the slopes is equal to the storativity ratio. His analysis methods allow evaluating the fractures transmissibility time the square of the hydraulic fracture length.

Wattenbarger et al.[21] presented new analysis methods for tight gas wells showing linear flow with a boundary effect but no pseudo-radial flow. The OGIP can be calculated once the outer boundary is reached and a drainage area with the value of $\sqrt{k}\, x_f$ can be calculated. The authors developed equations for transient linear flow. These calculations can be done without the need to know porosity, thickness or formation's permeability. The paper also showed the equation provided for linear flow with constant p_{wf} are different from constant rate analysis.

Helmy and Wattenbarger.[22] presented different was to analyze production data subjected to shut-in intervals of gas wells producing linear flow at constant p_{wf}. First they showed the application of the superposition principle which enables calculating the reservoir parameters and OGIP. Then the authors presented new analytical solutions for

production data subjected to periodic shut-ins. This solution filters the data and generates a trend with no interruptions.

Bello and Wattenbarger[23] studied the gas transient rate and identified five flow regions for multi-stage hydraulically fractured wells in shale gas formation. They presented equation for each of these regions and described an early skin effect for the linear flow region. A suggested procedure to analyze field data is also presented.

2.3 Work Done for Bilinear Flow

For the hydraulically fractured horizontal wells, the bilinear flow occurred as a result of simultaneous drainage form the matrix and hydraulic fracture.

Cinco-Ley and Samaniego[24] were the first who introduced the idea of bilinear flow or the transient linear flow in both formation and fracture. They demonstrated it in vertically fracture well with a plot of p_{wf} vs $t^{1/4}$ that produces a straight line with a slope inversely relative to $h_f (k_f b_f)^{1/2}$. A new interpretation technique was presented to analyze production data in the bilinear flow period and presented new type curve analysis.

Du Kuifu and Stewart [25] described many cases in which bilinear flow regime can occur in various geological situations that include horizontal wells in dual porosity reservoirs, vertical well in leaky channels or wells near high conductive fault.

Wong et al.[26] presented techniques with type curves to analyze wells with finite conductivity fractures which uses pressure and derivative for the bilinear flow period. The authors suggest the use of pressure derivative to curve improves the flow regime detection.

Cinco-Ley et al.[27] explained the case for wells having long fracture with low permeability and relatively high formation permeability. They illustrated that this type of system shows mainly two flow periods which are the bilinear and pseudo-radial flow with a transition region between them.

England et al.[28] showed results of an ongoing study of production data of a hydraulically fractured wells. It compares the performance of two different completion approaches which are the conventional hydraulic fracturing and the "waterfrac" with low proppant concentration. The authors illustrate different analysis techniques for the production from fractured wells to estimate formation and fracture properties utilizing bilinear, linear and pseudo-radial flow regimes. From these analyses, the fracture half-length, fracture conductivity, effective permeability of formation can be determined.

Branajaya et al.[29] explains how the transient bilinear flow occurs in tight naturally fractured formation. Some of the conditions in which bilinear flow occur: vertical well with finite fracture conductivity, horizontal well with transient dual porosity behavior during intermediate linear flow and transient dual porosity behavior in linear reservoir. The authors simulated different cases for wells producing at constant rate and constant pressure. The papers verify Cinco-Ley and Samaniego for constant rate production solutions and Guppy et al[30] for constant pressure solutions.

Arevalo-Villagran et al.[31] studied different cases of tight gas wells production data showing linear and bilinear flow behaviors and described systematic method to analyze the production data and estimate reservoir properties and OGIP for linear, bilinear and boundary dominated flow.

CHAPTER III

DATA PREPARATION AND DIAGNOSIS

3.1 Introduction

Production data for 378 shale gas wells from the Barnett shale were provided and used for analysis in this thesis. An additional 18 wells were used to compare the results from Fayetteville shale formation which differs significantly in its low reservoir pressure compared the Barnett shale. A supplementary report showing the analysis result is published. The data include the production rates for gas, oil and water in addition to surface tubing and casing pressures. Completion reports were also provided, which include fracture water volumes. The completion reports are available for 209 wells and well's diagram available for 173 wells. The production data of the 378 wells were distributed among 10 counties. This chapter will show how the data being prepared for analysis. A systematic data evaluation can be done using Andersons et al.[32] suggested procedure to perform the following tasks:

1. Evaluate the Production Data Viability.
2. Check for Production Data Correlations.
3. Perform a Preliminary Diagnosis.
4. Apply the Model-Based Analysis.

3.2 Evaluating the Data Viability

The first task before using the field data is to evaluate and determine if we can use the data provided for analysis or not. In this process the data are checked for being complete and realistic. Three things need to be checked are:

- The daily or monthly production data
- Formation and fluid properties.
- Completion report and stimulation history.

3.2.1 Checking the Historical Production Availability

The first step to be checked is the availability of complete historical production data. The main are the production rates and pressure. Out of the 378 wells provided, there were 150 wells having only the gas production data available. The flow behavior still can be analyzed for these wells, yet a better understanding would have been possible with complete data. Fig. 3.1 shows example of well #107 having 205 days of gas production data available. No water production, casting / tubing pressures or the completion history were available. This well shows low rates of scattering or fluctuating production data with long shut-in intervals. This well shows an example of a bad candidate that should not be analyzed yet more data is required to have a complete understanding of the causes of such behavior.

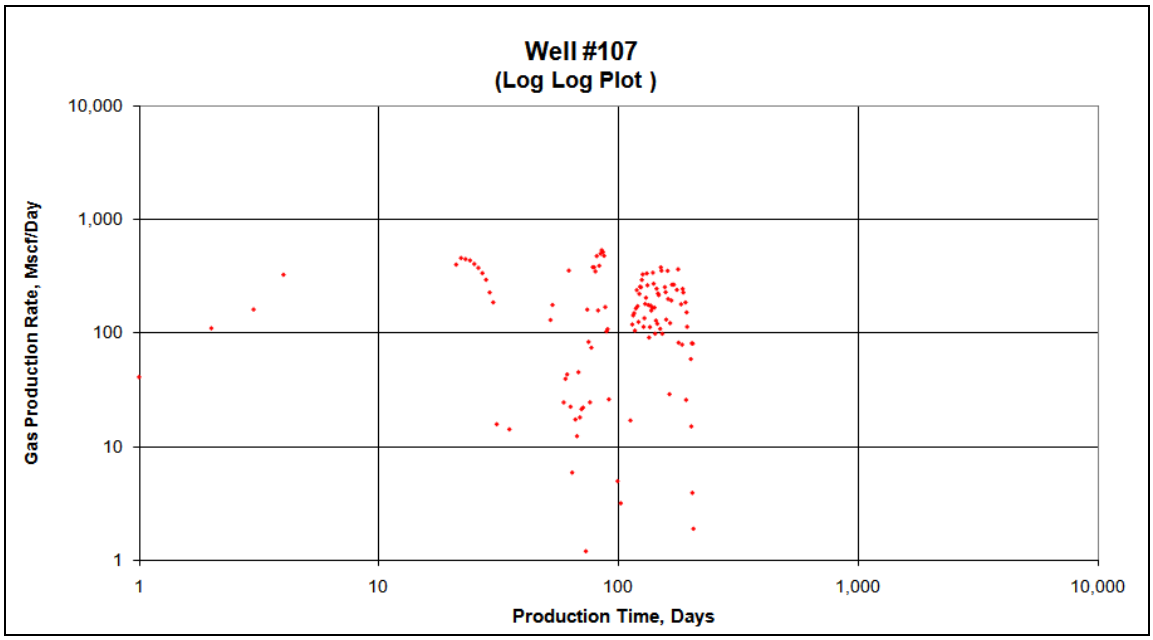

Fig. 3.1 – Well having short and fluctuating data with no complete production data or completion history available.

Unlike the previous case, well #302 shows a complete historical gas, water, casing/tubing pressure and completion data available. This makes it good candidate to be added to the production analysis list. Fig. 3.2 shows well #302 with 1062 days of complete production data available that will help to explain any abnormal behavior that might occur as will be shown later.

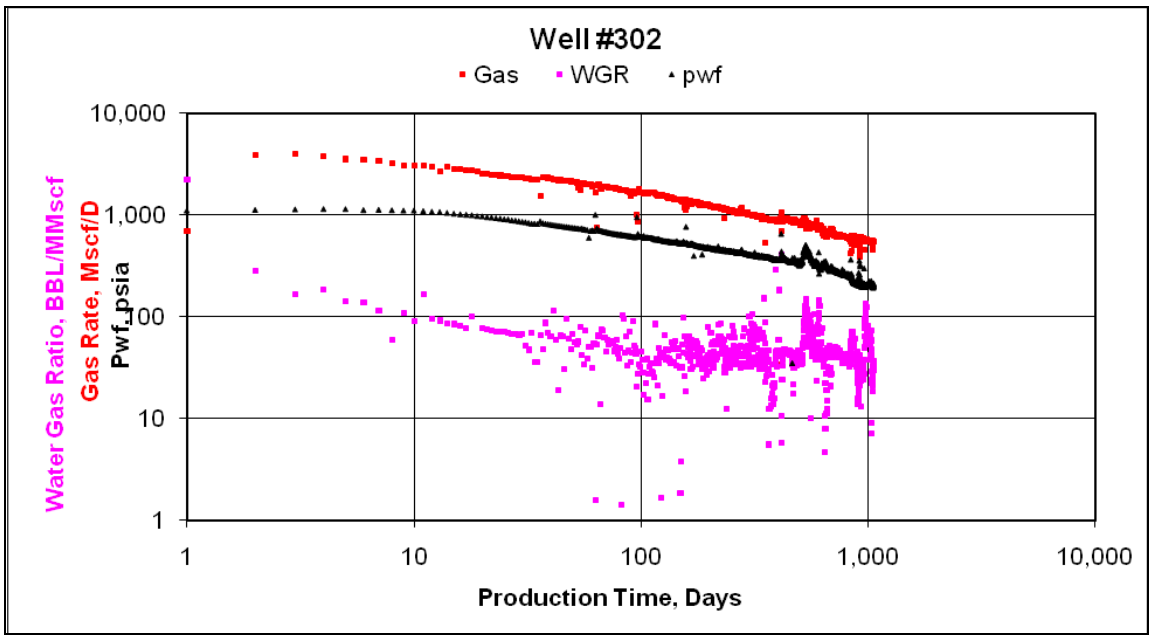

Fig. 3.2 – Well having complete and correlated production history that can be used to perform production analysis.

3.2.2 Gathering Fluid and Formation Properties

Both fluid and formation properties are important when using the data for analysis. These data will be used in the model-based analysis and when preparing the data for analysis. For example the pressure data were available for surface casing and tubing. These pressure need to be calculated for bottom hole pressure. This can be done using Cullender and Smith method based on mechanical energy balance for calculating the subsurface pressures for static and flowing gas production wells. It calculates the pressure drop along tubing for the gas phase. The method assumes single phase in the tubing and ignore the liquid oil and water, yet the effect is minimal because of the square pressure effect between the average formation pressure and the bottom hole flowing pressure which minimized the difference. In the data provided, the wells produced

though the tubing, however, the surface casing pressure was used and converted to bottom hole flowing pressure because no packers installed.

Some of the fluid and formation properties that were not available have been assumed. Tables 3.1 shows an example of some the assumed values that are used when imposing the model or in other calculations.

Table 3.1 – Example of the assumed formation and fluid properties for the Barnett shale.	
T	610 °R
h	200 ft
ϕ	0.6
k_m	1.5 x 10^{-4} md
p_i	2950 psi
μ	0.02009 cp
c_t	2.2x10^{-4} psi^{-1}

3.2.3 Well Completion and Stimulation History

The well's completion and stimulation history information will be used in the model such as the cluster spacing of the hydraulic fracture, well's horizontal length and water volumes. Some of this information is important especially when using the model to calculate the original gas in place, *OGIP*. Other data such as water volumes and cluster spacing might also be used to correlate the results and eventually improve the job. This could be done by determining the best cluster spacing or the optimum water volumes to be used based on previous completion results. Moreover, the completion information regarding the well's total vertical depths along with the formation tops can be used to

explain some of the production behavior and formation water production depending on the proximity to the under-laying water bearing formation as shown in Fig. 1.6.

3.3 Check for Production Data Correlations

After the three steps for evaluating the data, a quick check for the production data correlation is performed on the data. Different plots are created to make sure that the abnormal behavior correspond to the events occur on different plots at the same time for the same well. For example, a quick check between the production rate and pressure along with completion events could explain any abnormal behavior. An example is shown for well # 73 on Fig. 3.3. The well was producing normally but after 550 days of production, sudden increase in water rate and gas production rates were observed along with an increase in the pressure. Since both rates and pressure correspond to the same event at the same time, this indicates the data with good correlation. Moreover, the completion reports show that a gas lift system was installed at that time which led to an increase in gas and water production after a period of shut-in. The well history report has any recompletion data or change in the production conditions to explain any abnormal behavior during the production.

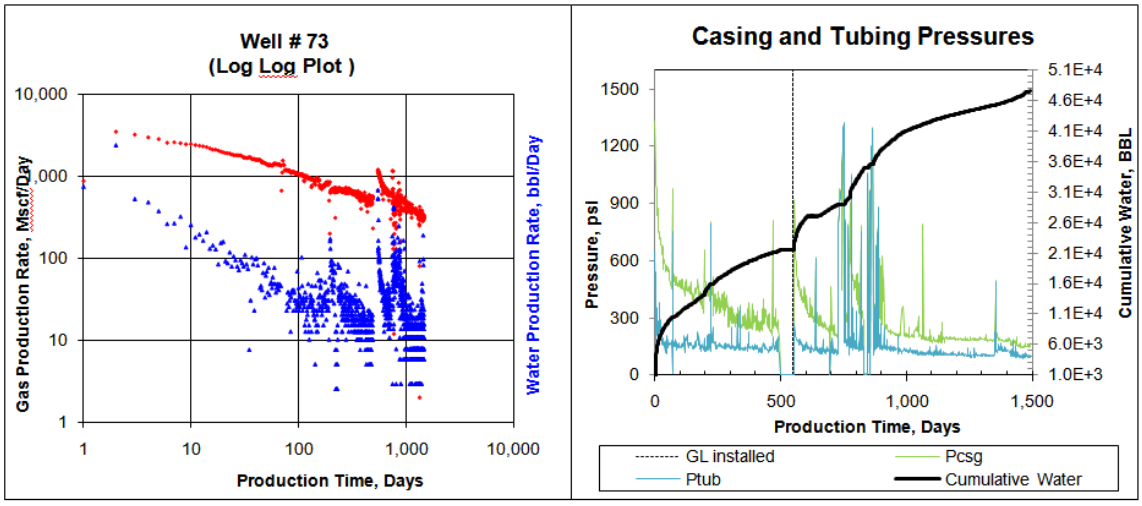

Fig. 3.3 –Checking basic correlations between rates, pressures and well history indicating gas lift installment which explains the sudden increase in rates and pressures at 550 days.

3.4 Preliminary Production Data Diagnosis

A quick data analysis is performed before imposing the model. This part will help in better understanding the data and determine which calculations can be done for each flowing interval. The preliminary production data diagnosis includes:

- Quick interpretation.
- Identifying different flow regimes.
- Filtering and eliminating unclear data.
    - Identifying interference between wells.
    - Identifying the liquid loading affect.
    - Identifying gas lift installment.

3.4.1 Quick-look Interpretation

This part performs a quick-look on the data to evaluate and classify different intervals of the production data. Fig. 3.4 shows example of a Blasingame type curve generated using Fekete RTA software [33]. The type curve can give an idea about pressure loss or pressure support from the production data behavior. From this plot, quick interpretations can be performed such as:

- Damage or stimulated well: The appearance and the y-intercept of the data on type curve plot can give an idea about the well whither it is damaged or stimulated from the transient part:
    - Steady/flat appearance with low= Skin effect.
    - Steep decline with high intercept = Stimulation.
- Indication if the production in transient or boundary dominated: This is clear in the plot because the all the BDF should follow the harmonic decline.
- Boundary dominated behaviors:
    - Above the harmonic unit slope = pressure support (gas lift, communicating layers "when upper and lower Barnett are separated").
    - Bellow the harmonic unit slope = pressure loss (liquid loading, interference).

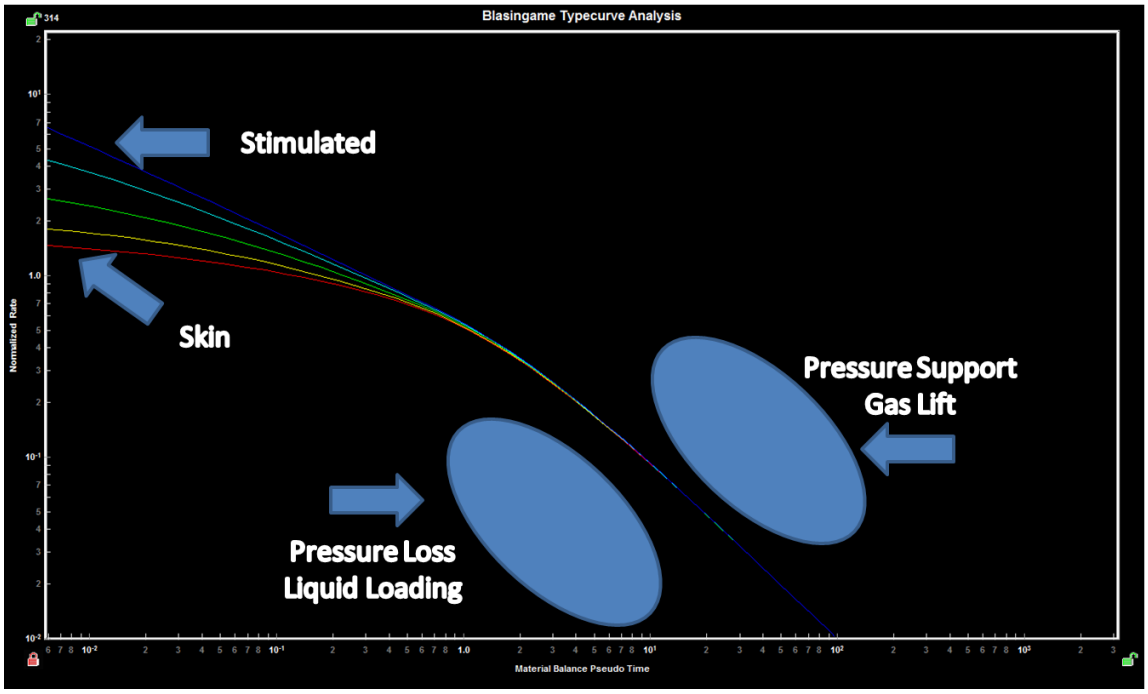

Fig. 3.4 –Quick check when applying decline curve analysis gives indication about the production behavior as shown in different areas of this Blasingame Type Curves generated using Fekete RTA software.

3.4.2 Identifying Flow Regimes with Derivatives and Normalized Pseudo- time with Superposition Plots

Identifying the flow regimes will enable us to decide what calculations can be applied on each well and the model that can be imposed to analyze this flowing period. The low permeability in shale gas formation causes the flow regimes to occur in a longer duration. Bello and Wattenbarger[8] identified five different flowing regions for fractured horizontal wells. These regions are shown in Fig. 3.5.

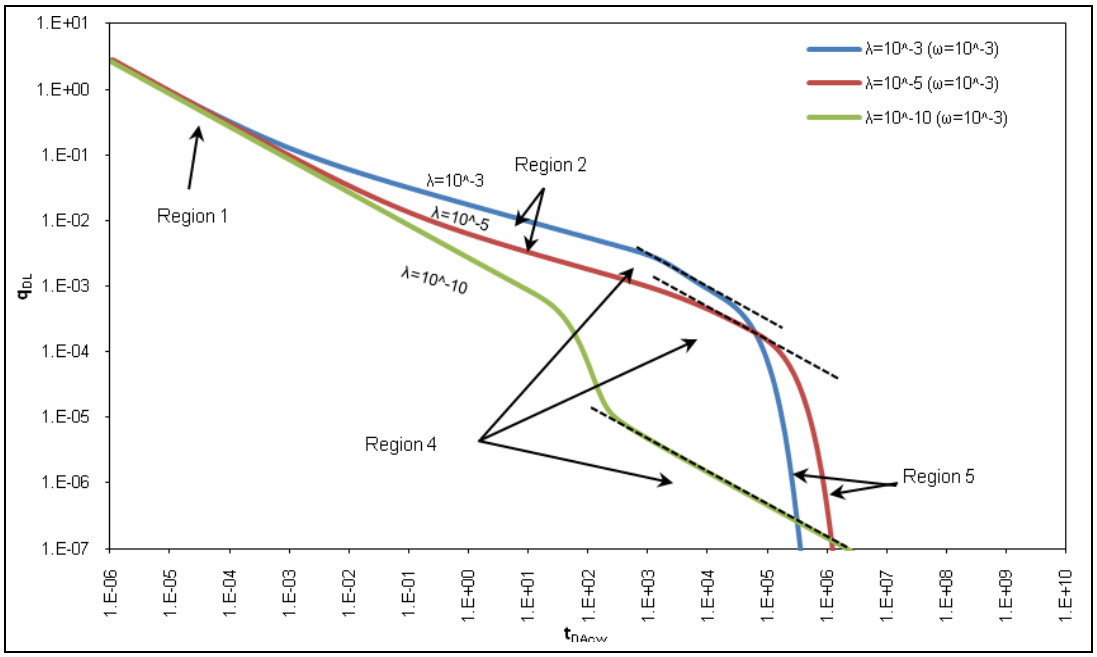

Fig. 3.5 – Five flow regions are shown for different values of dimensionless interporosity parameter, λ_{Acw} and dimensionless storativity ratio, ω. [34]

Different flowing regions are observed in shale gas production data of well being hydraulically fractured. The first flowing region is the bilinear flow, which occurs as a result of simultaneous drainage form the matrix and hydraulic fracture. This region is identified by a quarter slope in the log-log plot of production rate vs. time or by a slope of zero when plotting the derivative on log-log plot of $\frac{\Delta m(p)/q}{d\sqrt[4]{t}} vs. \sqrt[4]{time}$. Fig. 3.6 shows an example of Well #225 having a long bilinear flow for more than 426 days. The green line on the log-log plot, indicates a quarter slope.

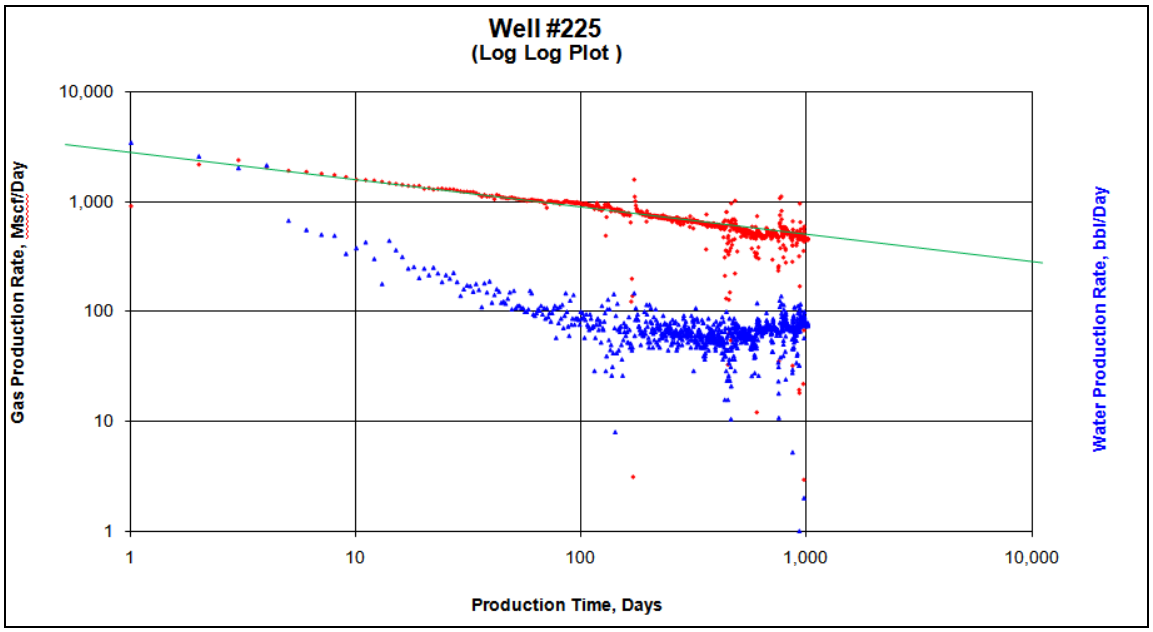

Fig. 3.6 – Long bilinear flow up to 426 days in shale gas well might indicate a poor completion job.

The second flowing regime and the dominant flow is the linear flow or the transient drainage from the formation matrix toward the hydraulic fracture. This flow could extend up to years of production. It can be identified by half slop on the log-log plot of the gas rate against time or by using the derivative plot of $\frac{\Delta m(p)/q}{d\sqrt{t}} vs. \sqrt{time}$ with a zero slope indicating a linear flow. Fig. 3.7 shows an example of well #171 having long linear flow indicated by the black line.

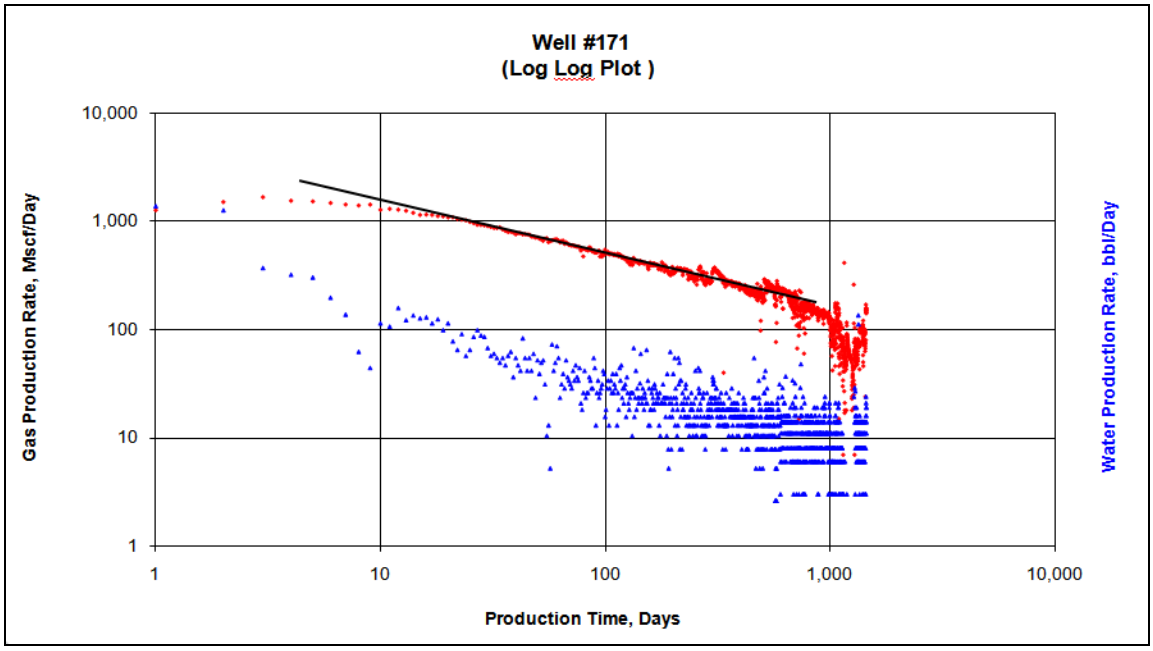

Fig. 3.7 –Linear flow indicated by a half slop black line on log-log plot.

The third flowing period is the boundary dominant. It occurs when the pressure drop reaches a no-flow boundary located between the hydraulic fractures. This region is identified by an exponential decline on the log-log plot of rate vs. time or zero slope of the derivative log-log plot of $\frac{\Delta m(p)/q}{dt}_{vs.time}$ Fig. 3.8 shows an example of well that is suspected to have reached the boundary dominant flow. More production data might be required to confirm this flow regime.

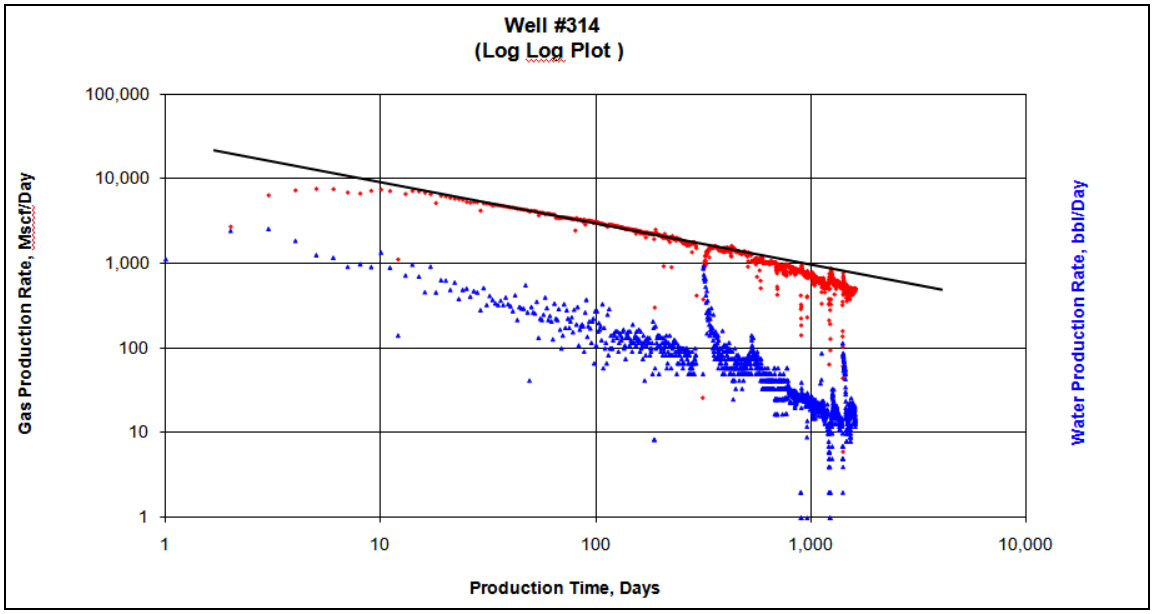

Fig. 3.8 –Boundary dominated flow was reached as the data depart from the half slope line following an exponential decline.

In addition to the linear, bilinear and boundary flow, there is an early flow period observed which last less than 30 day. This flow period was described by Bello[7-8] as a convergence skin effect period that is observed in shale gas wells as a result of linear flow distortion around the wellbore. Also, it might be resulted from well cleanup when gas creates flow paths inside the hydraulic fractures that are filled with water.[34] This flowing period can be observed in Fig. 3.7 where it extends up to 20 days of production. Table 3.2 shows a summary of the different plots that can be used to identify the flow regimes of gas production data.

Table 3.2 - Quick ways to identify different flow regimes.		
Flow Regime	Log-Log	Derivative (Cartesian)
Bilinear	*Quarter slope line*	Derivative is constant $\frac{\Delta m(p)/q}{d\sqrt[4]{t}} vs. \sqrt[4]{time}$
Linear	*A half slope line*	Derivative is constant $\frac{\Delta m(p)/q}{d\sqrt{t}} vs. \sqrt{time}$
Boundary Dominant flow	*Exponential decline*	Derivative is constant $\frac{\Delta m(p)/q}{dt} vs. time$
Transient or Boundary Dominated Flow	Using type curves	

3.4.3 Filtering and Eliminating Unclear Data

Events that occur during the production and disturb the flow behavior are identified in this section. Some of these events are liquid loading, gas lift installations, well completion changes and interference.

3.4.3.1 Identifying Liquid Loading Effect

Liquid loading is common problem in shale gas wells. It occurs whenever the producing well's rate drop to a level that it would not have a sufficient energy to carry the water droplets to the surface. This could be due to dropping reservoir pressure, oversized

production tubing or an increase in the well's surface pressure. As a result, liquid water or gas condensate will start to accumulate in the wellbore. The accumulated liquid will increase the back pressure on the formation which will further drop the gas flow rate.[35]

The presence of liquid in gas wells results in different flowing regime. The flow regime of high rate wells will be mist flow, in which the wells produces at rate above the critical rate and liquid droplets will be carried to the surface. With time, the gas production rate will drop and this will result in changing the flow regime from mist to slug and finally bubble flow. During this process, liquid is accumulating in the tubing causing an increase in the back pressure on the formation and additional reduction in the gas rate will occur. If no action is taken to remove the liquid loading, this will results in dead well. [36]

Different methods[36] are applied to identify the effect of liquid loading in gas wells. Some of these methods are:

1. Observing the pressure difference between the casing and tubing. The greater the pressure difference means additional hydrostatic pressure is accumulating in the tubing and resulting in lower tubing pressure.
2. The production rate will start to fluctuate and drop as the flow behavior changes from mist flow to slugging. This approach is not applicable for the Barnett shale data because of the average daily production data are provided which does not show the fluctuation in rate.
3. Comparison of the production rate to the critical rate is very useful approach.

The liquid loading can be identified by comparing the production rate to the critical rate or minimum rate required to remove the liquid droplets from the wellbore to the surface Turner Method.[35] In some cases, rates having liquid loading tend to show production behavior similar to reaching the boundary dominant flow. Therefore, it is important to identify the liquid loading to avoid mistakes in calculations. Fig. 3.9 shows a well having liquid loading which causes difficulties when trying to identify the boundary dominant flow. The liquid loading will also cause error when trying to calculate OGIP or try to forecast a production lift of the well.

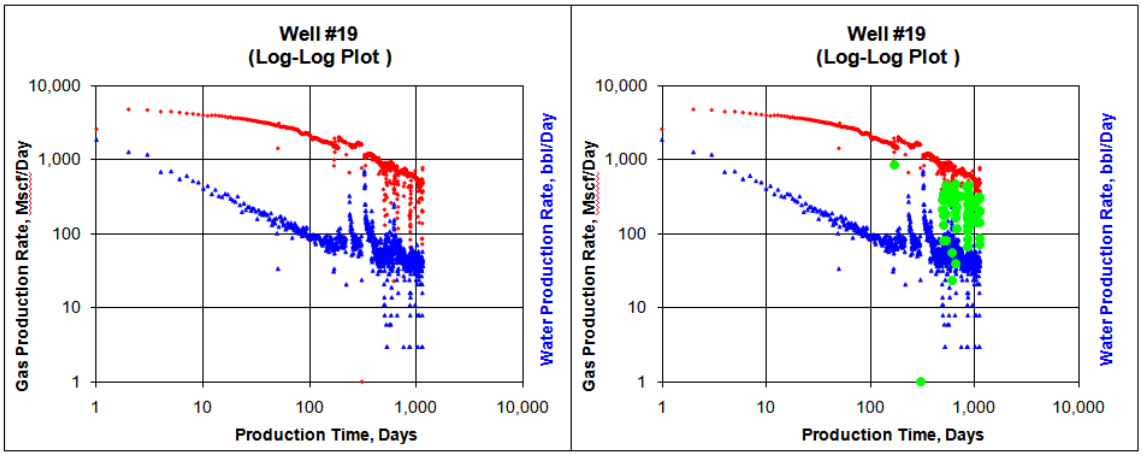

Fig. 3.9 –Liquid loading intervals are ignored when analysis is performed. Rates bellow critical highlighted in green on right disturb the flow behavior.[14]

The production data having liquid loading will need to be ignored when analyzing or imposing the models. Removing the water from the bottom of the tubing can be done using different methods. One way to remove the water is by reducing the production tubing size. This is common and cheap action that will result in higher gas

velocity as a result of reducing the flow cross sectional area and a higher frictional flow inside the tubing. However, this method might not be effective at later production as the gas production rates start to drop again bellow the critical rate. Another ways to remove water is by installing socker rod pumps, plunger lift, electrical submersible pumps or installing gas lift.[36]

3.4.3.2 Filtering and Identifying Gas Lift Effect

Gas lift installment is used in the Barnett shale to remove the water from loading wells. The net gas rates were provided, which subtracts the injected gas and gives the formation's gas production rate. The gas lift and the former liquid loading affect the flow behavior and result in different flow trends. Fig. 3.10 shows well #113 with gas lift effect of on the well production behavior.

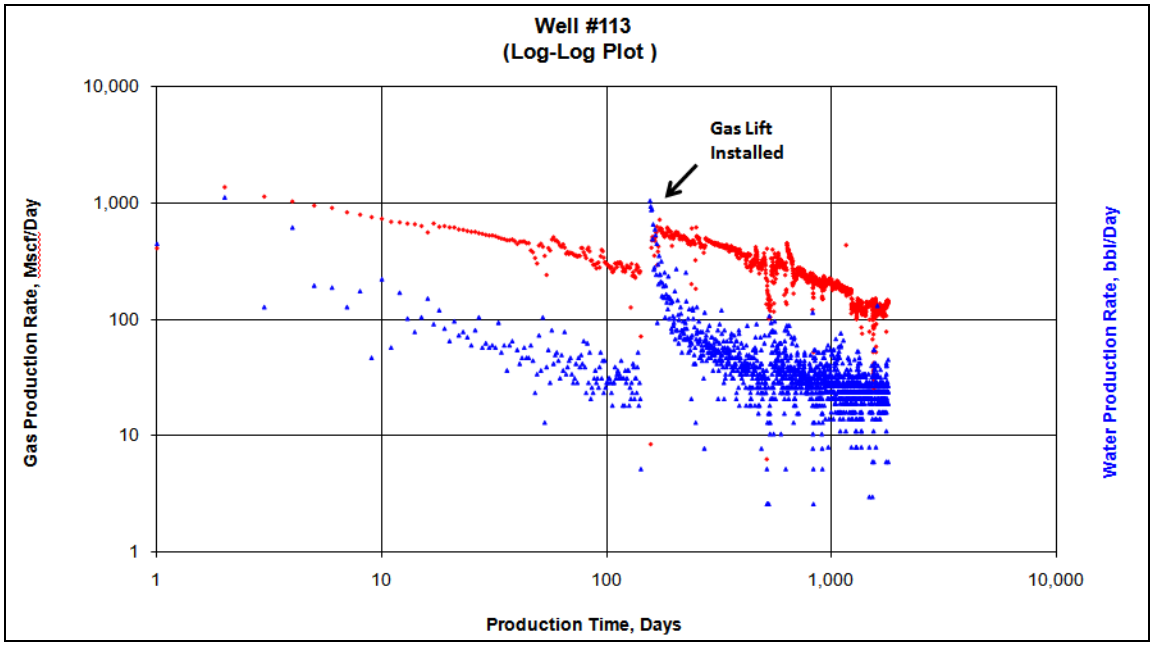

Fig. 3.10 –Gas lift was installed after 155 days affected the production behavior by increasing the gas and water production rates and disturbing the flow regime.

Four production trends were observed as a result of installing gas lift and performing different operational conditions. These trends were observed on the square root of time plot when trying to evaluate the linear flow behavior. Fig. 3.11 through Fig. 3.14 show these trends with an example of field case illustrating.

The first trend is shown on Fig. 3.11, which is expected to result from intermittent gas lift injection. After injecting gas to remove the water, the production data goes back to continue the earlier linear trend and whenever the injection stops, liquid will start to load causing a drop in the rate. The behavior will occur as a bouncing production rate where the liquid loading will shift the production data upward while the gas lift will return the trend back to the original linear flow behavior.

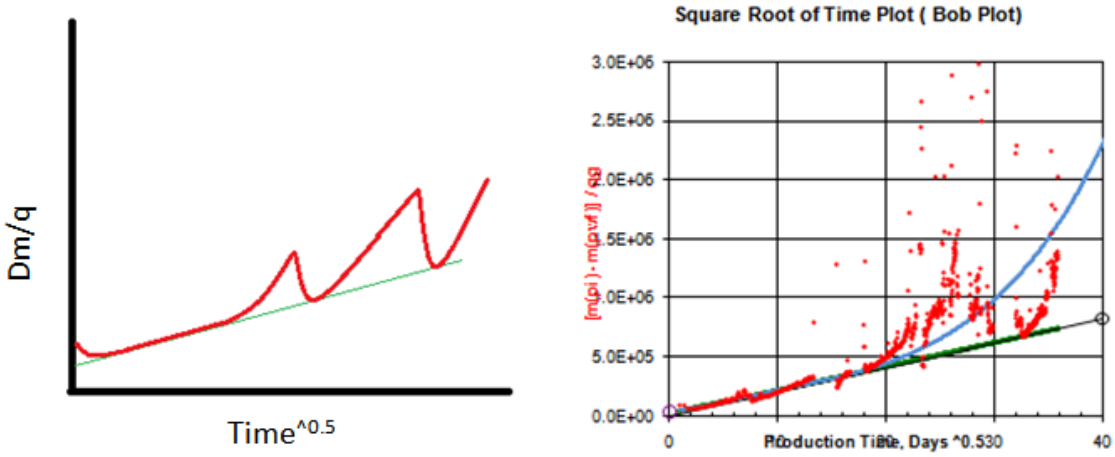

Fig. 3.11 –Gas lift is installed and gas was irregularly injected resulting in bouncing behavior on the square root of time plot. The green line represents the linear flow trend while the red points show the gas production rate.

The second trend shown on Fig. 3.12, is expected to occur as a result of a continuous and excessive gas injection rates. A new trend line will be formed while the liquid is being removed from the tubing. During this trend, it is hard to match and forecast the production data for this well. This trend will give a higher OGIP when trying to analyze the production data.

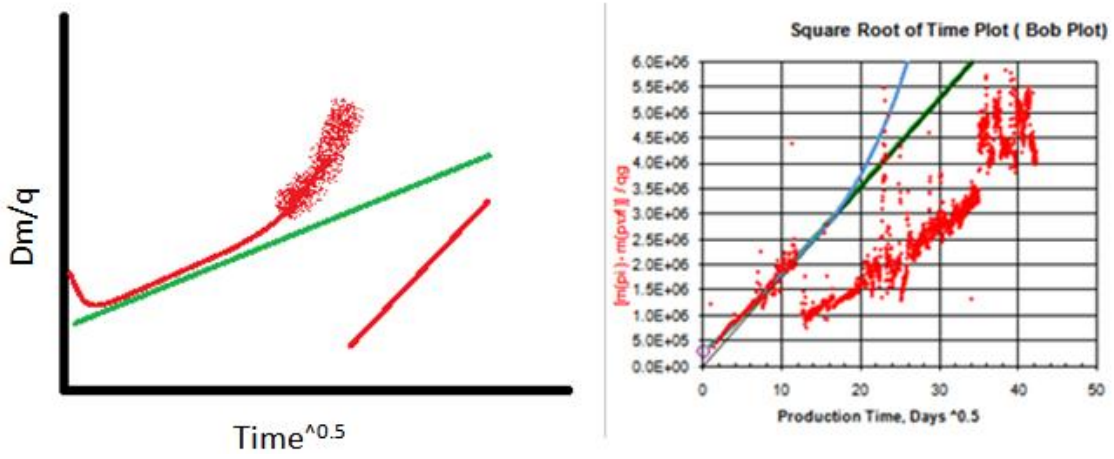

Fig. 3.12 –Gas lift is installed and excessive gas volumes are injected that resulted in new line production trends on the square root of time plot. The green line represents the linear flow trend while the red points show the gas production rate.

The third trend shown on Fig. 3.13, is expected to occur as a result of a gas being injection at optimum rates. The gas lift removed the accumulated liquid in the tubing and production trend starts converging towards the original linear flow trend as shown in green line.

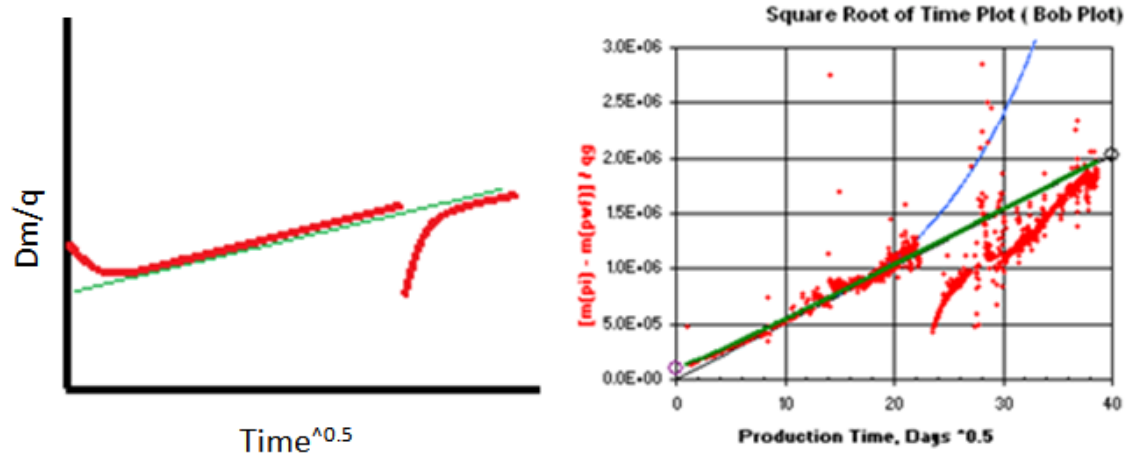

Fig. 3.13 –Gas lift is installed and injected at an optimum rate that ensured removing liquid loading and continue on the same trends. The green line represents the linear flow trend while the red points show the gas production rate.

The fourth gas lift trend shown on Fig. 3.14, is expected to occur as a result of a gas being injection at low and insufficient rates. The low rate resulted in fluctuating production data and long time to remove the liquid from the tubing.

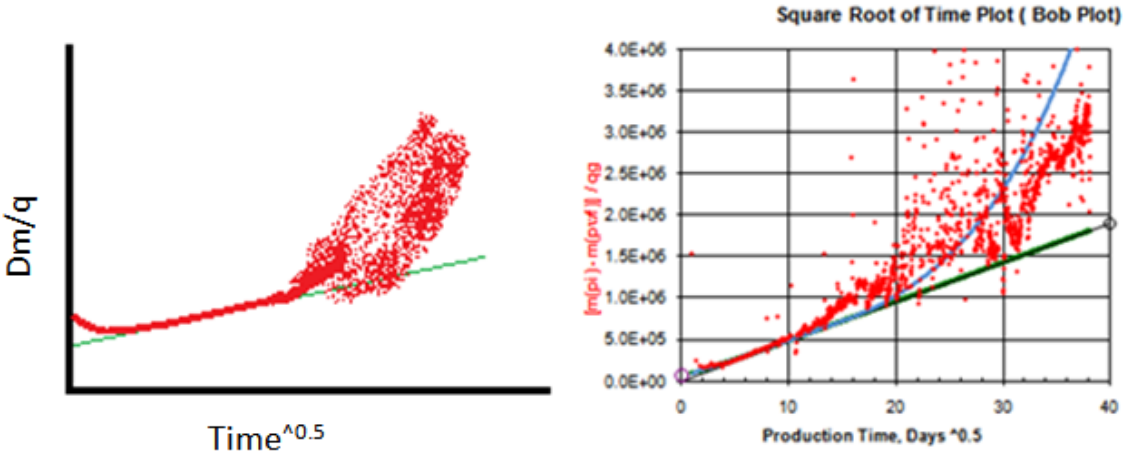

Fig. 3.14 –Gas lift is installed and injected at insufficient rate that resulted in intermittent flow and fluctuation in production rates. The green line represents the linear flow trend while the red points show the gas production rate.

The gas lift effect can be numerically compared to the hydraulic fracture if the production shows a straight line trend on the square root of time plot. Fig. 3.15 shows the production data for well #113 on a square root of time plot. After installing a gas lift, new production trend is observed with a straight line. To numerically compare the effect of gas lift, Wattenbarger's model was imposed and calculations similar to one on Chapter 4 section 4.2.4 were completed for both of the intervals. First, we evaluate the linear flow interval before the gas lift was installed.

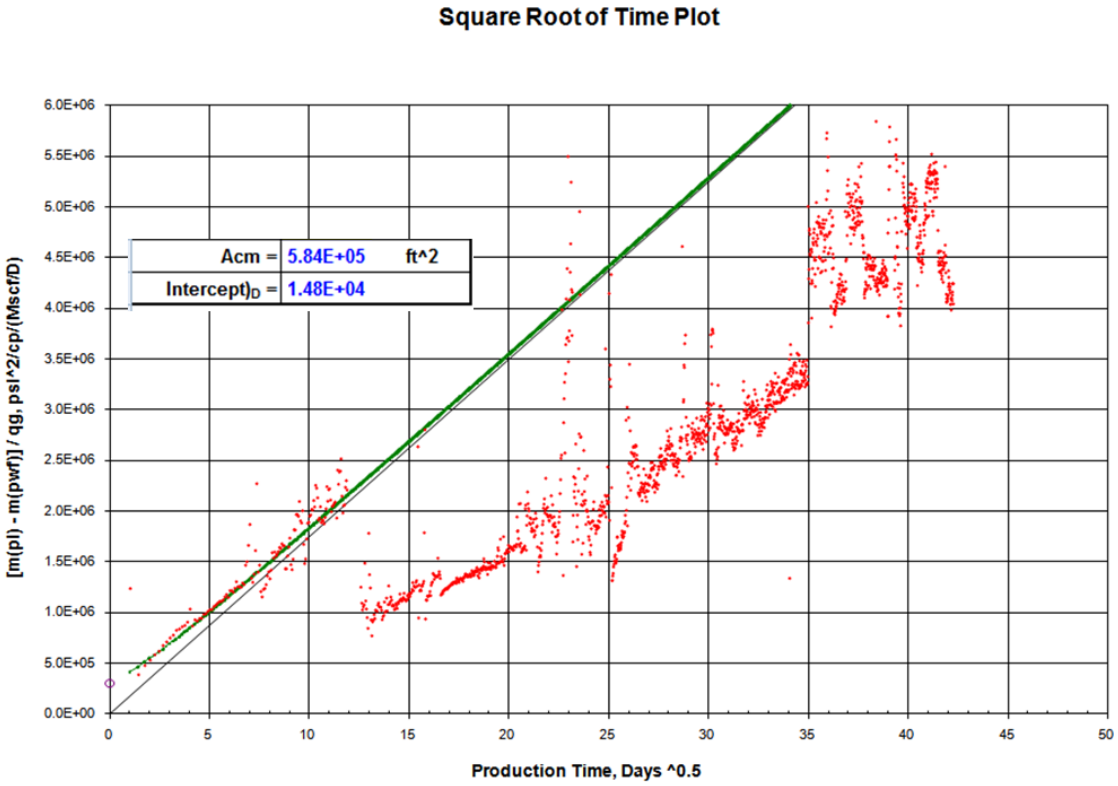

Fig. 3.15 –Matching the linear flow interval to evaluate A_{cm} using the Shale Gas VBA.[14]

Then, the time has to be re-set to zero at the day the gas lift installed and re-evaluate the completion job using the procedure. Fig. 3.16 shows the matching for the second linear flow interval. From the results, the new trend is showing 1.17 x 10^6 ft^2 fractured surface area compared to 5.84 x 10^5 ft^2 that was originally generated. This shows that installing a gas lift has the same effect of re-fracturing the well to generate an additional 5.86 x 10^5 ft^2 of fracture surface area to have the same results.

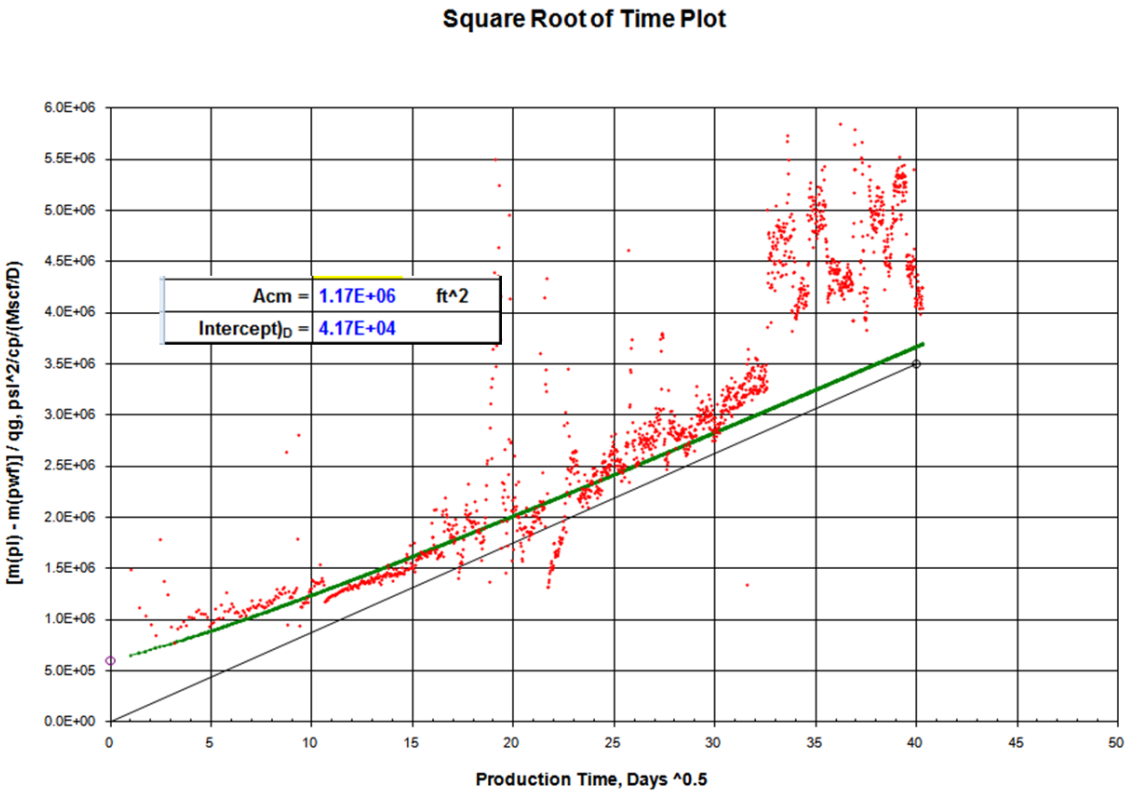

Fig. 3.16 –After resetting the time to zero and matching the interval with gas lift effect, the same calculations were cared to evaluate A_{cm} using the Shale Gas VBA.[37]

3.4.3.3 Identifying Interference Cases

The third case that needs to be filtered is the interference between wells. Although the low permeability makes it unlikely to observe interference in the shale gas formation, different cases occurred as a result of the short well spacing. Fig. 3.17 shows well #254 that was having linear flow for more up to 970 days when a nearby well #255 was completed. The completion of Well #255 resulted in drop in the gas production rate and an increase in water volumes of Well #254.

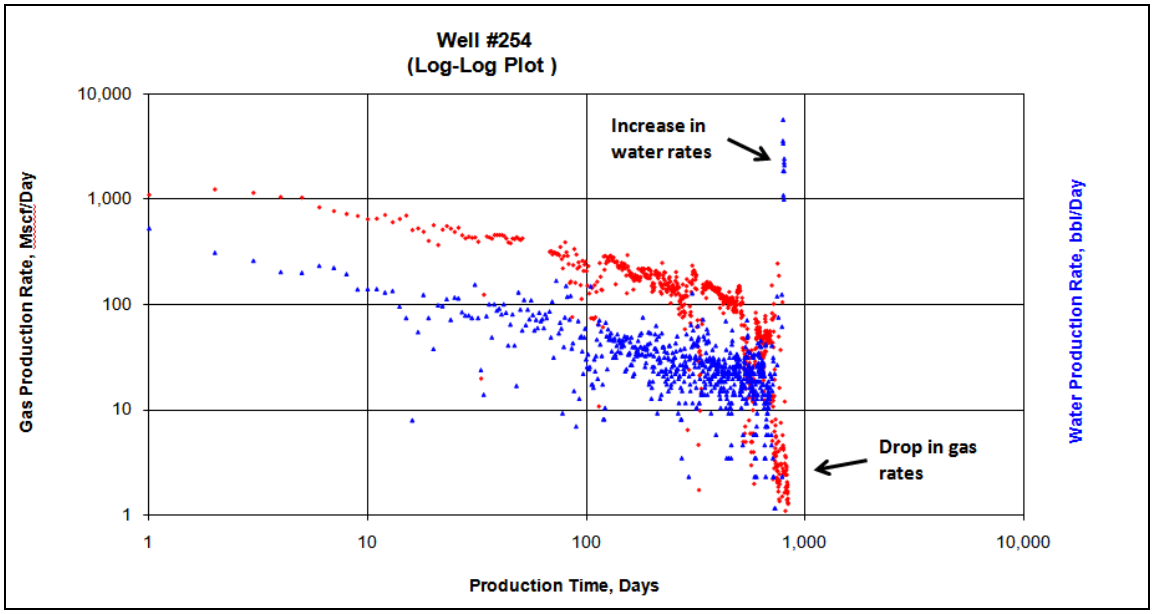

Fig. 3.17 –Nearby well completion resulted in interference disturbing the linear flow causing a drop in gas and increase in water rates.

3.5 Model-Based Analysis

The candidate wells prepared have a complete and viable data for analysis. The common approach is to first evaluate the reservoir properties form the transient, linear and

bilinear flow, and then evaluate the reservoir volume once the boundary dominated flow is observed. The analysis will enable us to:

- Estimate original gas in place.
- Estimate Reservoir characteristics.
- Evaluate the effectiveness of the completion job.

Both analytical and numerical methods are performed and compared using field data. Some assumptions will be required during interpretations and this might affect the accuracy of the results. Different decline curve techniques and different methodologies are available for analyzing the production data such as; Fraim and Wattenbarger[14], Palacio and Blasingame[15], Agarwal et al. [16], Ibrahim et al.[18], and Doublet et al[38]. Next chapters will show the methods and models used for production data analysis.

CHAPTER IV

IMPLICATIONS OF LINEAR AND BILINEAR FLOW

4.1 Implications of the Linear Flow

The first part of this section shows the implications of the linear flow of shale gas wells for a transient dual porosity solutions were presented first by El-Banbi[10]. The transient linear flow occurs in hydraulically fractured shale gas wells during the drainage from the formation matrix towards the hydraulic fracture and it could last up to years of production as shown in Fig. 3.6. The production data with the completion report can be utilized to evaluate different parameters such as the interface area between the hydraulic fracture and the matrix, A_{cm}, drainage area width, x_e, the permeability of the formation, and the OGIP.

4.2 Evaluating OGIP from Hydraulically Fractured Wells

Different models imposed for hydraulically fractured wells available in the literature. The first transient dual porosity model for linear reservoir was presented by El-Banbi[10]. He presented new semi-analytical and numerical Laplace solutions for the analysis of production data. He used both old solution to new interpretation models and new solution to solve different cases including the dual porosity models for linear reservoirs with constant pressure and constant rates with variety of boundary conditions. In this chapter, three models are discussed and a sample of the calculations is shown using field

data. The models imposed can be used as guidance for the expected flow regimes that may occur.

4.2.1 Model-1: Slab Model Using Anderson et al.[39]

Anderson et al.[33] model uses the transient slab model with the following assumptions:

1. Well completed horizontally.
2. Multiple hydraulic fractures finite conductivity that perpendicularly intersect the well.
3. The pore volume in contact with the fracture network is the Stimulated reservoir Volume (SRV).
4. Matrix blocks are homogeneous and occupy the space between the fractures.
5. Fluid in the pores assumed to be free gas while the adsorbed gas is not considered.
6. The SRV is bounded by infinite homogenous formation with properties similar to the matrix blocks. Anderson's model differs from Wattenbarger model in the way production progresses from linear to boundary and back to infinite acting linear flow. This occurs as a result of the unstimulated formation contribution to the production.

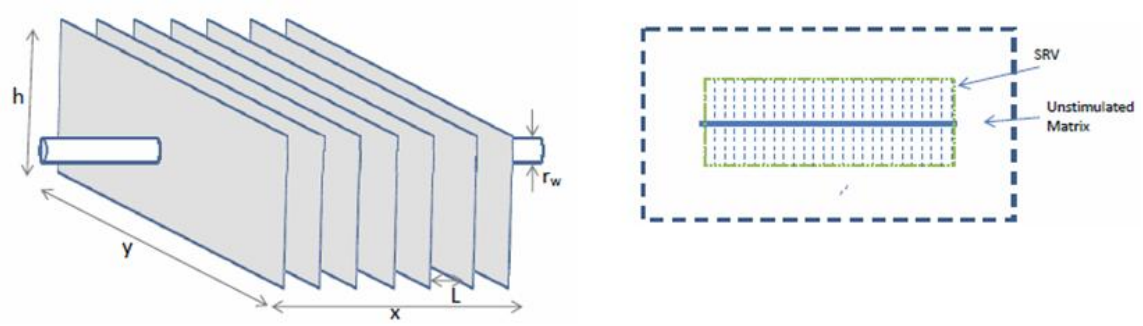

Fig. 4.1 –3D and plan view of Anderson et al. model. [39]

Fig. 4.1 shows a 3D diagram and a plan view of slab model using Anderson et al.[39] In their approaches, three plots are being utilized to evaluate different formation and completion properties such as the product of $A\sqrt{k}$, hydrocarbon pore volume (HCPV), and apparent skin. These results can be utilized to forecast the wells production and estimated the reserves. Some of the utilized plots include; square root of time plot, log-log plots, and the flowing material balance plot.

- **Log-log plot**

  This plot can identify different flow regimes based on the straight lines and slopes. Moreover plots of normalized rate and derivatives may be used on log-log plots such as plotting the semi-log derivative. We can use the plot of:

$$\left[\frac{d}{d\ln t_a}\left(\frac{p_{pi}-p_{pwf}}{q}\right)\right]^{-1} vs.t_a \quad \text{.....(4.1)}$$

  For interrupted and variable production conditions use the plot of:

$$\left[\frac{d}{d\ln t_{ca}}\left(\frac{p_{pi}-p_{wf}}{q}\right)\right]^{-1} vs. t_{ca} \quad \text{.....(4.2)}$$

- **Square root of time plot**

  The specialized square root of time plot or $(p_{pi}-p_{pwf})/q$ *vs.* $t^{0.5}$ can be used to evaluate different parameters from the linear flow period which appears as a straight line. From the slope of this line, *m*, the product $A\sqrt{k}$ can be evaluated using:

$$LFP = A\sqrt{k} = \frac{315.4T}{m}\times\frac{1}{\sqrt{(\phi\mu_g c_t)_i}} \quad \text{.....(4.3)}$$

and the fracture spacing can be evaluated by:

$$L = \frac{xyh\sqrt{k}}{LFP} \quad \text{.....(4.4)}$$

From the y-intercept, b, of the square root of time plot the apparent skin, s', can be evaluated using:

$$s' = \frac{kh}{1417T}b \quad \text{.....(4.5)}$$

- **Flowing Material Balance plot**

This plot utilized the Normalized Rate vs. Normalized Cumulative from Mattar and Anderson[40] and defined as:

$$Normalized\ Rate = \frac{q}{p_{ip} - p_{wf}} \quad \text{……..……(4.6)}$$

$$Normalized\ Cumulative = \frac{2qt_{ca}p_i}{(\mu c_t Z)_i (p_{ip} - p_{wf})} \quad \text{……..……(4.7)}$$

From this plot, the x-intercept (HCPV) of this plot, the stimulated reservoir width can be evaluated using:

$$A_{SRV} = \frac{HCPV \times B_{gi}}{\phi h S_g} \quad \text{……..……(4.8)}$$

$$y = \frac{A_{SRV}}{x} \quad \text{……..……(4.9)}$$

- **Forecasting the production**

In Anderson et al[39] model, the SRV is bounded by infinite action homogenous formation with properties similar to the matrix blocks. This will result in two components in forecasting the production data for the model:

1. The production from the stimulated reservoir volume.
2. The contribution of the bounded unstimulated formation. Depends on:

    a. The outer contact area with SRV which is defined by:

$$A_{outer} = (x + y)h \quad \text{……..……(4.10)}$$

    b. Permeability of the unstimulated formation:

A minimum and maximum forecast for the expected range of permeability is calculated.

Analysis Procedures:

1. Identify the different flow regimes by checking the slopes on log-log plot of rate against time with a half slope indicating the transient linear flow regime. The same period should appear as a straight line on a of [m(pi)-m(pwf)]/qg vs. $t^{0.5}$.
2. If BDF is observed, then calculate the HCPV from the Flowing Material Balance plot using Equations 4.6 and 4.7.
3. Determine the slope ($\tilde{m}_4$) and the y-intercept to evaluate $A\sqrt{k}$ and the apparent skin, s' using equations 4.3 and 4.5.
4. Evaluate fracture spacing, L, or stimulated reservoir width, y using equation 4.4.

4.2.2 Model-2: Slab Model Using Wattenbarger et al.[21]

In this transient slab model as shown in Fig. 4.2, a horizontal shale gas well is located at the center of a rectangular dual porosity reservoir which does not extend beyond the fracture system. It appears as the center of Anderson et. al[39]model with the following assumptions:

1. Well drilled horizontally for cased hole.
2. The hydraulic fractures have finite conductivity and perpendicularly intersect the well.
3. The Stimulated reservoir Volume (SRV) that is pore volume in contact with the fracture network.
4. Matrix blocks occupy the space between the fractures and assumed to be homogeneous.

5. Fluid in the pores assumed to be free gas.
6. The reservoir does not extend beyond fracture system.

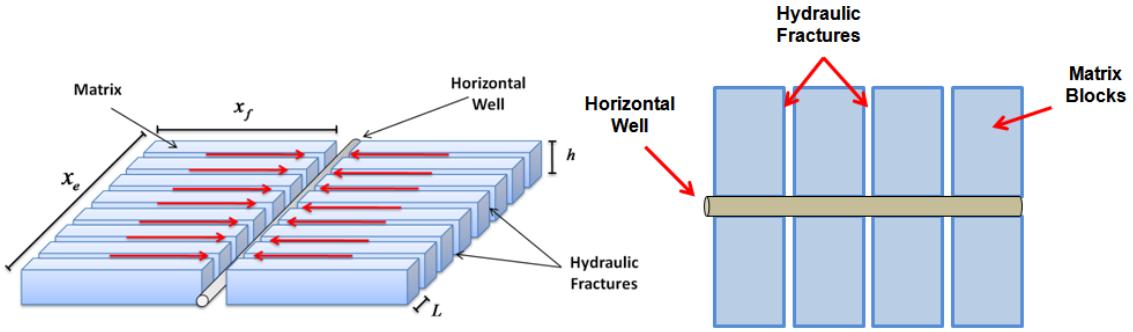

Fig. 4.2 –3D and plan view of Wattenbarger et al.[21] slab model. Unlike Anderson et al.[33] model the SRV is not bounded by unstimulated formation and the reservoir does not extend beyond the fracture system.

Analysis Procedures:

1. Identify the flow regime by checking the half slope on log-log plot of rate against time indicating the transient linear flow regime. The same period should appear as a straight line on a plot of $[m(p_i)-m(p_{wf})]/q_g$ vs. $t^{0.5}$.
2. Determine the slope ($\tilde{m}_4$) of the linear flow interval line on the square root of time plot.
3. Calculate the dimensionless drawdown, D_D, and the correction factor, f_{CP}, using Ibrahim and Wattenbarger[52]:

$$f_{CP} = 1 - 0.0852\, D_D - 0.0857\, D_D^2 \qquad (4.11)$$

$$D_D = \frac{m(p_i) - m(p_{wf})}{m(p_i)} \qquad (4.12)$$

4. If matrix permeability, km, is know, calculate Acm using:

$$\sqrt{k_m}A_{cm} = f_{CP}\frac{1262T}{\sqrt{(\varphi\mu c_t)_m}}\frac{1}{\tilde{m}_4} \quad \text{.....(4.13)}$$

5. Calculate end of transient time, t_{esr}, and fractures half-length, xf, using:

$$t_{esr} = \frac{1}{0.1591^2}\left(\frac{L}{2}\right)^2\frac{(\varphi\mu c_t)_i}{k_m} \quad \text{.....(4.14)}$$

$$x_f = \frac{A_{cm}}{4hn_f} \quad \text{.....(4.15)}$$

6. Calculate the OGIP using either the end of transient time or the fracture half length:

$$OGIP = f_{CP}\frac{200.8\,T\,S_{gi}}{(\mu c_t B_g)_i}\left(\frac{\sqrt{t_{esr}}}{\tilde{m}_4}\right) \quad \text{.....(4.16)}$$

$$V_{bm} = \frac{L_1}{2}A_{cm} \quad \text{.....(4.17)}$$

$$OGIP = \frac{V_{bm}\varphi(1-S_{wi})}{B_{gi}} = \frac{2Ln_f x_f h\varphi(1-S_{wi})}{B_{gi}} \quad \text{.....(4.18)}$$

4.2.3 Model-3: Cube Model Using Mayerhover et al.[41]

This model is similar to Warren and Root[9] idealized reservoir model which has heterogeneous porous medium. This model assumes transient cube model in which the hydraulic fractures enhance the conductivity of the natural fractures network. A 3D and a plan view diagram of the model is shown in Fig. 4.3. The assumptions that can be used with this model are:

1. Well completed horizontally for cased hole.

2. The hydraulic fractures only enhance the existing fracture network.
3. The Natural fracture spacing, L_2, is unknown and should be assumed.
4. Suggested a Stimulated reservoir Volume (SRV) that is pore volume in contact with the fracture network.
5. Matrix blocks occupy the space between the fracture network and assumed to be homogeneous with low permeability.
6. The reservoir does not extend beyond fracture system.

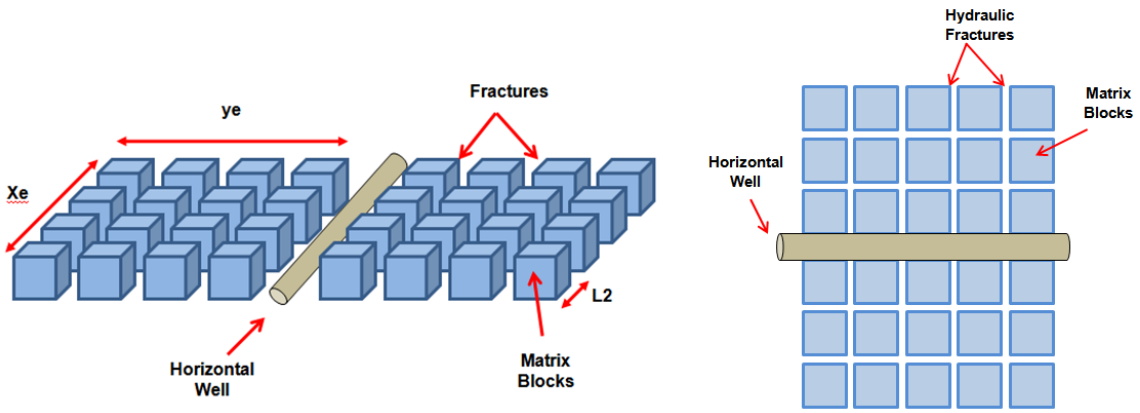

Fig. 4.3 –3D and plan view of transient cube model similar to Mayerhover et al.[41] This model assumes spacing between the enhanced natural fractures.

Analysis Procedures:

The procedures are illustrated in the paper published by Al-Ahmadi et al[34]. In this Model we evaluates the reservoir volume differently using the a fracture spacing from seismic or assumed by:

$$V_{bm} = \frac{L_2}{6} A_{cm} \text{ ……..……(4.19)}$$

Then using Equation 4.18 to estimate the OGIP.

4.2.4 Comparison of the Results Using Filed Data

Well #314 will be used to show example calculations for the slab model using Wattenbarger's and the cube model similar to Mayerhover's models. After identifying the linear flow interval on the log-log or the derivative plots, a specialized square root of time utilized to evaluate the slope, $\tilde{m}_4$. Fig. 4.4 shows the production data on a specialized square root of time plot. The green line is utilized to evaluate the slope $\tilde{m}_4$ = 1.88 x 10^4 psi^2/cp/(Mscf/D)/day$^{0.5}$. Table 4.1 shows the formation properties that are used in the calculations while Table 4.2 shows the fracture properties.

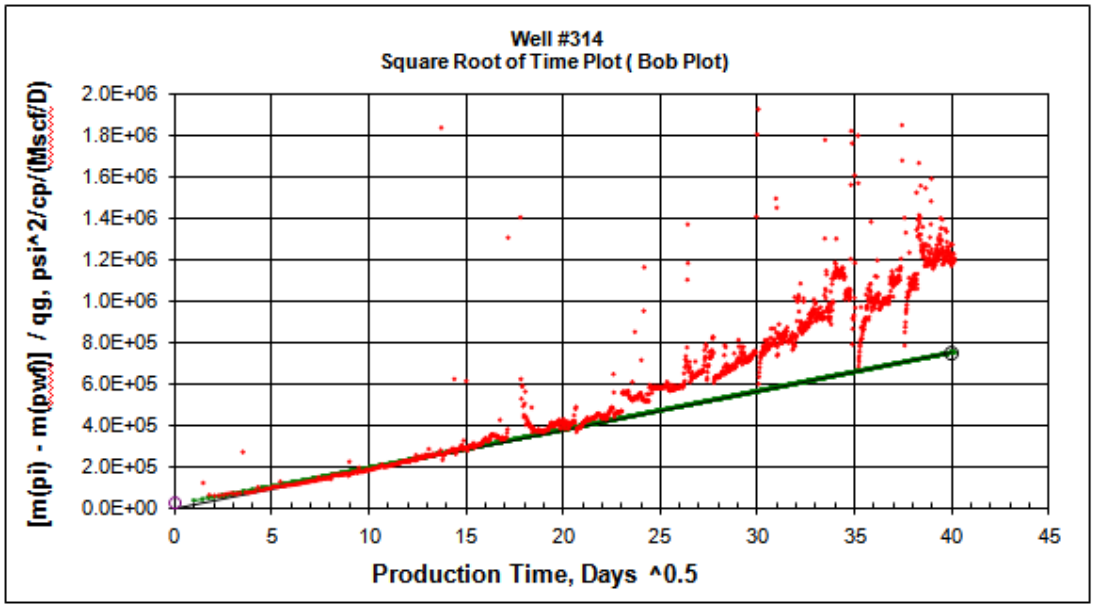

Fig. 4.4 –Square root of time plot showing the linear flow regime followed by BDF. The linear interval is matched and the slope is utilized to calculate the $\sqrt{k_m}A_{cm}$.

Table 4.1 - Formation properties for calculation.	
ϕ (fraction)	0.06
μ (cp)	0.02009
c_t (psi^{-1})	220E-06
T (^oR)	610
k_m (md)	0.00015
Bgi (rcf/scf)	0.00509
m(p)i (ps^2/cp)	5.91E+08
$m(p_{wf})$ (ps^2/cp)	2.03E+07

Table 4.2 - Fracturing Properties.	
fracture spacing , *L(ft)*	106
Number of hydraulic fractures, n_f	28
Thickness *(ft)* =	300
Drainage area length, x_e *(ft)*	2968
End of matrix transient (day)	391

After evaluating the slope $\tilde{m}_4$ = 1.88 x 104 psi2/cp/(Mscf/D)/day0.5 the dimensionless drawdown, D_D, and the correction factor, f_{CP} is calculated in order to evaluate the $\sqrt{k_m}A_{cm}$ product. The calculations go as follows:

$$D_D = \frac{m(p_i) - m(p_{wf})}{m(p_i)} = \frac{5.91\times10^8 - 2.03\times10^7}{5.91\times10^8} = 0.9657$$

$$f_{CP} = 1 - 0.0852\,D_D - 0.0857\,D_D^2 = 1 - 0.0852(0.9657) - 0.0857\,(0.9657)^2 = 0.8378$$

$$\sqrt{k_m}A_{cm} = f_{CP}\frac{1262T}{\sqrt{(\varphi\mu c_t)_m}}\frac{1}{\tilde{m}_4}$$

$$\sqrt{k_m}A_{cm} = (0.8378)\frac{1262\,(610)}{\sqrt{(0.06\times0.02009\times220\times10^{-6})}}\frac{1}{(1.88\times10^4)} = 66{,}618\ md^{0.5}.ft^2$$

The $\sqrt{k_m}A_{cm}$ production cannot be separated unless there is another source to provide an estimation for the permeability, $\sqrt{k_m}$, which was assumed in our case to be 0.00015 md. Using the assumed value to evaluate the total matrix drainage surface area into the fracture system, Acm using:

$$A_{cm} = \frac{66{,}618}{\sqrt{0.00015}} = 5.44\times10^6\ ft^2$$

Now, the OGIP can be estimated using either the volumetric of Wattenbarger Model or utilizing the end of straight line time on the square root of time plot or the time to reach the BDF, t_{esr}. From Fig. 4.4 the straight line ends at 289 days. Equation 4.16 can be used to evaluate OGIP using:

$$OGIP = f_{CP}\frac{200.8\,T\,S_{gi}}{(\mu c_t B_g)_i}\left(\frac{\sqrt{t_{esr}}}{\tilde{m}_4}\right)$$

$$OGIP = 0.8378\frac{200.8\ (610)(0.7)}{(0.02009\times220\times10^{-6}\times0.00509)}\left(\frac{\sqrt{289}}{1.88\times10^4}\right) = 2.80\times10^9\ scf$$

Using the volumetric of Wattenbarger's Model to calculate OGIP can be done utilizing the A_{cm} and knowing the hydraulic fracture spacing from the completion report. First we calculate the reservoir volume, V_{bm}:

$$V_{bm} = \frac{L_1}{2} A_{cm} = \frac{106}{2} \times (5.44 \times 10^6) = 2.88 \times 10^8 \ ft^3$$

The OGIP using the Volumetric of Wattenbarger's Models is calculated using:

$$OGIP = \frac{V_{bm} \varphi (1 - S_{wi})}{B_{gi}} = \frac{(2.88 \times 10^8) \times (0.06) \times (0.7)}{0.00509} = 2.38 \times 10^9 \ scf$$

The hydraulic fracture half length, x_f, can be evaluated using the A_{cm} value by:

$$x_f = \frac{A_{cm}}{4 h n_f} = \frac{5.44 \times 10^6}{4(300)(28)} = 161.9 \ ft$$

Mayerhover's models starts with the same calculations for A_{cm} while different definition for the V_{bm} definition based on the model. The natural fracture spacing, L_2 is assumed to be 90 ft and V_{bm} is calculated using:

$$V_{bm} = \frac{L_2}{6} A_{cm} = \frac{95}{6} (5.44 \times 10^6) = 8.61 \times 10^7 \ ft^3$$

$$OGIP = \frac{V_{bm} \varphi (1 - S_{wi})}{B_{gi}} = \frac{(8.61 \times 10^7) \times (0.06) \times (0.7)}{0.00509} = 0.711 \times 10^9 \ scf$$

Error might occur when calculating OGIP using t_{esr} time because of the false boundary which is caused by the natural fracture communication with the hydraulic fracture, resulting in different boundary than the one between the hydraulic fractures.

4.3 Implications of Bilinear Flow

Bello[7] showed that the occurrence of the bilinear flow is controlled mainly by the Warren and Root Interporosity[9] flow parameter for the slab matrix case which is defined as

$$\lambda_{AC} = \frac{12}{L^2}\frac{k_m}{k_f} A_{cw} \quad \text{.....} \quad (4.20)$$

where

$$A_{cw} = \frac{12}{L^2}\frac{k_m}{k_f} \quad \text{.....} \quad (4.21)$$

and it occurs only when $y_{De} > \sqrt{3/\lambda_{AC}}$. This flow interval can be plotted using $\Delta m(p)/q$ *vs.* $t^{0.25}$ to give a straight line with a slope, $\tilde{m}_2$ to evaluate the shape factor, σ and the fracture permeability using:

$$\sqrt{k_f} A_{cw} = \frac{4064T}{\tilde{m}_2 \sqrt[4]{k_m \sigma (\phi \mu_g c_t)_i}} \quad \text{.....} \quad (4.22)$$

Arevalo-Villagran et al.[31] presented systematic methods to evaluate different parameters from the production data. They investigated linear and bilinear flow using a model that was ran for dual porosity formation with two different media having different properties. The first medium is the fracture while the other one is matrix. The fracture has high flow capacity with low storage while the matrix has the storage with the low permeability.

Branajaya et al.[29] ran different simulation cases for bilinear flow where they changed the fracture half length and its permeability to verify Cinco-Ley and Samaniego

solutions. Their simulation were for a single matrix block model having a specified length, a, and width, b. Fig. 4.5 shows the imposed model and from this model, the upper half of the block has identical geometry which allows the assumption to use the rate of q/2 and fracture width w/2. This will also let the fracture half length x_f equal to a+b.

4.3.1 Bilinear Model: Arevalo-Villagran et al.[31]

This model utilized the symmetry element to reduce the field model to quarter of its original size. Table 4.3 summarizes the equation that can be used for bilinear flow. The model used has the following assumptions:

1. The model geometry has length, a, width, b, and height, h.
2. When simulating runs, the width is fixed while changing the length, a, and running it for different ratios of a/b.
3. Model cross section area, A_c :

$$A_c = 2h(a+b) \text{ ……..……} (4.23)$$

4. The upper half of the block has identical geometry which allows the assumption to use the rate of q/2 and fracture width w/2. This will also let the fracture half length x_f equal to (a+b)/2.
5. Matrix blocks assumed to be homogeneous with low permeability.

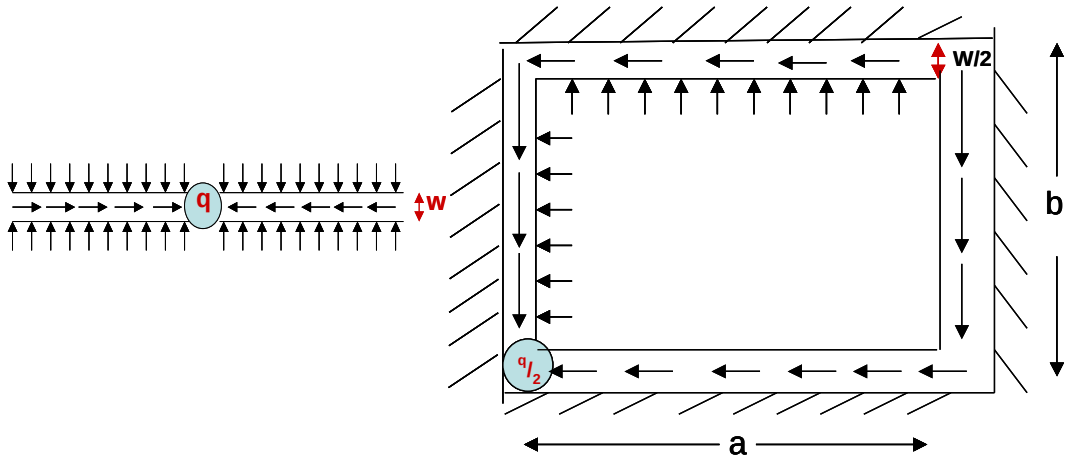

Fig. 4.5 –Branajaya et al.[29] model shows the matrix block with length, a, width, b and the fracture half length, x_f is equal to a+b. [29]

Table 4.3 – Bilinear equations for gas. [29]
Gas
$\frac{1}{q_D} = \frac{k_m h\left[m(p_i) - m(p_{wf})\right]}{1422\ q_g T} = \frac{C}{\sqrt{F_{CD}}} t_{Dxf}^{1/4}$ $C = 2.722\ or\ 2.45\ depending\ on\ case$
$p_{WD} = \frac{k_m h\left[m(p_i) - m(p_{wf})\right]}{1422\ q_g T}$
$t_{Dxf} = \frac{0.00633\ k_m t}{(\phi\ \mu\ c_t)_i (x_f)^2}$

4.3.2 Analysis Procedure

1. As shown in Table 3.2, a quick way to identify the bilinear flow can be done using different plots such as:
    - Quarter slope in a log-log plot of rate vs. time.
    - Zero slope derivative plot of $\frac{\Delta m(p)/q}{d\sqrt[4]{t}} vs. \sqrt[4]{time}$ on log-log scale.
    - Straight line is a plot of $\Delta m(p)/q \ vs. \sqrt[4]{time}$.

    Fig. 4.6 shows example of well #255 having long bilinear flow period identified on the log-log plot by a quarter slope and straight line on the $\Delta m(p)/q \ vs. \sqrt[4]{time}$.
2. After identifying the bilinear flow, specialized plots are done using the superposition time and plotting $\Delta m(p)/q \ vs. \sqrt[4]{time}$.
3. Determine the slope, intercept and the beginning of the boundary dominated flow from the $\Delta m(p)/q \ vs. \sqrt[4]{time}$ plot.
4. Reservoir properties can be calculated utilizing the transient flow period while the boundary effect can be utilized to calculate the V_p and OGIP shown in Table 4.2.

No early linear flow, from the hydraulic fracture, was observed from the analyzed shale gas wells.

Tables 4.4 through 4.6 show summary of the equations that can be used for different flow regimes during the production life of well that has been hydraulically fractures. Different equations represent different conditions for constant rate and constant pressure production.

Table 4.4 – Early linear flow equations for constant p_{wf} production. [31]

$$\sqrt{k_1}A_{c1} = \frac{631T}{\tilde{m}_{CPEL}\sqrt{(\phi\mu_g c_t)_i}}$$

$$s_f = \frac{b_{CPEL}k_1\sqrt{A_{c1}}}{1424T}$$

Table 4.5 – Bilinear equations for gas for constant q_g production. [31]

$$\sqrt{k_1 w} = \frac{984T\,A_c^{1/4}}{\tilde{m}_{CRB}\sqrt[4]{k(\phi\mu_g c_t)_i}}$$

$$s_1 = \frac{b_{CRB}k\sqrt{A_c}}{1424T}$$

Table 4.6 – Late linear equations for gas for constant p_{wf} production. [31]

$$\sqrt{k_m}A_{cm} = f_{CP}\frac{1262T}{\sqrt{(\varphi\mu c_t)_m}}\frac{1}{\tilde{\tilde{m}}_4}$$

$$A = \frac{225T}{(\varphi\mu_g c_t)_i}\left(\frac{\sqrt{t_{esr}}}{\tilde{m}_{CPL}\,h}\right)$$

$$V_p = \frac{225T}{(\mu_g c_t)_i}\left(\frac{\sqrt{t_{esr}}}{\tilde{m}_{CPL}}\right)$$

$$OGIP = \frac{225TS_{gi}}{(\mu_g c_t B_g)_i}\left(\frac{\sqrt{t_{esr}}}{\tilde{m}_{CPL}}\right)$$

$$b = \frac{b_{CRB}k\sqrt{A_c}}{1424T}$$

$$y_e = 0.1779\sqrt{\frac{kt_{esr}}{(\varphi\mu_g c_t)_i}}$$

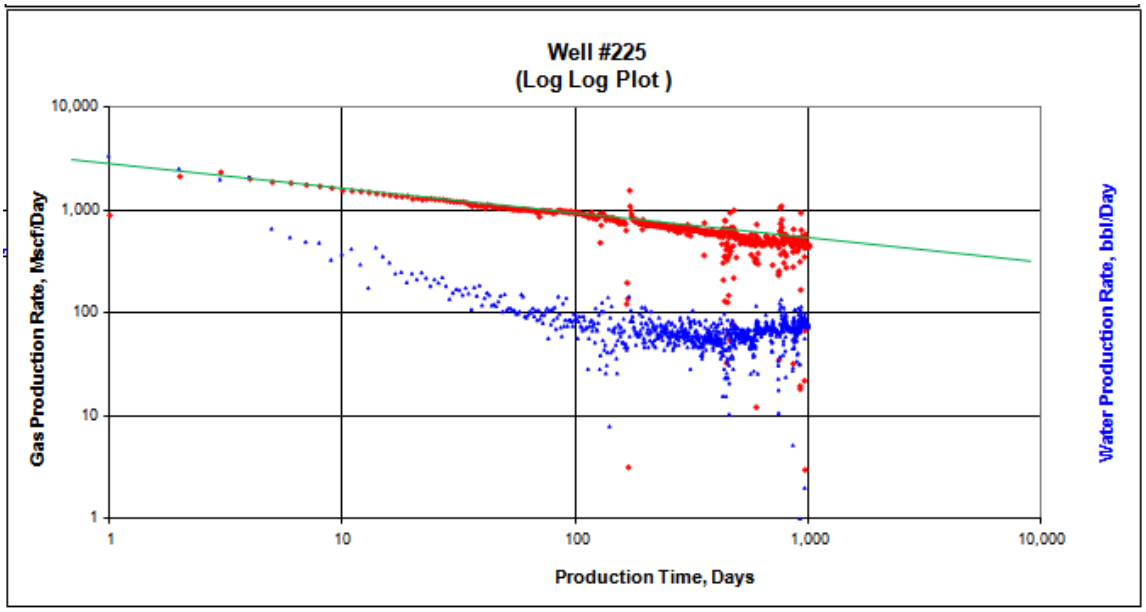

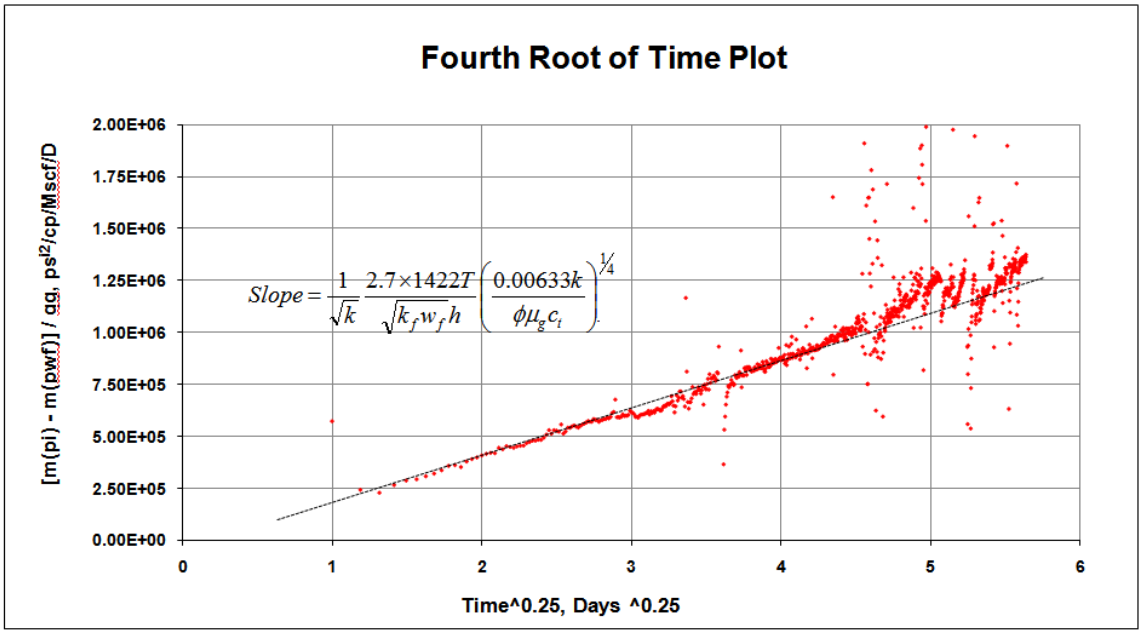

Fig. 4.6 –Showing bilinear flow on log-log appearing as quarter slope line and on the fourth root of time plot with a slope that can be utilized in Eq. 4.20.

From the plot of $\Delta m(p)/q$ $vs.\sqrt[4]{time}$, the slope is equal to:

$$Slope = C\frac{1}{\sqrt{k}}\frac{T1422}{\sqrt{k_f w_f}\,h}\left(\frac{0.00633k}{\phi\mu_g c_t}\right)^{1/4} \quad \text{……..……(4.24)}$$

4.3.3 Sample Calculation for Field Case Having Bilinear Flow

First step is to identify the interval of the bilinear flow using log-log plot, fourth root superposition time, derivative plot, and specialized plot using the fourth root of time as shown in Fig. 4.5. After evaluating the slope of the straight line on the fourth root of time plot, we can evaluate the fracture conductivity using:

$$Slope = C\frac{1}{\sqrt{k}}\frac{T1422}{\sqrt{k_f w_f}\,h}\left(\frac{0.00633k}{\phi\mu_g c_t}\right)^{1/4}$$

$$\sqrt{k_f w_f} = (2.722)\frac{1}{\sqrt{0.00015}}\frac{(610)\times 1422}{(2.5\times 10^5 \times 300}\left(\frac{0.00633(0.00015)}{0.06\times 0.02009\times 220\times 10^{-6}}\right)^{1/4}$$

$$\sqrt{k_f w_f} = 3.54\,md^{0.25}.ft^{0.25}$$

4.3.4 Simulating Bilinear Flow Regime and Checking Derivatives

From Branajaya et. al.[31], Constant rate production tend to have linear flow more than the constant pressure production for different a/b ratio. From the simulated runs, the constant pressure production show linear flow for a/b ratios greater than 16 while the constant rate production show it for a/b ratios above 3. Gassim VBA Software[42] was used to simulate a hydraulic fracture in matrix formation having input data as shown in Fig. 4.7. Results of the simulated run showed that the pressure drop reach the tip of the fracture and the bilinear flow ends in less than a day of production as shown in Fig. 4.8.

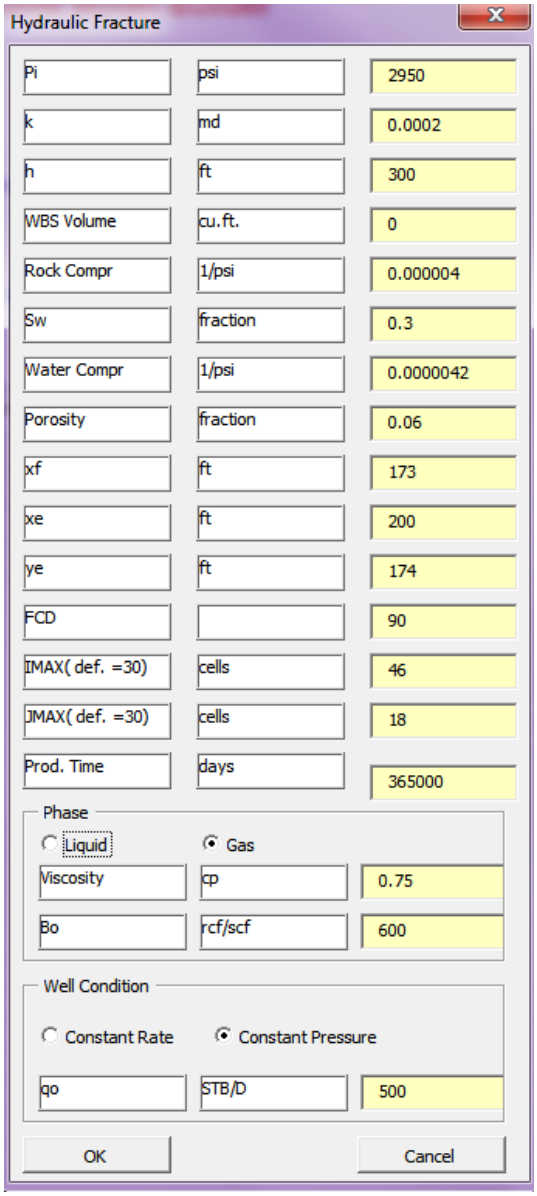

Fig. 4.7 –Showing the input data window in Gassim VBA[42] for hydraulic fracture model.

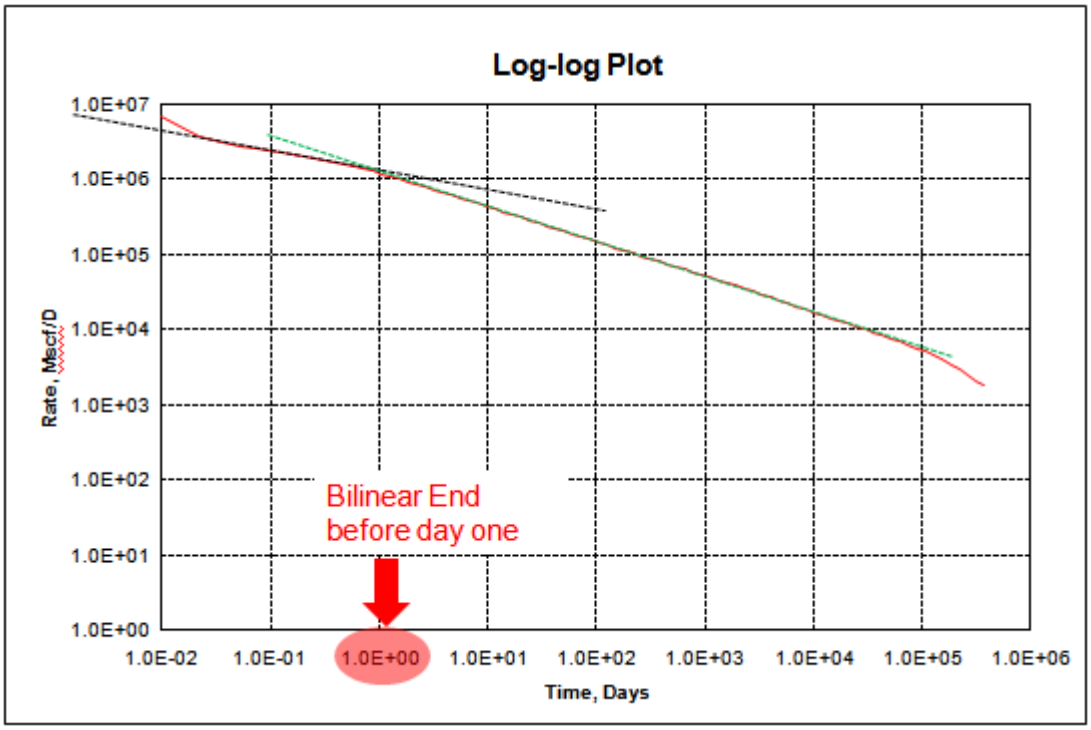

Fig. 4.8 –Showing the bilinear flow with quarter slope ended in less than one day of production followed by a linear flow indicated by a green line with a half slope.

If we use the derivative with respect to the fourth root of normalized pseudo time with super position, the results will look as in Fig. 4.9. The derivative plot does not identify the bilinear flow which also ended in less than normalized pseudo time with super position equal to 1. Another derivative plot with respect the square root of the normalized pseudotime with superposition is shown in Fig. 4.10 and the linear flow interval is indicated by constant derivative or zero slope line.

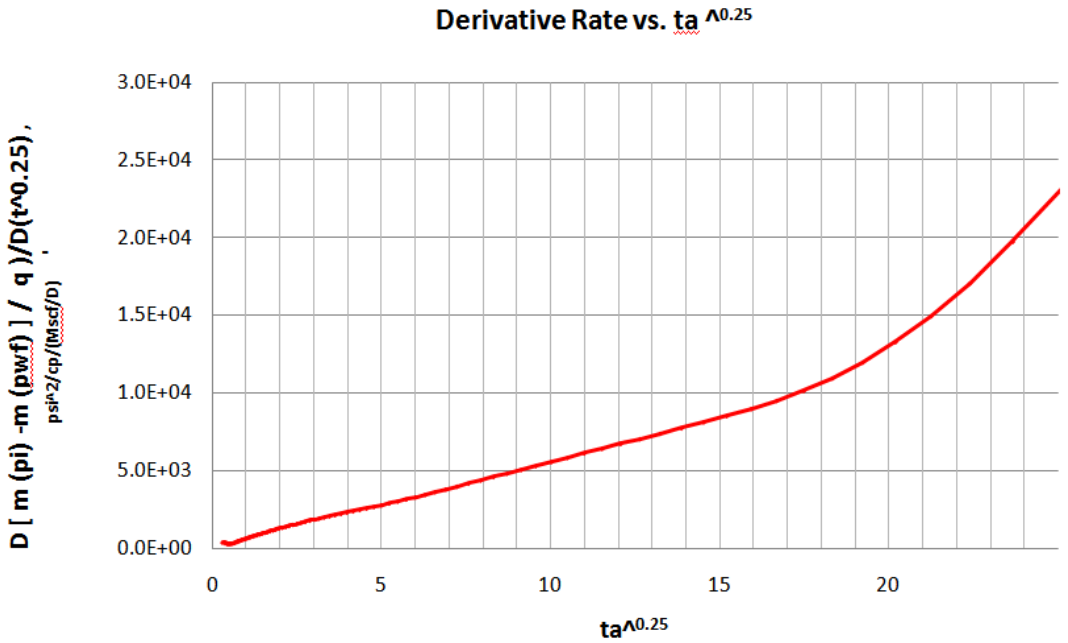

Fig. 4.9 –Showing the bilinear flow in the derivative plot ending in less than 1 which makes it difficult to be identified using the derivative plot.

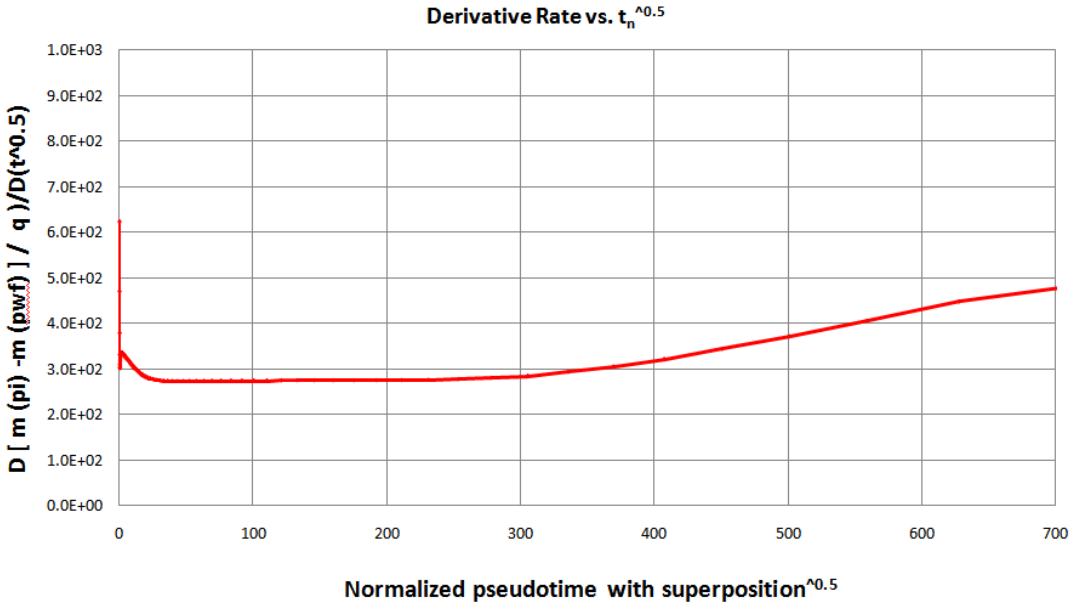

Fig. 4.10 –The derivative plot with respect to square root of normalized pseudotime with superposition showing constant derivative indicating the linear flow regime.

This could explain the reason why it is not common to observe bilinear flow in field data which are provided in average daily production. The daily production data will show the bilinear period as one day point in production. However, it is more commonly to observe the bilinear flow in wells that have poor hydraulic fracture jobs which have low hydraulic fracture conductivity.

Another simulated run is performed to check whether the end of the bilinear flow will appear as the beginning of the linear flow when using the derivative plots. For this case the hydraulic fracture properties are changed to extend the effect of the bilinear flow. The dimensionless fracture conductivity value was changed from 90 to 5. The resulted log-log plot is shown on Fig. 4.11 with a transition interval between the bilinear and linear flow reaching 757 days.

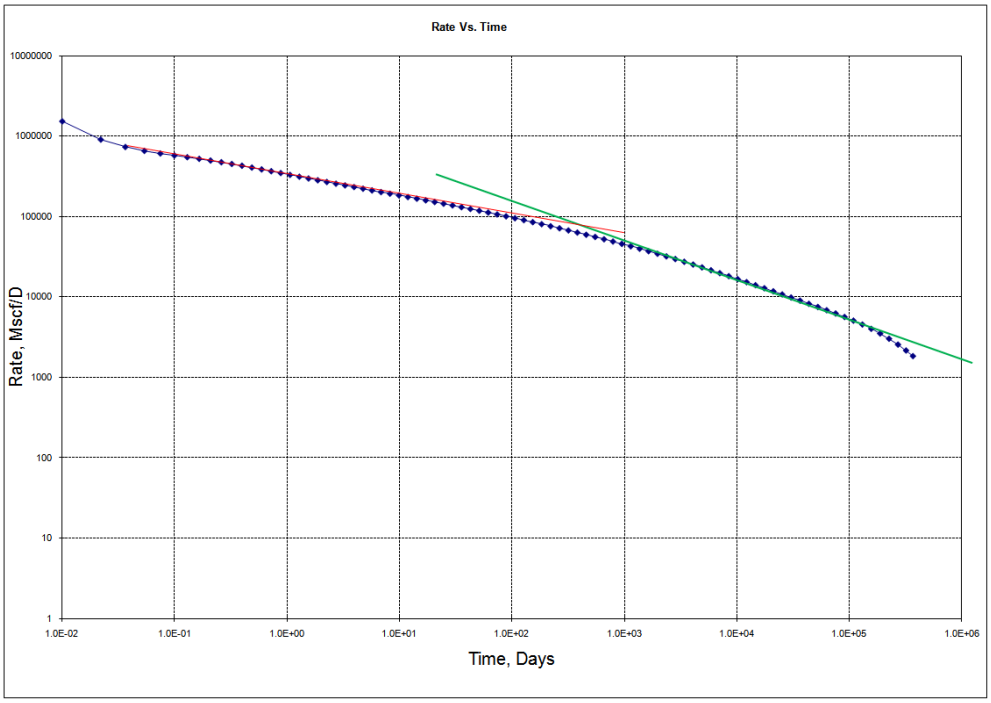

Fig. 4.11 –Simulated run to investigate the transition time from the bilinear flow to linear flow. Red line with a quarter slope representing the bilinear flow while the green line with a half slop showing the linear flow. There is a long transition interval between the two flow regimes estimated to be around 757 days.

CHAPTER V

ADVANCED PRODUCTION DATA ANALYSIS

5.1 Introduction

Different methods in the literature are available for analyzing the production data. Some of them use type curve to analyze the production data while others uses different methodologies that does not involve type curve. Examples of these techniques include; Fraim and Wattenbarger[14], Palacio and Blasingame[15], Agarwal et al. [16], Ibrahim et al.[18], Doublet et al[38]. Anderson et al[39]. Fetkovich et a.[43-44] and Carter[45]. The first production data analysis was developed in 1945 by Arps[46]. His decline curves were developed to analyze oil and gas production data during the transient flow regime. Fetkovich et al.[43-44] modified Arps procedure and developed decline curves to analyze gas production during the BDF intervals. Both of these traditional decline curve analysis are based on matching the historical production data to a model. The approaches will fail to forecast or evaluate reserves if the production conditions were changed. They are both assuming the production conditions applied in the past will not change in the future. However, field data have operating conditions that are not stable and the well's production is affected by re-completion operations and shut-in interruptions. The modern decline curve analysis and new methodologies account for variable production conditions and variable fluid properties that will result in more accurate estimates for OGIP and forecasting results. Now, with many analysis approaches available, it is difficult to determine which method will give the most accurate results.

The traditional decline curve analysis, such as Arps[46] and Fetkovich et al.[43-44], were not applied in the Barnett shale neither to estimate the EUR nor to forecast the production. This is because their limitation for operating conditions to be stable while this is not the case for field data. The material balance approach for calculating the OGIP requires the reservoir pressure as a function of cumulative production. This approach will require long shut-in time to measure the average pressure in shale gas formation because of the low permeability of the formation.

In this chapter, different methods available to analysis production performance of gas wells are tested. The approaches will be presented and field cases will be applied with different flow regimes to evaluate the original gas in place. Then the results will be tested to forecast the production and evaluate the best method to be applied in the Barnett shale.

5.2 Production Data Analysis

The decline curve analysis use the production data such as the fluid rates and pressures to evaluate fluid in place. They are cheap alternative which uses the pressure transient theory similar to the well testing when evaluating the permeability and skin. Although the welltest data analysis is more accurate, the production data provide more of long term analysis.

Once the pressure drop reaches the no flow boundary, the transient linear or bilinear flow regime will end and the boundary dominated flow starts. Different methods utilize the beginning of the BDF to evaluate the OGIP. A review of the different

production analysis approaches was presented by Mattar and Anderson[47] where they evaluated the different methods and summarized in Table 5.1.

Table 5.1 - Comparison of different production data analysis approaches showing the strength and limitations. Data in this table generated by Mattar and Anderson.[47]

Blasingame Type Curve Analysis[15, 38]	
Strength	Limitations
• uses the rate-integral which tend to smooth the data • All BDF decline curve combine to one harmonic curve which and make it easy to match	• Flow regimes cannot be identified when rate-integral derivative is used. • the accuracy of the of the rate-integral is sensitive to early time inaccuracy.
Agarwal-Gardner Type Curve Analysis[16]	
Strength	Limitations
• Flow regimes can be identified more accurately.	• Requires smoothing.
Flowing Material Balance[40, 48]	
Strength	Limitations
• Simple and similar to applying the conventional MB plot and give OGIP • Doesn't require shut-in pressures.	• Applicable to BDF only.

5.3 Normalized Pseudotime with Superposition[18]

This approach starts from the Fraim and Wattenbarger's[14] normalized time for constant pressure production that linearize the gas production rate vs. normalized time. Their method will allow type curve matching using the exponential decline curve. The normalized time will bring the boundary dominant flow to the analytic solution of exponential decline with b=0. Moreover, it will account for the change in gas properties and can be used for transient and boundary dominated flow. The method differs from Lee and Holditch[49] pseudotime in the pressure where the fluid properties are calculated. Lee and Holditch evaluated the formation properties at the of bottom hole pressure, while Fraim and Wattenbarger's[14] utilized the average reservoir pressure to evaluate the normalized pseudotime, t_n and it is defined as:

$$t_n = \int_0^t \frac{(\mu c_t)_i}{\mu(\bar{p})c_t(\bar{p})}\, dt \qquad \text{.....(5.1)}$$

From their simulated runs, it has been observed that the more the pressure drawdown compared to initial pressure, the more the separation between production curve with normalized time and the real time.

The procedure starts by assuming value for the original gas in place. The OGIP value is utilized to calculate the normalized time and to match the curve with an exponential decline type curve to re-evaluate the new OGIP. The process repeated until OGIP value converges for exponential decline cure with b=0. The Calculation Procedure starts by evaluating (p/z) for each completive production step. Then evaluating storage

pseudopressure, $\bar{p}_p$ and Δt_n to calculate the normalized time. Finally plotting the production rate vs. normalized time and calculate the OGIP. The steps are repeated until the value of OGIP converges.

Ibrahim, Wattenbarger, and Helmy[18] utilized the normalized pseudotime with the superposition to come with a new plotting function method which enables analyzing variable rate and variable pressure production data to calculate the OGIP to more accurately. The normalized pseudotime with the superposition will correct for the error in superposition due to the change in gas properties. This new tangent method calculates the OGIP utilizing the current reservoir properties in the boundary dominant flow.

Method-1: Plotting $[m(p_i)-m(p_{wf})]/q_g \ vs. \ t$, the slope can be utilized to evaluate the OGIP at current reservoir properties using:

$$OGIP=\left(\frac{2pS_g\phi}{z}\right)_i\left(\frac{1}{\phi(\bar{p})\mu(\bar{p})c_t(\bar{p})}\right)\left(\frac{1}{\tilde{m}_{PSS}}\right) \qquad \text{.....(5.2)}$$

Method-2: utilizing the slope of the plot of $[m(p_i)-m(p_{wf})]/q_g \ vs. \ \text{sup}osition-t$. The OGIP can be evaluated using initial properties:

$$OGIP=\frac{2p_i S_{gi}}{z_i(\mu_g c_t)_i}\left(\frac{1}{\tilde{m}_{PSS}}\right) \qquad \text{.....(5.3)}$$

Method-3: The OGIP can be calculated more accurately taking into account the change in properties, rate and pressure. This can be done using the normalized pseudotime with superposition by plotting $\frac{m(p_i)-m(p_{wf})}{q_g} vs. \sum_{j=1}^{m}\frac{(q_{gj}-q_{gj-1})}{q_{gm}}(t_{nm}-t_{nj-1})$ and using

equation 4.56 while the slope is from the normalized pseudotime with superposition plot. The normalized pseudotime can be calculated using:

$$t_n = (\phi\mu_g c_t)_i \int_0^t \frac{1}{\phi(\bar{p})\mu_g(\bar{p})c_t(\bar{p})} dt \quad \text{.....(5.4)}$$

OGIP Calculation Procedure:

1. Assuming an OGIP value.

2. Calculating the average pressure, $\bar{p}$ using the material balance equation:

$$\frac{\bar{p}}{\bar{z}} = \frac{p_i}{F_R z_i}(1 - \frac{G_P}{G}) \quad \text{.....(5.5)}$$

3. Calculating the fluid properties at each average pressure, $\bar{p}$.

4. Calculating the normalized pseudotime using:

$$t_n = (\phi\mu_g c_t)_i \int_0^t \frac{1}{\phi(\bar{p})\mu_g(\bar{p})c_t(\bar{p})} dt$$

5. Calculating the normalized pseudotime with superposition using:

$$\text{super} - t_n = \sum_{j=1}^{m} \frac{(q_{gj} - q_{gj-1})}{q_{gm}}(t_{nm} - t_{nj-1})$$

6. Plotting $\frac{m(p_i) - m(p_{wf})}{q_g} vs. \sum_{j=1}^{m} \frac{(q_{gj} - q_{gj-1})}{q_{gm}}(t_{nm} - t_{nj-1})$ and evaluating the slope, $\tilde{m}_{PSS}$.

7. Calculating the OGIP using $OGIP = \frac{2p_i S_{gi}}{z_i(\mu_g c_t)_i}\left(\frac{1}{\tilde{m}_{PSS}}\right)$.

8. Repeating the steps from 1 to 7 until the calculated OGIP converges.

Example Cases for evaluating the OGIP for the Barnett shale. Well #314 is selected as a field example to show the results of different calculations. Fig. 5.1 shows the log-log plot of well #314 as a quick way to identify the flow regimes.

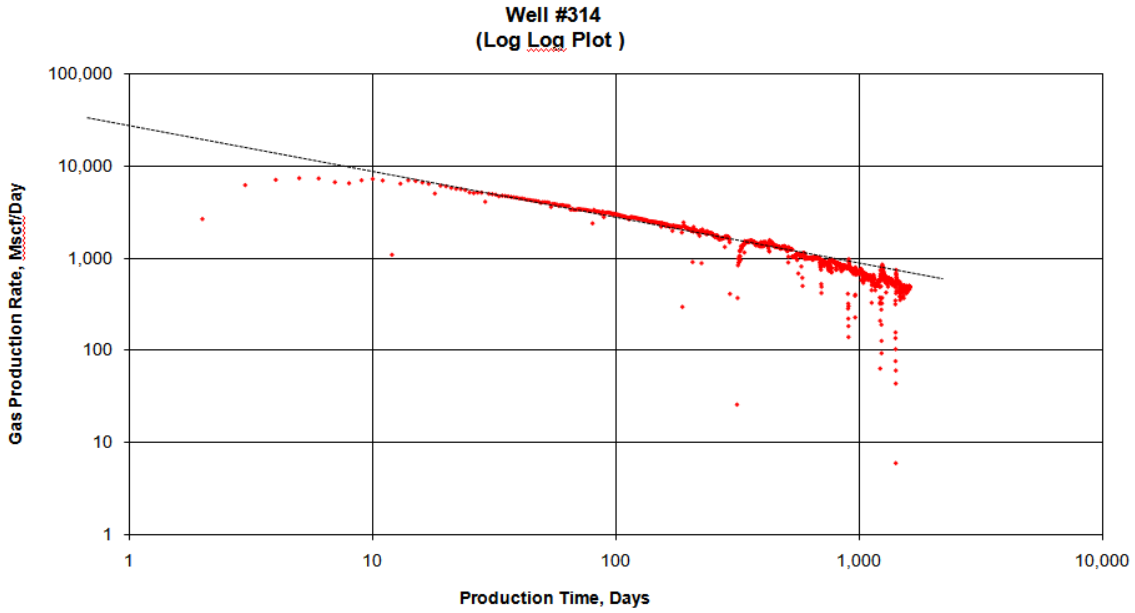

Fig. 5.1 – A quick look at the log-log plot to identify the flow regime of well #314. The plot shows a half slope line indicating the linear flow up to 450 days followed by BDF.

The linear flow regime is clearly identified by the half slope line from the log-log plot, but we need to confirm the BDF regime. The derivative plot was used with the normalized pseudotime and superposition as shown in Fig.5.2.

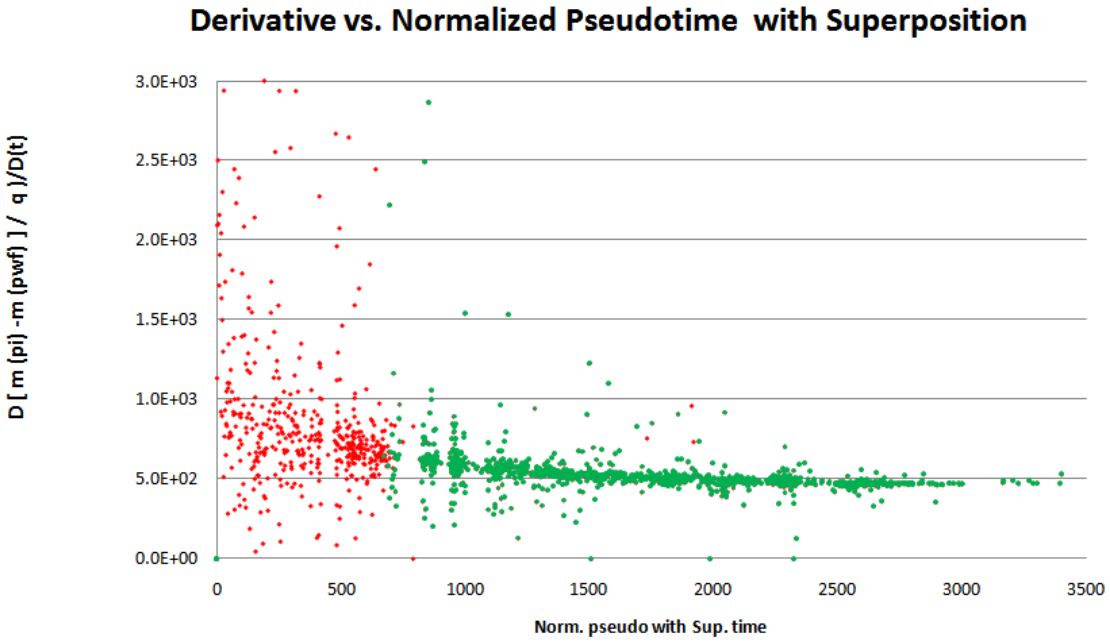

Fig. 5.2 – Derivative plot with respect to normalized pseudotime with superposition was applied. Highlighted in green is the interval after 500 days indicating the BDF with zero slope.

Case 1: Using the $\frac{m(p_i)-m(p_{wf})}{q_g} vs.\ t$ plot with the current properties.

The slope of this plot can be utilized to evaluate OGIP using the current fluid properties.

The points highlighted in green representing the BDF will be used when evaluating the slope of $\frac{m(p_i)-m(p_{wf})}{q_g} vs.\ t$ as shown in Fig. 5.3.

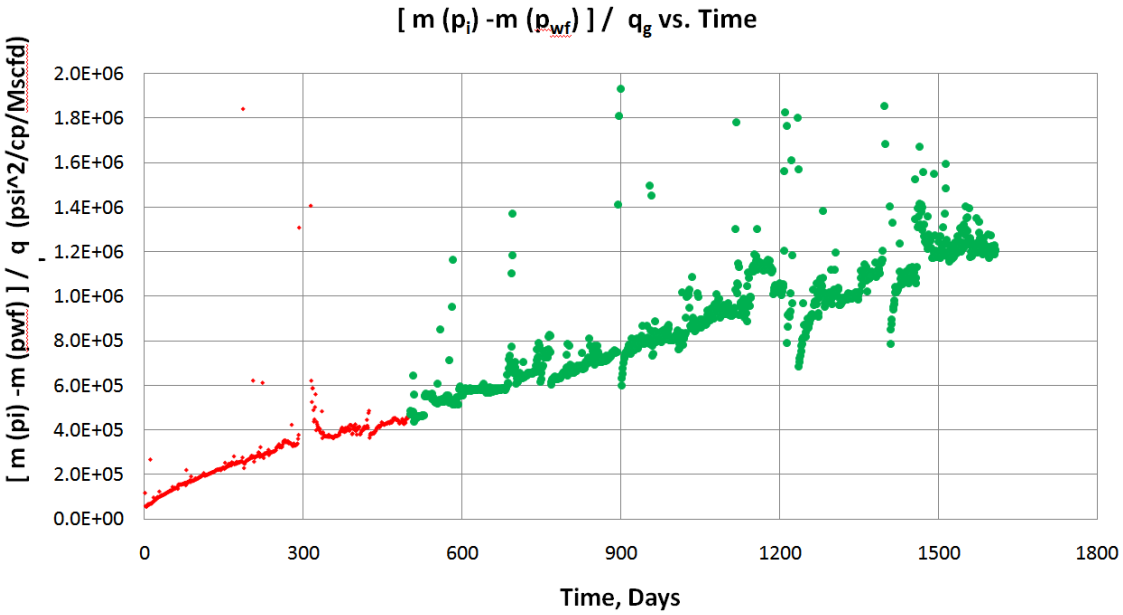

Fig. 5.3 – The points highlighted in green represent the BDF identified from the derivative plot. The slope of the line will be used to evaluate OGIP using the current fluid properties.

the slope value, $\tilde{m}_{PSS} = 625$ will be used to evaluate the OGIP as follows:

$$OGIP = \left(\frac{2pS_g\phi}{z}\right)_i \left(\frac{1}{\bar{\phi}(\bar{p})\bar{\mu}(\bar{p})\bar{c}_t(\bar{p})}\right)\left(\frac{1}{\tilde{m}_{PSS}}\right)$$

$$OGIP = \left(\frac{2\times 2950\times 0.8\times 0.6}{0.873567}\right)\left(\frac{1}{0.6\times 1.249\times 10^{-5}\times 0.000928}\right)\left(\frac{1}{625}\right)$$

OGIP= 0.746 Bscf.

Case 2: Using normalized pseudotime with superposition and initial properties by plotting the $\frac{m(p_i)-m(p_{wf})}{q_g}$ $vs.$ $\sum_{j=1}^{m}\frac{(q_{gj}-q_{gj-1})}{q_{gm}}(t_{nm}-t_{nj-1})$ as shown in Fig. 5.4.

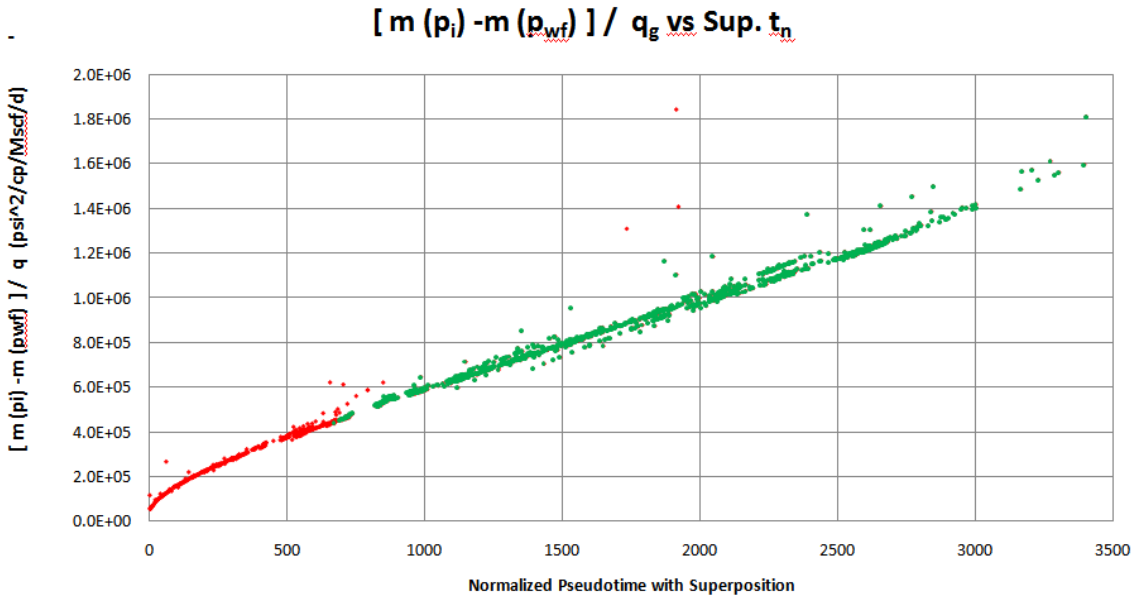

Fig. 5.4 – The points highlighted in green represent the BDF identified from the derivative plot. The slope of the line will be used to evaluate OGIP using the initial fluid properties.

By using the slope, $\tilde{m}_{PSS}$ = 4.4x10^5 from in Fig 5.4 to evaluate OGIP using:

$$OGIP = \frac{2 p_i S_{gi}}{z_i (\mu_g c_t)_i} \left(\frac{1}{\tilde{m}_{PSS}} \right) = \frac{2 \times 2950 \times 0.8}{0.873567 \times 0.02009 \times 0.000221} \left(\frac{1}{4.44 \times 10^5} \right)$$

OGIP=0.274 Bscf.

5.4 Dynamic Material Balance[40]

Because of the low permeability in shale gas formation, it takes long time to measure the average reservoir pressure. This fact affected the classical approach of calculating the OGIP using the material balance equation where the well is shut-in and average reservoir pressure is being measured.

Mattar and Anderson[40] presented the "Dynamic Material Balance" as an extension to the previous work of the Flowing Material Balance [48] that has an advantage of being applicable variable rate productions and use the conventional material balance plot. The new approach converts the flowing pressure to reservoir pressure at any given time and it is applicable only when the boundary dominant flow is reached. Once the pressure is converted to reservoir pressure, the traditional material balance plot and calculations can be performed to evaluate the OGIP. The calculation of the average reservoir pressure is done by:

$$\bar{P}_{PR} = P_{Pwf} + b_{PSS} q_g \quad \text{.....(5.6)}$$

where b_{PSS} is obtained from y-intercept of the:

$$\frac{m(p_i) - m(p_{wf})}{q_g} \text{ vs. } \textit{Mateial Balance Pseudotime}, t_{ca}$$

OGIP Calculation Procedure:

1. Converting pressure and flowing pressure to pseudopressures.

2. Assume a initial OGIP that will be re-evaluated in next steps.

3. Calculating the material balance pseudo-time at each pressure.

4. Evaluating b_{PSS} from the y-intercept of the plot $\frac{m(p_i) - m(p_{wf})}{q_g} \text{ vs. } t_{ca}$

5. Calculating the average reservoir pseudopressure from

$$\bar{P}_{PR} = P_{Pwf} + b_{PSS} q_g \quad \text{.....(5.7)}$$

6. Calculate the $\bar{P}_R$ from the average reservoir pseudopressure, $\bar{P}_{PR}$.

7. Evaluate $\bar{P}_R / z$ for each reservoir pressure and plot $\frac{\bar{P}_R}{z} vs. G_p$.

8. Evaluate the new OGIP from the x-intercept.

9. The value of the OGIP should be used repeat the procedure from 2 to 8 until the OGIP value convergence.

The following is an example field case to evaluate the OGIP using dynamic material balance. The procedure starts by identifying the flow regimes and determining the beginning of the BDF. Different plots are used to identify the beginning of the BDF such as the square root of time plot as shown in Fig. 5.5 and the derivative plot shown in Fig. 5.6. The reservoir constant $b_{PSS,}$ is evaluated from the y-intercept as shown in Fig. 5.7. Then the procedure listed above is applied as shown to create the dynamic material balance plot shown in Fig. 5.8.

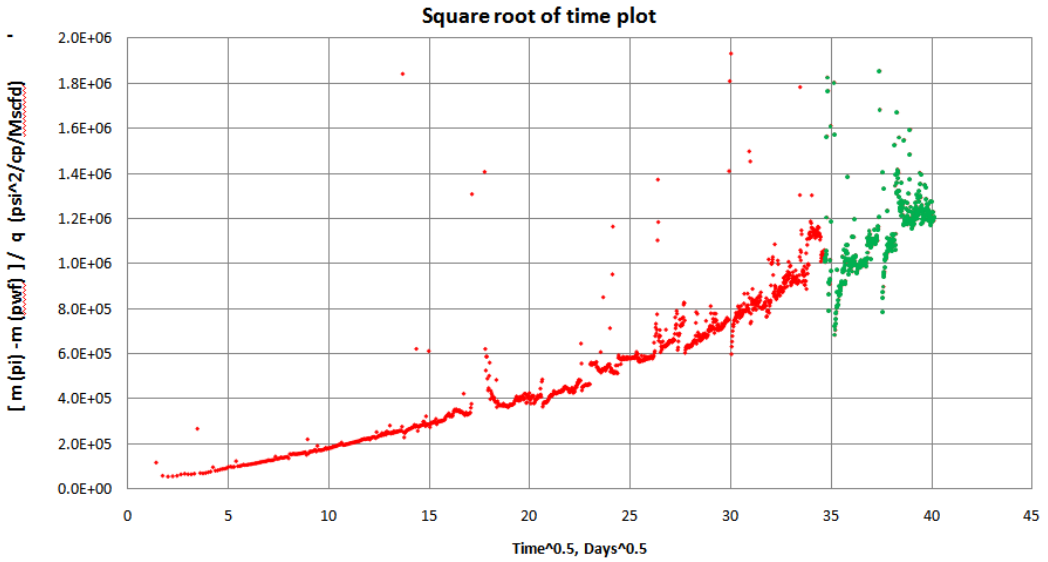

Fig. 5.5 –Showing well # 314 with the specialized square root of time plot and highlighted in green are flowing points that will be evaluating the flow regime for BDF confirmation.

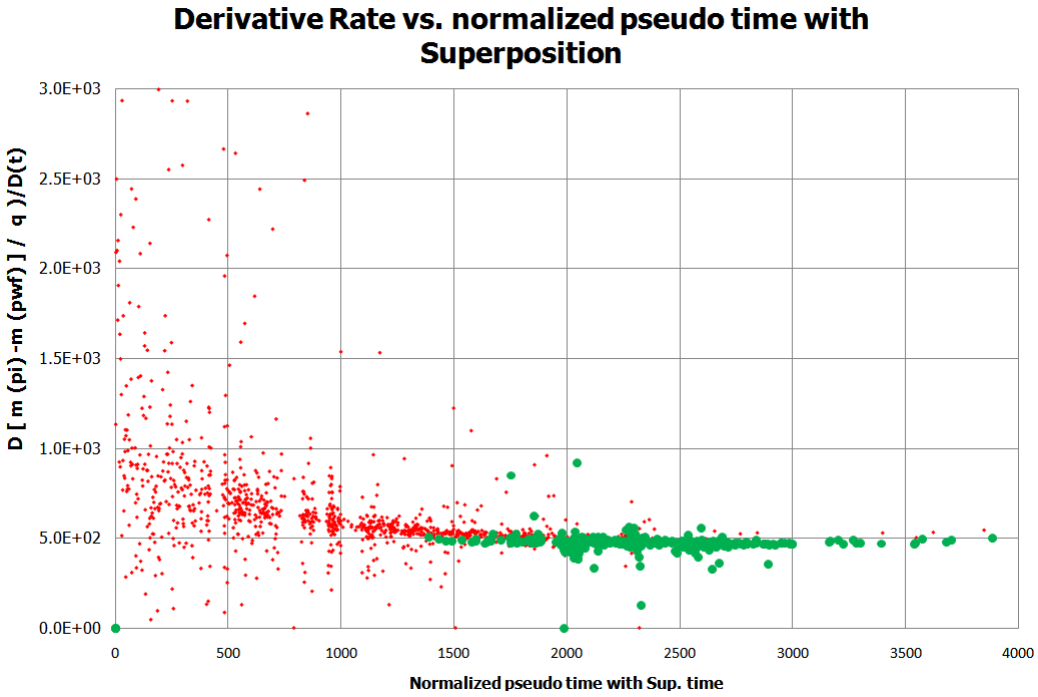

Fig. 5.6 –The highlighted points show zero slope when using the derivative with respect to normalized pseudotime with superposition.

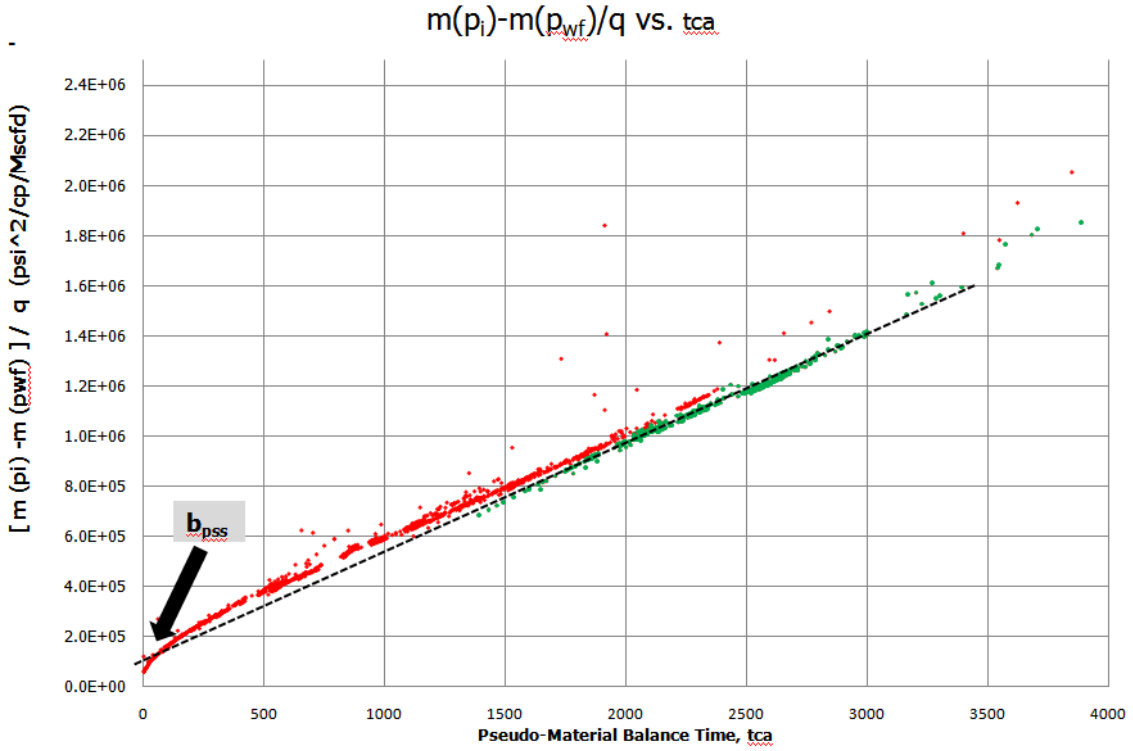

Fig. 5.7 –The identified BDF interval shown in green is being utilized to evaluate the y-intercept, b_{pss} which will be used to calculate the average reservoir pressure.

The y-intercept value, b_{pss}= 1.3x10^5 psi^2/cp/(Mscf/D) is used to evaluate the reservoir pseudopressure using:

$$\bar{P}_{PR} = P_{Pwf} + b_{PSS} q_g$$

Then converting the average pseudopressure to average reservoir pressure and plotting the p/z vs. cumulative gas production as shown in Fig. 5.8.

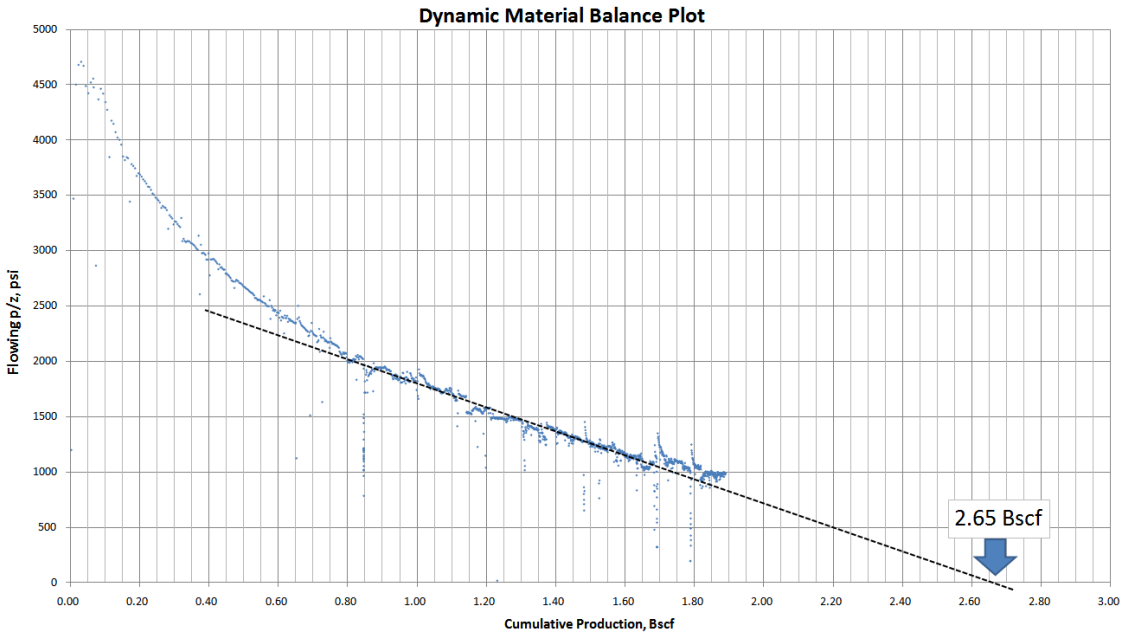

Fig. 5.8 –Matching and exploration the BDF using the dynamic material balance to evaluate the OGIP.

One observation on the Dynamic Material Balance approach, the selection of the beginning of the BDF and can lead to different values when evaluating the OGIP. Moreover, the material balance time tends to bias the BDF so that even scattering point or point still in transient flow will appear as a BDF which makes the estimation of b_{pss} very sensitive.

5.5 Blasingame's Type Curves

Palacio and Blasingame's Material Balance Pseudotime[15], $\bar{t}_a$ allows modeling variable rate and pressure production conditions using Fetkovich[50] harmonic decline type curves where b=1. When plotting the production data, the replacement of real time by the material balance time will result in converting the exponential decline to a harmonic

decline curve so that even the constant pressure production will appear as a constant rate production similar to liquid. During the BDF interval all production will be forced to follow a single curve of a harmonic decline. If a production data fall above this curve, then this is an indication of a pressure support while points falling below are indication of pressure loss such as the cases of liquid loading. The OGIP is calculated using a log-log plot of $\frac{q_g}{Pp_i - Pp_{wf}} vs. \bar{t}_a$ where $\bar{t}_a$ is defined as:

$$\bar{t}_a = \frac{\mu_{gi} c_{ti}}{q_g} \int_0^t \frac{q_g}{\mu_g(\bar{p}) c_t(\bar{p})} dt \quad \text{.....(5.8)}$$

The average reservoir pressure is calculated using the material balance using estimated value of the OGIP. In their paper, Palacio and Blasingame use a modified Fetkovich[48] and Carter [51] type curves solutions applied for gas in a liquid equivalent form. The modified type curves changes Carter's dimensionless variables which include the pseudopressure for gas solutions to equivalent Fetkovich variables for liquid.

OGIP Calculation Procedure:

1. Converting the pressure and to pseudopressure.

2. Obtain an initial value for OGIP and evaluate the reservoir pressure using the material balance equation.

3. Calculating the material balance pseudo-time at each pressure using:

$$\bar{t}_a = \frac{\mu_{gi} c_{ti}}{q_g} \int_0^t \frac{q_g}{\mu_g(\bar{p}) c_t(\bar{p})} dt$$

4. Calculate the normalized rate integral, which is the average rate up to the time of calculation, function/vertical axis integral of $\frac{q_g}{Pp_i - Pp_{wf}}$ with respect to $\bar{t}_a$ using:

$$\left(\frac{q_g}{Pp_i - Pp_{wf}}\right) = \frac{1}{\bar{t}_a}\int_0^{\bar{t}_a} \frac{q_g}{Pp_i - Pp_{wf}} d\bar{t}_a$$

5. Both the normalized rate and rate integral can be plotted against the material balance time on log-log plot to confirm the matching of the data. The field production data are moved across the type curve to find best matching for the data and both type curve axis and production data axis should be kept parallel.

6. After fitting the data, select a match point and identify the value of the best curve fitting which is the (re/xf) value and the match point of (normalized rate and tca) along with (q_{Dd} and t_{Dd}).The matching point can be used to evaluate OGIP for the selected model.

The production data of well #314 has been used with (Fekete RTA software[33]) which provides user friendly interface software with different models that uses the type curve to match the production data and evaluate the OGIP. The data was loaded the software, corrected units, formation, completion and fluid properties were used. Then the data were matched using Blasingame type curves with the normalized rate as shown in Fig. 5.9 with an estimation of OGIP = 2.25 Bscf.

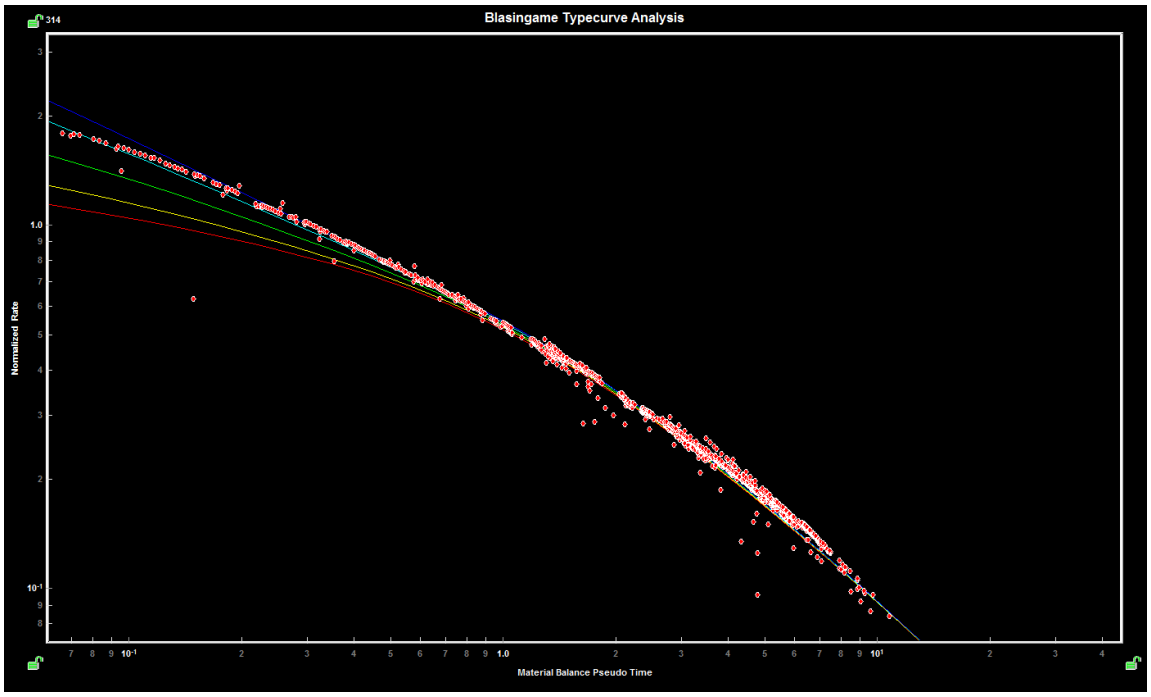

Fig. 5.9 –Fekete software[33] matching the production data on normalized rate vs material balance pseudotime on Blasingame's type curve using Fekete RTA software. The data match the BDF period with no sign of pressure support or pressure loss due to gas lift or liquid loading.

5.6 Normalized Rate and Normalized Cumulative [39,40, 48]

The plot of this approach is similar to the conventional material balance method. It plots the normalized cumulative production with the normalized rate to create linear plot. It is applicable only when the boundary dominant flow has occurred which appears as a straight line in the plot and it is extrapolated to evaluate the x-intercept or the OGIP. Unlike the conventional material balance, approach does not require shutting the well to measure the average reservoir pressure.

OGIP Calculation Procedure:

1. Obtain an initial value for the OGIP.

2. Calculate the material balance pseudotime and evaluate the normalized cumulative Q_n pressure normalized rate, using:

$$\text{Normalized Cumulative} = Q_n = \frac{2q_g\, t_{ca}\, p_i}{(\mu_g c_t z)_i\, \Delta p_p} \quad \ldots\ldots\ldots\ldots\ldots\ldots\ldots\ldots (5.9)$$

$$\text{Normalized Rate} = \frac{q_g}{\Delta p_p} \quad \ldots\ldots\ldots\ldots\ldots\ldots\ldots\ldots (5.10)$$

3. Plot the Normalized Rate vs. Normalized Cumulative on a Cartesian scaled plot.

4. Identify the BDF which appears as a straight line and extrapolate to evaluate OGIP.

5. The procedure is repeated until the value of OGIP converges.

Fig. 5.10 shows the plotting results applied to well #314. After matching and extrapolating the BDF production to evaluate the OGIP = 3.7 Bscf.

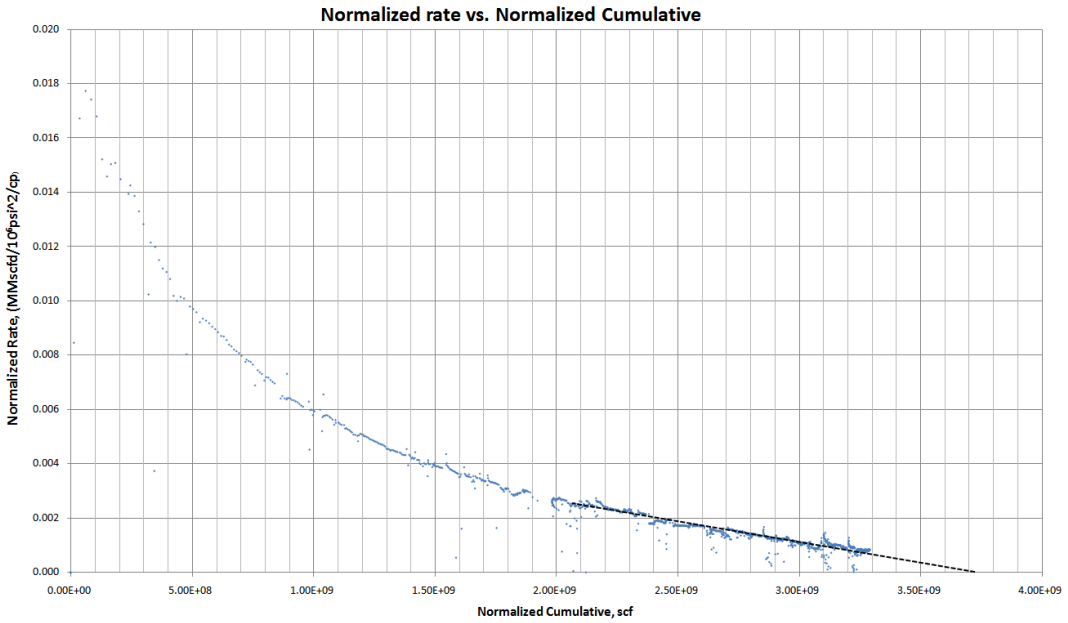

Fig. 5.10 –Matching and exploration the BDF using the flowing material balance to evaluate the OGIP.

5.7 Results and Discussion

The best way to check which method fits the Barnett shale and gives the most accurate OGIP, is by utilizing the evaluated OGIP to forecast the well's production and see which value will result in the most accurate forecast.

The only certain case of having the evaluated OGIP wrong if it gives a value that has already been produced. In other words, the well has recovered 100% of the OGIP and still producing. Table 5.2 summarizes the results of calculating the OGIP using the different methods. The OGIP varies from 0.711 Bscf to 3.65 Bscf. The volumetric models include the correction of Ibrahim and Wattenbarger.[52]

Table 5.2 Summary of the results for calculating OGIP using different methods for field data using well #314.

Method	Calculated OGIP (scf)
Using the End of Transient Time	2.80×10^9
Volumetric (Hydraulic Fracture Model-2*)	2.38×10^9
Volumetric (Hydraulic Fracture Model-3*)	0.711×10^9
Normalized Rate and Normalized Cumulative	3.7×10^9
Blasingame Type Curve	2.25×10^9
Dynamic Material Balance	2.65×10^9

The procedure will be as follows:

1. The production data are divided into two parts with the second part being the BDF interval.

2. After identifying the flow regimes and the beginning of the BDF, OGIP is calculated as shown early in this chapter.

3. Perform forecasting based on the material balance and the OGIP evaluated from the different methods.

4. Compile the BDF interval production data to see which method gives the best fitting for the data.

5. For the OGIP evaluated form the type curves, it can be checked by tracing the BDF interval with production data and comparing.

When evaluating the OGIP results for Blasingame's type curves, the forecasting is done by tracing the decline curve and comparing it to the matched production data. In the BDF interval, all production is forced to follow a single curve of a harmonic decline which makes it easy to compare with the actual production data. However, matching the BDF becomes difficult whenever there is a loss or gain in pressure resulted from the liquid loading or installment of gas lift. If we look at well #314 production as shown in Fig. 5.11 a clear effect of the gas lift installment is shown on the production rate of the water. The gas lift will affect matching Blasingame type curve in which the data will be shifted upward as having a pressure support and the actual field data will not follow or trace the harmonic decline curve as shown in Fig. 5.12.

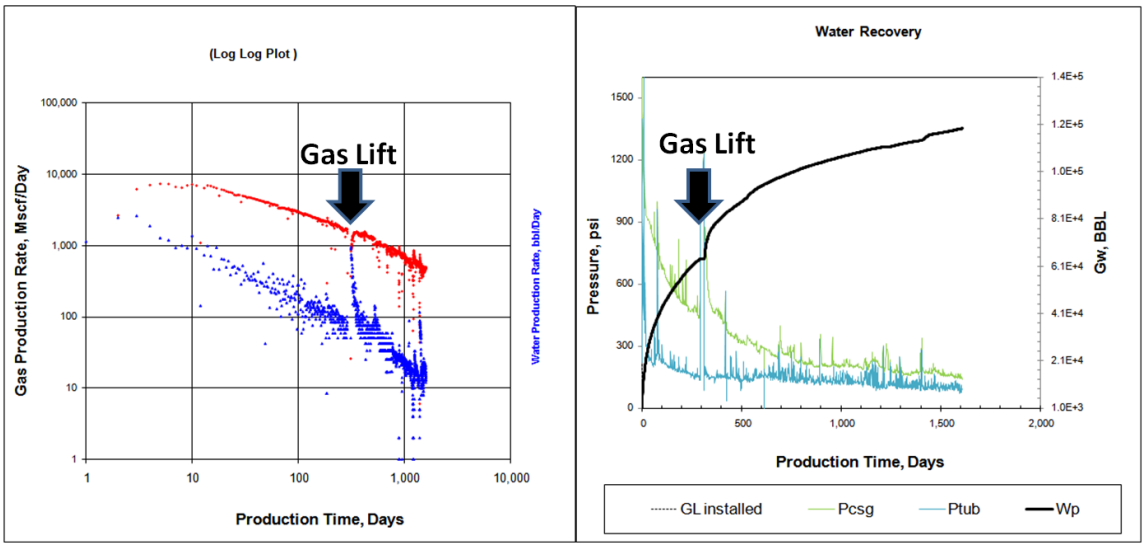

Fig. 5.11 – Showing the effect of gas lift installment can be identified from the production behavior as an increase in water production shown in daily and cumulative production.

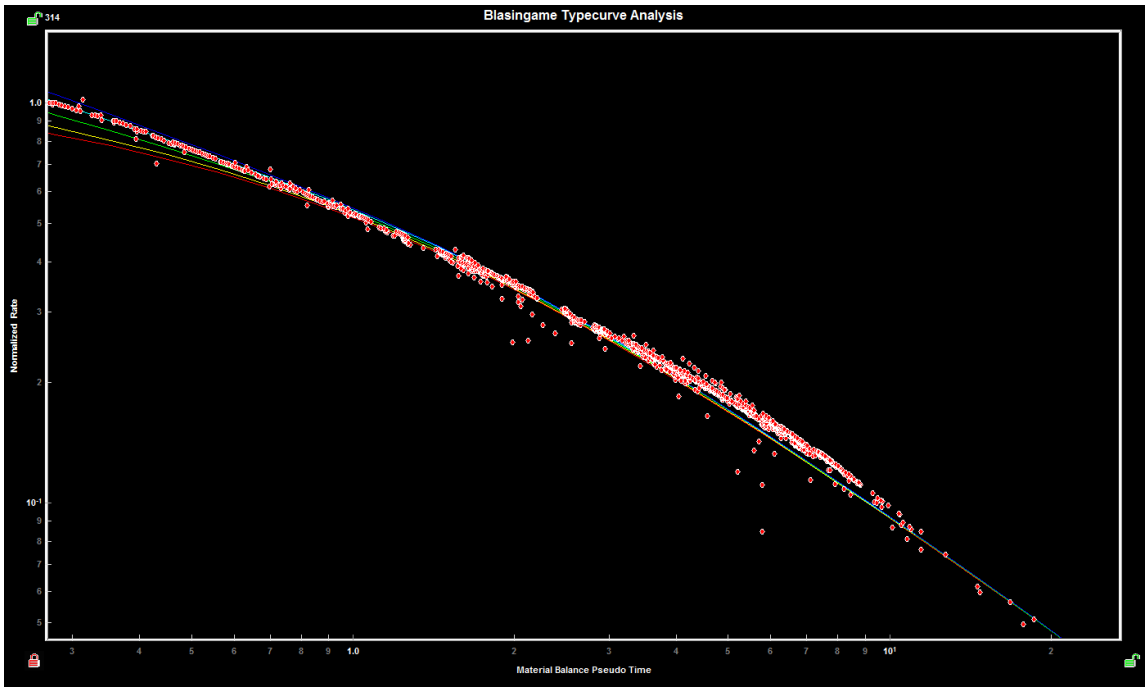

Fig. 5.12 –Fekete software shows Blasingame type curve and the effect of the pressure support caused by gas lift is shown. The production data are shifted upward and the will not match the forecasted production.

Fig. 5.13 through Fig. 5.16 show the forecasting plots for the BDF interval based on OGIP for different methods. Both the log-log plot and the square root of time plot are shown. When trying to forecast the production, different factors may affect the result such as the assumed formation permeability. Shale Gas VBA[37] was used for this part where the forecasting of the BDF is based on the material balance calculations that will account for change in real gas properties. Fig. 5.13 through Fig. 5.16 will show the effect of gas lift as the forecasting line underestimates the production rate for different cases. Moreover, if a pressure loss or liquid loading occurs, then the forecasting curve will overestimate the gas production.

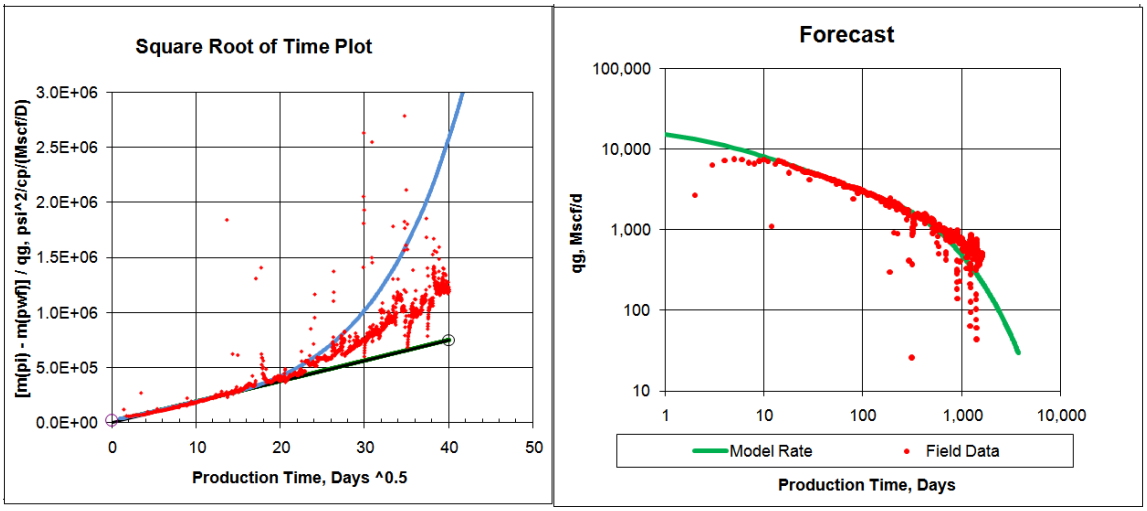

Fig. 5.13 –Forecasting the BDF interval based on OGIP = 2.38 Bscf.

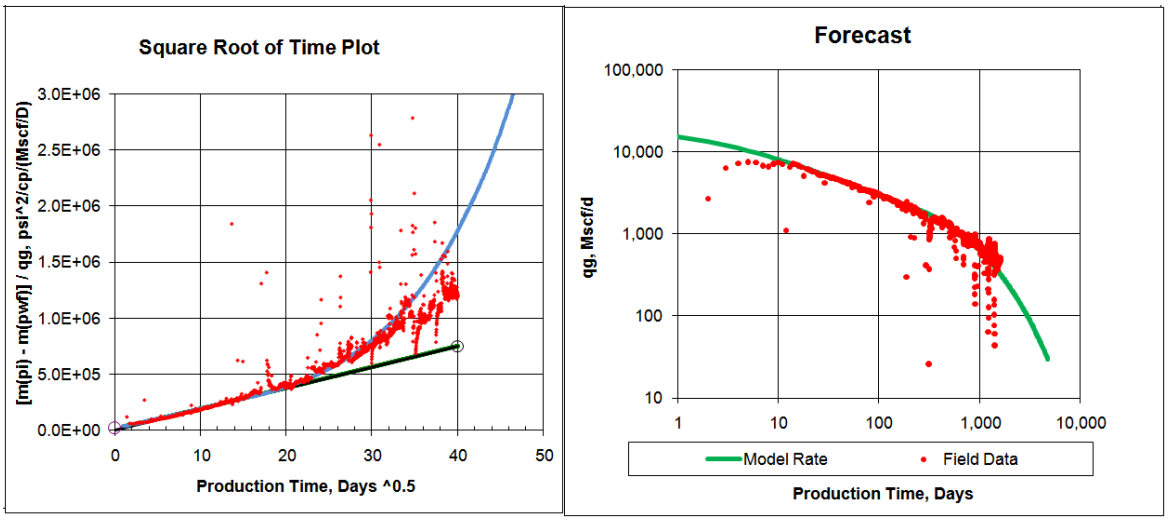

Fig. 5.14 – Forecasting the BDF interval based on OGIP= 2.8 Bscf.

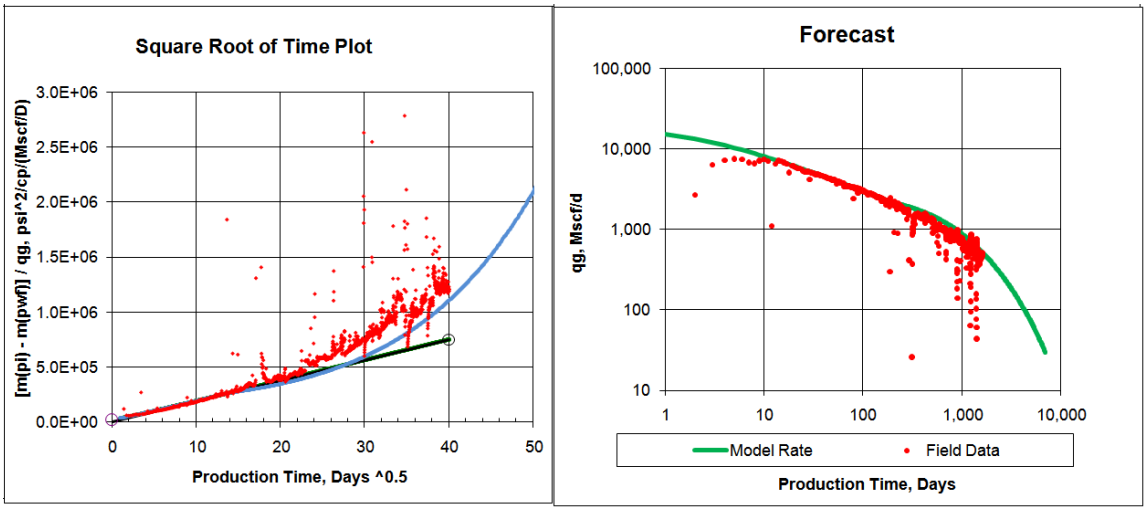

Fig. 5.15 – Forecasting the BDF interval based on OGIP=3.7 Bscf.

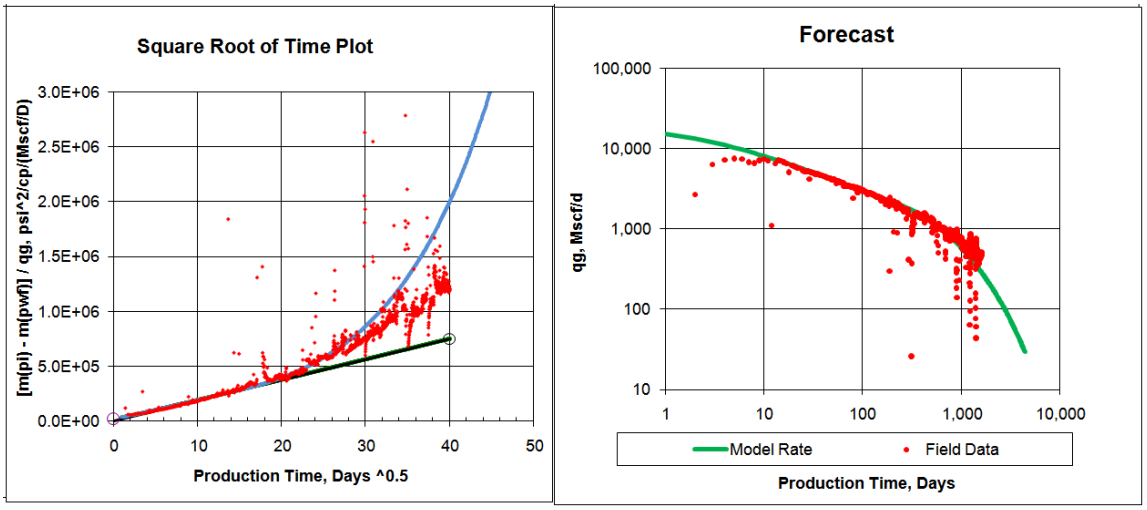

Fig. 5.16 – Forecasting the BDF interval based on OGIP=2.65 Bscf.

Because of the water production, liquid loading, interference, recompletion, and gas lift installment, an accurate forecasting of the BDF is difficult to obtain. None of the applied method perfectly matched the BDF interval. The BDF could be matched if we change some of the formation properties such as the permeability or modify the beginning of the BDF. One factor affecting the matching is the evaluated t_{esr} which could be subjective whenever there is a transition interval between the flow regimes. One approach could be done is to use the Barnett shale formation and fluid properties and run a simulated cases then use the different method to evaluate the OGIP. This is followed by forecasting the simulated run using the results from different methods which could give us the best approach analyzing procedure. However, these simulated data will not represent the field data and the conclusion would not be possible to make. Another factor that was not considered in this work is the gas desorption. It will be another factor that will significantly affect the forecasting at lower average reservoir pressure.

CHAPTER VI

CONCLUSION AND REMARKS

6.1 Conclusion and Remarks

In this study, 378 wells producing from the Barnett shale have been utilized to evaluate completion and formation properties. The data have been filtered and prepared for analysis through a systematic procedure and different models were utilized to evaluate the completion. A supplementary report show the results for evaluating completion jobs of these wells and showing the updated production for 149 wells from the same list.

Before imposing any model the data are prepared through different steps to make sure of their validity and completeness. During this procedure, the production data and completion reported are aligned to check for any abnormal behavior resulting from recompletion of the well. Then the basic correlations are checked and followed by identifying the flow regime for each well. One of the ways to identify the flow regimes was to plot the derivatives with respect to different time and using the normalized pseudotime with superposition to account for variable production conditions. The conclusion from this approach was that the derivative plots tend to make the data noisy and scattered when using the field data and smoothing approaches must be applied to evaluate the data more effectively. Moreover, there were long transition intervals between the flow regimes which makes identifying the beginning of the BDF more complicated.

The conclusions are summarized as follows:

1. Original gas in place can be evaluated using different methods and there is no best method to be applied to the Barnett shale production because of the variable factors such as liquid loading, gas lifting, interference and production interruption that occur at later stages of the well's production life.
2. Adsorption was not considered in this work as a critical factor at the current average reservoir pressure, but it can cause difficulties when trying to forecast the production or match the type curves at lower reservoir pressures.
3. Utilizing the production data to evaluate the effective of the completion job is simple and very useful way to improve completion jobs and field planning.
4. When evaluating the transient flow, the transition interval can be misinterpreted and wrong conclusion will be calculated. As shown in simulated run, the transition interval between the bilinear and linear could reach 700 days of production.
5. Determining the beginning of the BDF is subjective and the methodologies utilizing it will need to account for inaccuracies.
6. Occurrence of bilinear flow is depends mainly on the hydraulic fracture conductivity and it can be an indication of a poor fracturing job.
7. The Derivative plots tend to make field data noisy and require smoothing to better identify flow regimes.
8. Four flow trends were observed as results of installing gas lift.
9. The Following are shown in the supplementary report:
    - Evaluation of 378 hydraulic fracturing jobs from Barnett shale.

- Summary of production data for 149 wells.

6.2 Recommendations for Future Work

The following recommendations are listed:

1. Investigation of the effect of the normalized pseudotime with superposition and the material balance pseudotime on the BDF.
2. Investigation of the effects of injected water volumes on the fracture surface area.
3. Investigation of the effects of adsorption on forecasting and type curve matching.
4. The effects of gas lift on the flowing bottom hole pressure calculations.
5. Utilized smoothing approaches with the derivative to reduce the noise in the data.
6. Investigate the transition intervals between the flow regimes.
7. Investigate the effect of natural fracture interference on BDF.

NOMENCLATURE

A_{cm} = total matrix surface area draining into fracture system, ft^2

A_{cw} = well-face cross-sectional area to flow, ft^2

A_{c1} = cross sectional area along the high permeability flow path of Arevalo-Villagran et. al model, ft^2

A_{SRV} = area of stimulated reservoir volume, ft^2

A_{outer} = area defined by the interface between the SRV and the unstimulated reservoir, ft^2

B_{gi} = formation volume factor at initial reservoir pressure, rcf/scf

b= intercept of the square root of time plot, psi^2/cp/Mscf/Day

b_{CPEL} = intercept of constant p_{wf} early linear flow of $\Delta m(p)/q$ $vs. \sqrt[2]{time}$ plot, psi^2-D/Mscf-cp

b_{CRB} = intercept of constant q_g early linear flow of $\Delta m(p)/q$ $vs. \sqrt[2]{time}$ plot, psi^2-D/Mscf-cp

b_{PSS} = reservoir constant obtained from the y-intercept of $\frac{m(p_i)-m(p_{wf})}{q_g}$ $vs.\ t_{ca}$

c_t = liquid total compressibility, psi^{-1}

c_{ti} = total compressibility at initial reservoir pressure, psi^{-1}

D_D= dimensionless drawdown, dimensionless

f_{CP} = slope correction factor, dimensionless

h = reservoir thickness, ft

k = homogeneous reservoir permeability, md

k_f = bulk fracture permeability of dual porosity models, md

k_m = matrix permeability, md

l =half of fracture spacing, ft

L_1 = fracture spacing for Wattenbarger's model (slab), ft

L_2 = fracture spacing for Mayerhover model (cube), ft

LFP= linear flow parameter, $ft^2md^{1/2}$

$\tilde{m}_{CPL}$ = slope of square root of time plot with a constant p_{wf} production., $(psia^2\text{-}D^{1/2})/(Mscf\text{-}cp)$.

$\tilde{m}_{CRL}$ = slope of square root of time plot with a constant rate production., $(psia^2\text{-}D^{1/2})/(Mscf\text{-}cp)$.

$\tilde{m}_{PSS}$ = slope of the plot $\lfloor m(p_i)-m(p_{wf})\rfloor/q_g$ *vs.* $superposition-t$, $(psia^2)/(Mscf\text{-}cp)$.

$m(p)$ = pseudopressure (gas), psi^2/cp

p_i = initial reservoir pressure, psi

p_{wf} = wellbore flowing pressure, psi

p_f = fracture pressure, psi

p_i = initial pressure, psi

p_{pi} = pseudo-pressure at initial pressure, psi^2/cp

p_{pwf}= pseudo-pressure at flowing pressure, psi^2/cp

p_{PR}= pseudo-pressure at averag reservoir pressure, psi^2/cp

q_D = dimensionless rate (transient dual porosity model)

q_g = gas rate, Mscf/day

Q = cumulative production, STB

s' = apparent skin

s_c = convergence skin

S_g = gas saturation, dimensionless

t = time, days

t_n = normalized pseudotime

t_a = pseudo-time, days

t_{ca} = material balance pseudo-time, days

t_{esr} = end of transient flow time, days

T = absolute temperature, ^{o}R

V_{bm} = total matrix bulk volume, ft^3

V_p = matrix pore volume, ft^3

x_e = drainage area width (rectangular geometry), ft

x_f = fracture half length (rectangular geometry), ft

x = horizontal well length, ft

y_e = drainage area half-length (rectangular geometry), ft

z = gas compressibility factor

Greek symbols

λ = dimensionless interporosity parameter

μ = viscosity, cp

ω = dimensionless storativity ratio

ϕ = porosity

σ = shape factor, ft^{-2}

Subscript

Ac = cross-sectional area to flow

i =initial

f =fracture system

g = gas

m =matrix

f+*m* =total system (fracture+matrix)

REFERENCES

1. Railroad Commission of Texas, http://www.rrc.state.tx.us/data/wells/index.php, June 30, 2010.
2. Ayers, W. B.: "PETE 612 – Unconventional Reservoir Class Notes," Fall 2008.
3. Franz, J.H., Jr. and Jochen, V.: "Shale Gas," Schlumberger White Paper, 2005
4. Pickering Energy Partners, http://www.tudorpickering.com/pdfs/TheBarnettShale Report.pdf", June 28, 2010.
5. HPDI Data Service Company, U.S Production Data Application, Austin, TX. June (2010).
6. Railroad Commission of Texas, http://www.rrc.state.tx.us/data/fielddata/ barnettshale.pdf , June 28, 2010.
7. Bello, R. O.: "Rate Transient Analysis in Shale Gas Reservoirs with Transient Linear Behavior," PhD Dissertation, Texas A&M University, College Station, May (2009).
8. Bello, R. O. and Wattenbarger, R. A. 2009. Modeling and Analysis of Shale Gas Production with a Skin Effect. Paper *CIPC* 2009-082 presented at the Canadian International Petroleum Conference, Calgary, Alberta, Canada, 16-18 June.
9. Warren, J.E. and Root, P.J. 1962. The Behavior of Naturally Fractured Reservoirs. Paper *SPE* 426 presented at the 1962 Fall Meeting of the Society of Petroleum Engineers, Los Angeles, 7 – 10 October.
10. El-Banbi, A.H.: "Analysis of Tight Gas Wells," PhD Dissertation, Texas A&M University, College Station May (1998).

11. Arevalo, J. A.: "Analysis of Long-Term Behavior in Tight Gas Reservoirs: Case Histories," PhD Dissertation, Texas A &M University, College Station August (2001).
12. Yildiz, T and Ozkan, E. 1997. Influence of Areal Anisotropy on Horizontal Wells Performance. Paper *SPE* 38671 presented at the SPE Annual Technical Conference and Exhibition, San Antonio, TX, 5-8 October.
13. Arevalo-Villagran, J. A., Wattenbarger, R.A., Samaniego-Verduzco, F. and Pham, T.T. 2001. Production Analysis of Long-Term Linear Flow in Tight Gas Reservoirs: Case Histories. Paper *SPE* 71516 presented at the *SPE* Annual Technical Conference and Exhibition, New Orleans, Sept. 20-Oct. 3.
14. Fraim, M.L., and Wattenbarger, R.A. 1985. Gas Reservoir Decline-Curve Analysis Using Type Curve With Real Gas Pseudopressure and Normalized Time. Paper *SPE* 14238 presented at the *SPE* Annual Technical conference and Exhibition, Las Vegas, NV 22-25 September.
15. Placio, J.C and Blasingame, T.A. 1993. Decline-Curve Analysis Using Type Curves-Analysis of Gas Wells Production Data. Paper *SPE* 25909 presented at the 1993 *SPE* Joint Rocky Mountain Regional and Low Permeability Reservoir Symposium, Denver, CO, 26-28 April.
16. Agarwal, R.G, Gardner, D.C., Kleinsteiber S.W, and Fussel, D.D. 1998. Analyzing Well Production Data Using Combined Type Curve and Decline Curve Analysis Concepts. Paper *SPE* 49222 presented at the SPE Annual Technical Conference and Exhibition, New Orleans, LA 27-30 September.

17. Spivey, J.P. and Semmelbeck, M.E. 1995. Forecasting Long-Term Gas Production of Dewatered Coal Seams and Fractured Gas Shale. Paper *SPE* 29580 presented at the Rocky Mountain Regional/Low Permeability Reservoirs Symposium, Denver, CO, 20 -22 March.
18. Ibrahim, M., Wattenbarger, R.A. and Helmy, W. 2003. Determination of OGIP for Wells in Psedudosteady-State-Old Techniques. Paper *SPE* 84286 presented at the SPE Annual Technical Conference and Exhibition, Denver, CO, 5-8 October.
19. Gringarten A. C, Ramey, H.J., and Raghavan, R. 1975. Applied Pressure Analysis for Fractured Wells. *JPT* (July 1975); paper SPE 5496.
20. Aguilera, R. 1987. An Approximate Solution of Linear Flow in Naturally fractured Reservoirs. Paper *SPE* 16442 (available from SPE, Richardson, TX).
21. Wattenbarger, R. A., El-Banbi, A. H. Villegas, M.E. and Maggard, J.B. 1998. Production Analysis of Linear Flow into Fractured Tight Gas Wells. Paper SPE 39931 presented at the SPE Rocky Mountain Regional/Low Permeability Reservoirs Symposium and Exhibition, Denver, CO, 5-8 April.
22. Helmy, W.M. and Wattenbarger, R.A. 1999. A New Approach to the Analysis of Gas-Well Performance with Periodic Interruptions. Paper *SPE* 56695 presented at the *SPE* Annual Technical Conference and Exhibition, Houston, TX 3-6 October.
23. Bello, R. O. and Wattenbarger, R. A. 2010. Multi-stage Hydraulically Fractured Shale Gas Rate Transient Analysis. Paper *SPE* 126754 presented at the SPE

North Africa Technical Conference and Exhibition held in Cairo, Egypt, 14-17 February.

24. Cinco-Ley, H., and Samaniego, F. 1978. Transient Pressure Analysis for Fractured Wells. Paper SPE 7490, Presented at the *SPE* 53rd Annual Fall Meeting, Houston, TX, 1-3 October.
25. Du Kuifu and Stewart, G. 1995. Bilinear Flow Regime Occurring in Horizontal Wells and Other Geological Models. Paper *SPE* 29960 presented at the International Meeting on Petroleum Engineering Beijing, 14-17 November.
26. Wong, D.W, Harrington, A.G., and Cinco-Ley, H. 1984. Application of the Pressure Derivative Function in the Pressure-Transient Testing of Fractured Wells. Paper *SPE* 13056 presented at *SPE* Annula Technical Conference and Exhibition, Houston, TX, 16-19 September.
27. Cinco-Ley, H., Ramey Jr., H.J. , Samaniego, F. and Rodriguez F. 1987. Behavior of Wells with Low-Conductivity Vertical Fractures. Paper *SPE* 16776, Presented at the *SPE* 62nd annual Meeting, Dallas, TX, 27-30 September.
28. England, K.W., Poe, B.D., and Conger, J.G. 2000. Comprehensive Evaluation of Fractured Gas wells Utilizing Production Data. Paper *SPE* 60285, Presented at the *SPE* Rocky Mountain Regional/Low Permeability Reservoir Symposium, Denver, CO, 12-15 March.
29. Branajaya, R.T., Ibrahim, M. and Wattenbarger, R.A. 2004. Simulation of Bilinear Flow in Single Matrix Block Drainage. Paper CIPC 2004-052 presented

at the Canadian International Petroleum Conference, Calgary, Alberta, Canada 8-10 June.

30. Guppy, K., Cinco-Ley, H., Ramey, H. Transient Flow Behavior of Vertically Fractured Well Producing at Constant Pressure. Paper *SPE* 9963.
31. Arevalo-Villagran, J.A., Ganpule S.V, Wattenbarger, R.A., Yanez-Mondragon, M., Serrano-Lozano, J.R., Samaniego-Verduzco, F. 2002. Analysis of Long-Term Performance in Tight Gas Wells: Field Examples. Paper *SPE* 74360 presented at the SPE International Petroleum Conference and Exhibition, Villahermosa, Mexico, 10-12 February.
32. Anderson, D. M., Stotts, G.W.J, Mattar, L. Ilk, D. and Blasingame, T. A. 2006. Production Data Analysis-Challenges, Pitfalls, Diagnostics. Paper *SPE* 102048 presented at the Annual Technical Conference and Exhibition, San Antonio, TX, 24-27 September.
33. Fekete Associates Inc. 2010. RTA software Advanced Software Technology, Alberta, Canada, 2010.
34. Al-Ahmadi, H. A., Almarzooq, A.M., and Wattenbarger, R. A. 2010. Application of Linear Flow Analysis to Shale Gas Wells-Field Cases. Paper *SPE* 130370 presented at the SPE Unconventional Gas Conference held in Pittsburgh, Pennsylvania, 23-25 February.
35. Turner, R. G.; Hubbard, M. G.; Dukler, A. E. 1968. Analysis and prediction of minimum flow rate for the continuous removal of liquids from gas wells. Paper *SPE* 2198, 43rd Fall Meeting, Houston, TX, 1968 Sept. 29 to Oct 2.

36. Wattenbarger, R. A. 1996. Liquid Loading in Gas Wells. Class Notes, Texas A&M University. Spring 2009.

37. Wattenbarger, R. A. April 2010. Shale Gas VBA Software, College Station, TX.

38. Doublet, L.E, Pandie, P.K, Mccollum, T.J. and Blasingame, T.A. 1994. Decline Curve Analysis Using Type Curves Analysis of Oil Well Production Data Using Material Balance Application to Field Cases. Paper *SPE* 28688 presented at the Petroleum Conference and Exhibition of Mexico, Veracruz, 10-13 October.

39. Anderson, D.M. Nobakht, M., Moghadam, S., Mattar, L. 2010. Analysis of Production Data From Fractured Shale Gas Wells. Paper *SPE* 131787 preseted at the SPE Unconventional Gas Conference, Pittsburgh, PA, 23-25 February.

40. Mattar, L., and Anderson, D.M. 2005. Dynamic Material Balance (Oil or Gas-In-Place without Shut-Ins). Paper *CIPC* 2005-11 presented at the Canadian International Petroleum Conference, Calgary, Alberta, 7-9 June.

41. Mayerhofer, M. J., Lolon, E. P., Youngblood, J. E. and Heinze, J. R. 2006. Integration of Microseismic Fracture Mapping Results with Numerical Fracture Network Production Modeling in the Barnett Shale. Paper *SPE* 102103 presented at the 2006 Annual Technical Conference and Exhibition, San Antonio, TX, 24-27 September.

42. Lee, J. and Wattenbarger, R.A.: Gas Reservoir Engineering, *SPE* Textbook Series Vol. 5, Richardson, TX (1996).

43. Fetkovich, M.J, Vienot, M.E, Brandley, M.D., and Kiesow, U.G., "Decline-Curve Analysis Using Type Curves - Case Histories", *SPE* Formation Evaluation, pp 637-656, 1987 December.

44. Fetkovich, M.J., Fetkovich, E.J., and Fetkovich, M.D. 1996. Useful Concepts for Decline-Curve Forecasting, Reserve Estimation, and Analysis. Paper *SPE* Reservoir Engineering, 13-22 February.

45. Carter, R. D.: "Type Curves For Finite Radial and Linear Gas-Flow Systems: Constant-Terminal Pressure Case," *SPEJ* (Oct. 1985) 719-28.

46. Arps, J.J. 1945. Analysis of Decline Curves, Trans., *AIME* (1945), 160, 228.

47. Mattar, L. and Anderson, D. M. 2003. A Systematic and Comprehensive methodology for Advanced Analysis of Production Data. Paper *SPE* 84472 presented at the Annual Technical Conference and Exhibition, Denver, CO, 5-8 October.

48. Mattar, L. and McNeil, R.,: "The Flowing Gas Material Balance", Journal of *JCPT*, Vol. 37#2, page, 1998.

49. Lee, W.J. and Holditch, S.A. 1982. Application of pseudotime to Buildup Test Analysis of Low-Permeability Gas Wells With Long-Duration Wellbore Storage Distortion. (*JPT* December 1982) 2877-2887; paper *SPE* 9888.

50. Fetkovich, M.J.: "Decline Curve Analysis Using Type Curves," *JPT* (June 1980) 1065-77.

51. Carter, R.D. 1981. Characteristic Behavior of Finite Radial and Linear Gas Flow Systems - Constant Terminal pressure Case. Paper *SPE* 9887 presented at the 1981 SPE/DOE Low Permeability Symposium, Denver, CO, 27-29 May.

52. Ibrahim, M. and Wattenbarger, R. A. 2005. Analysis of Rate Dependence in Transient Linear Flow in Tight Gas Wells. Paper *CIPC* 2005-057 presented at the Canadian International Petroleum Conference, Calgary, Canada, 7-9 June.

VITA

Name:	Anas Mohammadali S. Almarzooq
Permanent Address:	Harold Vance Dept. of Petroleum Engineering TAMU, College Station TX 77843-3116.
Email Address:	Al-marzooq@msn.com
Education:	M.Sc., Petroleum Engineering Texas A&M University College Station, USA, 2010.
	B.Sc., Petroleum Engineering King Fahad University of Petroleum and Minerals Dhahran, Saudi Arabia, 2004.